OAK RIDGE NATIONAL LABORATORY LIBRARY
3 4456 0041266 7

ORNL/TM-9296

ornl

OAK RIDGE
NATIONAL
LABORATORY

MARTIN MARIETTA

FED LIBRARY MAR 1 1985

Noninductive Current Drive in Tokamaks

N. A. Uckan

FUSION ENERGY DIVISION LIBRARY

OPERATED BY
MARTIN MARIETTA ENERGY SYSTEMS, INC.
FOR THE UNITED STATES
DEPARTMENT OF ENERGY

Printed in the United States of America. Available from
National Technical Information Service
U.S. Department of Commerce
5285 Port Royal Road, Springfield, Virginia 22161
NTIS price codes—Printed Copy: A10 Microfiche A01

This report was prepared as an account of work sponsored by an agency of the United States Government. Neither the United States Government nor any agency thereof, nor any of their employees, makes any warranty, express or implied, or assumes any legal liability or responsibility for the accuracy, completeness, or usefulness of any information, apparatus, product, or process disclosed, or represents that its use would not infringe privately owned rights. Reference herein to any specific commercial product, process, or service by trade name, trademark, manufacturer, or otherwise, does not necessarily constitute or imply its endorsement, recommendation, or favoring by the United States Government or any agency thereof. The views and opinions of authors expressed herein do not necessarily state or reflect those of the United States Government or any agency thereof.

ORNL/TM-9296
Dist. Category UC-20a,d,f,g

Fusion Energy Division

NONINDUCTIVE CURRENT DRIVE IN TOKAMAKS

N. A. Uckan

Date Published - January 1985

Prepared by the
OAK RIDGE NATIONAL LABORATORY
Oak Ridge, Tennessee 37831
operated by
MARTIN MARIETTA ENERGY SYSTEMS, INC.
for the
U.S. DEPARTMENT OF ENERGY
under Contract No. DE-AC05-84OR21400

OAK RIDGE NATIONAL LABORATORY LIBRARY
3 4456 0041266 7

CONTENTS

ABSTRACT vii
INTRODUCTION 1

1. CURRENT DRIVE EFFICIENCY FACTOR 7

1.1. Simple Efficiency Calculation 7
1.2. Derivation of Efficiency Factor Using the Fokker-Planck Equation 10
1.3. Reactor Applications 15

2. CURRENT DRIVE BY NEUTRAL BEAM INJECTION 21

2.1. Simple Calculation of Beam-Driven Current 22
2.1.1 Fast Ion Current 22
2.1.2 Electron Return Current 24
2.1.3 Trapped Electron Correction 26
2.1.4 Current Drive Efficiency 30
2.2. Experiments 30
2.3. Future Applications 32
2.3.1 Near-Term Potential 32
2.3.2 Reactor Projections 33

3. LOWER HYBRID CURRENT DRIVE 37

3.1. Propagation of LH Wave and Choice of rf Frequency 40
3.1.1 Dispersion Relation 40
3.1.2 Choice of $\eta_{\parallel}$ and ω 50
3.2. Current Generation and Power Absorption 56
3.2.1 Electron Distribution Function 59
3.2.2 Current Density 67
3.2.3 Power Dissipation 70
3.2.4 Efficiency Factor 74
3.3. Experiments 77
3.3.1 Demonstration of Current Drive 78
3.3.2 Current Drive Efficiency 81
3.3.3 Density Limit 84
3.3.4 Spectral Gap 88

4. ELECTRON CYCLOTRON CURRENT DRIVE 91

4.1 Basic Mechanism of Current Generation 93
4.2 Experiments 99
4.3 Propagation and Wave Absorption of Electron Cyclotron Waves 101
4.3.1 Dispersion Relation and Polarization 101
4.3.2 Accessibility 104
4.4 Nonrelativistic Calculations 108
4.4.1 Resonance Condition 108
4.4.2 Fokker-Planck Equation 109
4.4.3 Projections of Efficiency Factor 113
4.4.4 Trapped Electron Effects 114
4.5 Relativistic Calculations 117
4.5.1 Resonance Condition 117
4.5.2 Strong Relativistic Limit 120
4.5.3 Weak Relativistic Limit 123
4.6 Comments 125

5. CURRENT DRIVE BY ION CYCLOTRON WAVES-MINORITY SPECIES HEATING 129

5.1 Basic Mechanism of ICRF Current Generation by Minority Species Heating 130
5.1.1 Power Dissipation 131
5.1.2 Current Density 132
5.1.3 Efficiency Factor 139
5.1.4 Simple Reactor Application 142
5.2 Wave Propagation and Absorption 145
5.2.1 Dispersion Relation 145
5.2.2 Absorption 147
5.2.3 $k_{\parallel}$ Spectrum 150
5.2.4 Resonance Condition 152
5.3 Results from Quasi-Linear Fokker-Planck Theory 152
5.4 Comments 157

6. BRIEF DISCUSSION OF OTHER CURRENT DRIVE SCHEMES 161

6.1. ICRF Enhancement of Beam Driven Currents 161
6.2. Current Drive by Alpha Particles-RF Wave Interaction 163
6.2.1 Asymmetric Heating of α-Particles with ICRF 163
6.2.2 Asymmetric Heating of α-Particles (Fast) Waves 165
6.3. Current Drive by Synchrotron Radiation 168
6.4. Current Drive with Low Frequency Waves 171
6.4.1 Dispersion Relation 172
6.4.2 Quasi-Linear Wave Diffusion Coefficient 175
6.4.3 Current Drive Efficiency 177
6.4.4 Compressional Alfvén Wave (CAW) 180
6.4.5 Low-Phase Velocity Magnetosonic Wave 183
6.4.6 High-Phase-Velocity Magnetosonic Wave 184

REFERENCES 187

ABSTRACT

This report provides a brief survey of possible noninductive current drive mechanisms for tokamaks. It was originally prepared as part of the lecture notes for fusion courses taught at The University of Tennessee by the author. The primary application of driving currents noninductively is the possible continuous (steady-state) operation of a tokamak reactor through the indefinite sustainment of the poloidal magnetic field. Thus, the amount of power required to maintain the current is of crucial importance. In these notes the discussions are restricted to those schemes that are studied the most (experimentally and/or theoretically) and to those that are likely to be reactor contenders. Various current drive mechanisms may be grouped into four classes: (1) injection of energetic particle beams; (2) launching of rf waves; (3) hybrid schemes, which are combinations of various rf schemes (rf plus beams, rf and/or beam plus ohmic heating, etc.); and (4) other schemes, some of which are specific to reactor plasma conditions requiring the presence of alpha particle or intense synchrotron radiation. Particle injection schemes include current drive by neutral beams and relativistic electron beams. The rf schemes include current drive by the lower hybrid (LH) waves, the electron waves, the waves in the ion cyclotron range of frequencies, etc. Only a few of these approaches, however, have been tested experimentally, with the broadest data base available for LH waves. Included in this report are (1) efficiency criteria for current drive, (2) current drive by neutral beam injection, (3) LH current drive, (4) electron cyclotron current drive, (5) current drive by ion cyclotron waves — minority species heating, and (6) current drive by other schemes (such as hybrids and low frequency waves).

INTRODUCTION

Present tokamaks depend on inductive processes for the maintenance of the plasma current, which is necessary for plasma confinement. Because the flux-swing capability of ohmic heating (OH) coils is limited, tokamaks must operate in a pulsed mode. Therefore, tokamak reactors must go through a periodic startup, burn, and shutdown cycle, lasting on the order of minutes. This cycling of the burn introduces many engineering problems associated with the thermal cycling of the first wall, the pulsing of the poloidal magnetic circuit, etc.

The reactor potential of the tokamak could be considerably improved if a method of driving the current continuously rather than inductively could be developed and demonstrated. Continuous (steady-state) operation of tokamaks would provide a number of important engineering simplifications. Naturally, steady-state operation eliminates the need for thermal storage to prevent pulsing from the power output to the electrical grid. Continuous operation would also produce steady power output without cyclic thermal excursion of any portion of the reactor; thermal cycling of the first wall is a particularly serious problem that must be avoided if the structural integrity of the wall is to be maintained over long periods. Noninductive steady-state operation greatly reduces the engineering required for the OH coil and its related circuit (switching gear). However, ohmic drive may be required in a reactor during the startup phase, even if current drive is successful. Further, pulsed magnetic fields will be greatly reduced; this eases the design constraints on the use of superconductors, which are sensitive to time-dependent fields.

In 1970 Ohkawa proposed neutral injection as a possible method of driving a steady-state current in a reactor [1]. In 1978 Fisch suggested confining a tokamak plasma with rf-driven currents, in particular, current generation with lower hybrid (LH) waves [2]. Since then, there has been a rapid expansion in both theoretical and experimental research into rf-driven schemes. Some of these schemes are listed in Table 0.1. In Table 0.1 various current drive schemes are grouped into four classes: (1) injection of energetic particle beams; (2) launching of rf waves; (3) hybrid schemes, which are combinations of various rf schemes, rf plus beams, rf and/or beam plus ohmic heating, etc.; and (4) other schemes, some of which are specific to reactor plasmas. Particle injection schemes include current drive

Table 0.1. Noninductive current drive schemes

RF-driven schemes

Slow waves:[a] $(\omega/k_{\parallel}) \ll v_e$ [small $(\omega/k_{\parallel})$][a]

Compressional Alfvén wave (CAW)
Shear Alfvén wave (SAW)
Ion cyclotron range of frequencies (ICRF) — minority heating

Fast waves: $(\omega/k_{\parallel}) \gg v_e$ [large $(\omega/k_{\parallel})$][a]

Lower hybrid (LH)
Fast magnetosonic (FM) wave
Electron cyclotron resonance heating (ECRH)

Particle injection — driven schemes

Neutral injection of single- and multiple-charged ions
Relativistic electron beams (REB)

Hybrid schemes

ICRF and neutral injection
ICRH of the fusion product α
Cyclic operation (ohmic plus any other scheme)

Other schemes

Phased injection of pellets
Anisotropic reflection of synchrotron radiation
Selective loss of α's

[a] In this table classification of slow or fast waves is with respect to comparison of the wave phase velocity $\omega/k_{\parallel}$ to v_e.

by neutral beams [1,3–13] and relativistic electron beams [14–15]. The rf schemes may be broadly classified into two categories: slow (or low-speed) waves ($\omega/k_{\parallel} \ll v_e$), whose parallel phase velocities are much smaller than the electron thermal velocity, and fast (or high-speed) waves ($\omega/k_{\parallel} \gg v_e$), whose phase velocities exceed the electron thermal velocity. Examples in the latter category include current drive by the LH waves [2,9,16–40] and the electron cyclotron waves [9,18,41–53]; those in the former category include minority species heating at the ion cyclotron range of frequencies [9,54–56]. Among the other approaches, some them are specific to reactor plasma conditions, requiring the presence of alpha particles or intense synchrotron radiation [9,57–61]. In these notes we do not attempt to cover the complete list but restrict the discussions to those schemes that are studied most (experimentally and/or theoretically) and those that are likely to be reactor contenders. For further information and for details not covered here see refs. [1–88].

To drive a current, one species of charged particles needs to be given a net velocity relative to the other. In general, any wave (or beam) with net momentum can generate a current by transferring its momentum via the appropriate damping mechanisms to the charged particles in the plasma. To the extent that current drive, and not heating, is the main interest, it is desirable to minimize the power dissipation necessary to drive the current. For a given amount of energy, current drive is most efficient if the momentum is transferred to the electrons rather than the ions. Although the momentum dissipation rate is the same for ions and electrons, the ratio of current to momentum is greater for electrons as compared to ions by an ion-electron mass ratio, (m_i/m_e). The current can be either carried by the whole electron distribution, by a small number of superthermal electrons, or through the outflow of electrons from the magnetic axis (enhanced radial electron diffusion).

In general, to generate a current asymmetry must be introduced into the toroidal geomery so that one toroidal direction is favored over the other. This is an ingredient in almost all of the theories of current drive by beams or waves. As listed in Table 0.1, several distinct current drive mechanisms have been studied. Only a few of these approaches, however, have been tested experimentally with the broadest data base available for LH waves. As an illustration, Fig. 0.1 shows schematically the energy-momentum transfer picture in rf current drive. Basically, an external rf source couples a

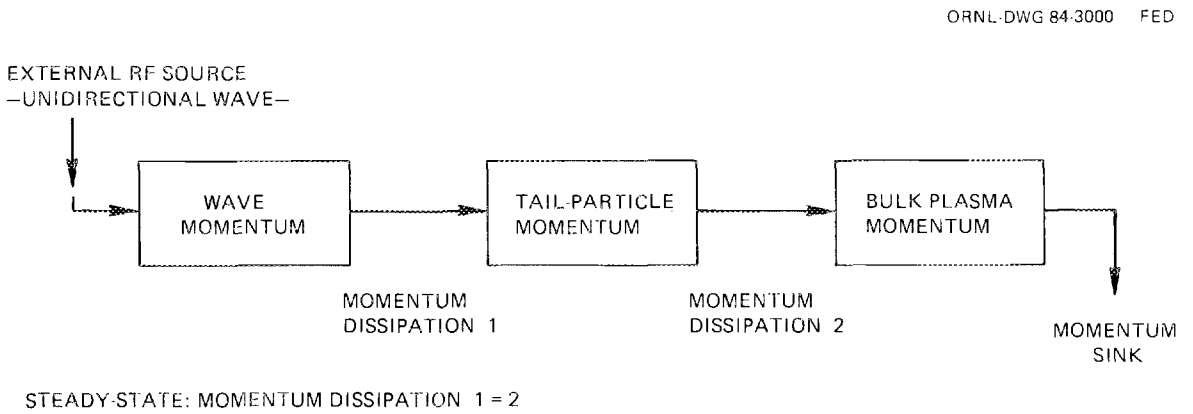

Fig. 0.1. Example of energy-momentum picture in rf current drive.

unidirectional wave to the plasma, which directs the power flow in one of the directions parallel to the magnetic axis. The waves traveling in the toroidal direction have net parallel momentum. The momentum from these waves can be dissipated by electron Landau or transit-time damping and/or by collisional damping, thereby transferring momentum to the electrons. This net toroidal momentum causes the electrons to drive toroidally, creating an electric current. The momentum is absorbed by electrons travelling with the wave parallel phase velocity ($v_{\parallel} = v_p = \omega/k_{\parallel}$). The current, in this example (Fig. 0.1), is mainly carried by these resonant ($\omega = k_{\parallel}v_{\parallel}$), high-velocity tail electrons because, being collisionless, they retain momentum longer than bulk electrons. (This is an example of a current being carried by superthermal electrons.) As these electrons move they lose momentum to the ions, so that a steady-state current is eventually achieved. As we will see, however, it is not necessary for waves to have net parallel momentum content to drive a current efficiently [41].

For current drive schemes to be practical for reactor applications, the current must be sustained at levels high enough for confinement while the power cost (and recirculating power fraction) is kept at a low level compared to the fusion power output. Before discussing the details of current drive schemes, we will derive a simple efficiency criterion for current drive (Sect. 1). This efficiency factor (namely, the power necessary to generate a given current) is a useful figure of merit in comparing various current generation techniques.

The organization of the remainder of this report is as follows: (1) current drive by neutral beam injection (Sect. 2); (2) LH current drive (Sect. 3); (3) electron cyclotron current drive (Sect. 4); (4) current drive by ion cyclotron waves-minority species heating (Sect. 5); and (5) current drive by other schemes (Sect. 6), which briefly covers various hybrid schemes and the use of low frequency waves. For each of the major driver options, we briefly review the basic mechanisms of current generation and discuss the tools used in the study. By and large, simple analytical derivations and estimates are used to point out the basic scaling relationships. If available, the discussion of experimental results is also included.

Because it is not the purpose of these notes to recommend one current drive scheme over another, and because these notes were prepared primarily for class lectures, no comparative assessment of driver options are included.

1. CURRENT DRIVE EFFICIENCY FACTOR

An ultimate measure of the efficiency of current drive by any scheme (rf, particle injection, etc.) is the ratio of excited current density to absorbed power density, J/P. In general, it is desirable to have as large a J/P as possible.

1.1. Simple Efficiency Calculation [8,10]

In its simplest form, we will calculate the ratio of current density generated to power density dissipated. As mentioned, to drive a current one species of charged particles density n (electrons or ions) needs to be given a net velocity relative to the other. Denoting this relative velocity as V_{rel}, the current density is given by

$$\mathbf{J} = ne\mathbf{V}_{rel} \qquad (A/m^2) \ . \tag{1-1}$$

The force on these particles due to Coulomb collisions is

$$\mathbf{F} = mn\nu\,\mathbf{V}_{rel} \ , \tag{1-2}$$

where m is the mass of the particle carrying the current and ν is the collision frequency. The power required to maintain the current is therefore

$$P = \mathbf{F} \cdot \mathbf{V}_{rel} = mn\nu V_{rel}^2 \qquad (W/m^3) \ . \tag{1-3}$$

We introduce the following normalizations to the current and power (i.e., we normalize both to their thermal values):

$$\hat{J} = J/nev_e \ , \tag{1-4a}$$

$$\hat{P} = P/m_e n v_e^2 \nu_o \ , \tag{1-4b}$$

where $J = |J|$ $v_e = (kT_e/m_e)^{1/2}$ is the electron thermal velocity and

$$\begin{aligned} \nu_o &= \omega_{pe}^4 \ \ell n \Lambda / 2\pi n v_e^3 \\ &= ne^4 \ \ell n \ \Lambda / 2\pi \epsilon_o^2 m_e^2 v_e^3 \ . \end{aligned} \tag{1- }$$

With these normalizations we can now write the efficiency factor as

$$\begin{aligned} \frac{J}{P} &= \frac{2\pi\epsilon_o^2 m_e v_e^2}{ne^3 \ \ell n \ \Lambda} \frac{\hat{J}}{\hat{P}} \simeq 9.6 \times 10^{17} \left(\frac{20}{\ell n \ \Lambda}\right)\left(\frac{T_e}{n}\right)\left(\frac{\hat{J}}{\hat{P}}\right) \\ &\simeq 10^{18} \left(\frac{T_e}{n}\right)\frac{\hat{J}}{\hat{P}} \ , \end{aligned} \tag{1-6}$$

where $\hat{J}$ and $\hat{P}$ are normalized dimensionless quantities [Eqs. (1-4a) and (1-4b)], $\ell n \ \Lambda \simeq 20$ is used, and the units are mks with temperature T_e in keloelectron volts. The normalized ratio $\hat{J}/\hat{P}$ hides most of the physics of current drive (rf, beams, etc.) and is a function of the characteristic velocity of the driver normalized to the electron thermal velocity. We can see this characteristic by considering Eqs. (1-4a) and (1-4b) and form the normalized ratio

$$\frac{\hat{J}}{\hat{P}} = \frac{m_e \nu_o}{m\nu} \frac{v_e}{V_{rel}} \tag{1-7}$$

(Note that if the current is carried by the electrons $m = m_e$.)

The normalized efficiency factor given by Eq. (1-7) can be written entirely as a function of $U_o = V_{rel}/v_e$ (ν/ν_o is also a function of $U_o = V_{rel}/v_e$): $\hat{J}/\hat{P} \sim f(U_o)$.

Without getting into any specifics of a given driver option, we can obtain the general characteristics of $\hat{J}/\hat{P}$, which is sketched in Fig. 1.1. The main point to note here is that the efficiency of current drive is high at both low values of $V_{rel}/v_e \equiv U_o$, where it

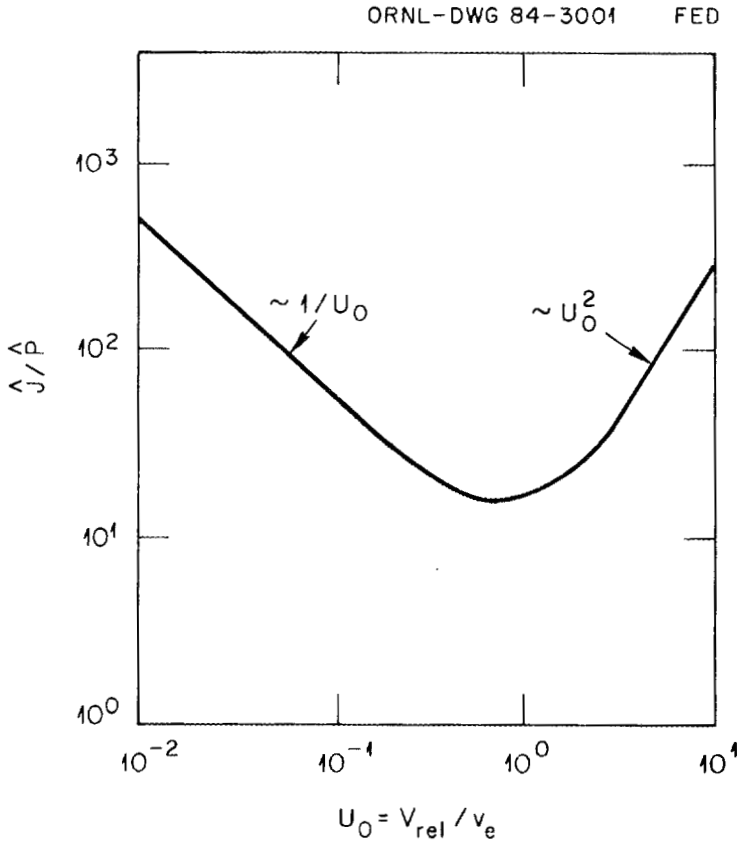

Fig. 1.1. Normalized efficiency factor $\hat{J}/\hat{P}$ vs $V_{rel}/v_e \equiv U_o$ (V_{rel} is the velocity of electrons that carry the current and v_e is the electron thermal velocity) (ref. [8]).

scales as $v_e/V_{rel} = 1/U_o$, and at high values of V_{rel}/v_e, where it scales as $(V_{rel}/v_e)^2 = U_o^2$. This is because in the limit of low $U_o = V_{rel}/v_e$ the current is carried mainly by the whole electron distribution and ν_o/ν is independent of V_{rel}/v_e, where V_{rel} is the velocity of the electrons that carry the current. In the limit of high U_o, ν_o/ν scales as U_o^3, where the current is carried by superthermal electrons. Thus, it is best to drive currents either in the high-velocity electron tail using, for example, fast waves ($\omega/k_{\parallel} >> v_e$) or in the low-velocity electrons using very slow waves ($\omega/k_{\parallel} << v_e$).

This simple expression for the efficiency factor, as pointed out earlier, hides most of the physics and, generally, cannot be used directly to find a current generated from the injected power. It should be noted, moreover, that both J and P are very sensitive functions of V_{rel}/v_e [Eqs. (1-1) and (1-3)] that vanish when the figure of merit becomes infinite.

One of the most-used methods in deriving the efficiency factor is the Fokker-Planck equation, which we will discuss briefly in the next section.

In terms of total current I_{tot} ($= J\pi a^2$, where a is the plasma radius) and required power P_{tot} ($= P2\pi^2 a^2 R_o$, where R_o is the major radius), Eq. (1-6) can be rewritten as

$$\frac{I_{tot}}{P_{tot}} \simeq 3 \times 10^{18} \frac{T_e}{nR_o \ln \Lambda} \frac{\hat{J}}{\hat{P}} \simeq 1.5 \times 10^{17} \left(\frac{20}{\ln \Lambda}\right) \frac{T_e}{nR_o} \frac{\hat{J}}{\hat{P}}$$

$$\simeq \frac{0.015}{R_o} \left(\frac{20}{\ln \Lambda}\right)\left(\frac{T_e}{10}\right)\left(\frac{10^{20}}{n}\right) \frac{\hat{J}}{\hat{P}} \quad (A/W) \qquad (1\text{-}8)$$

(mks, keV units).

1.2. Derivation of Efficiency Factor Using the Fokker-Planck Equation [2,4,8-9,16-18,45-46,67-70]

The general form of the electron Fokker-Planck equation is given by

$$\frac{\partial f_e}{\partial t} = C_{ei}(f_e, f_i) + C_{ee}(f_e, f_e) + L(f_e) \ , \qquad (1\text{-}9)$$

where C denotes the Fokker-Planck collision operator and L denotes the current drive operator. The subscripts in C refer to electron-ion [first term on the right side of Eq. (1-9)] and electron-electron [the second term on the right side of Eq. (1-9)] collisions.

The current drive operator L for rf schemes is different from that for injected beams. For the rf schemes, the operator L is derived using quasi-linear theory, whereas for the injection drive schemes, L is the beam-background plasma collision operator.

In this section, we do not derive these operators; we present instead a few examples for rf current drive schemes. Basically, $L(f_e)$ represents the velocity space diffusion caused by the wave. In general [75],

$$L(f_e) = -\frac{\partial}{\partial \mathbf{v}} \cdot \Gamma_e = \frac{\partial}{\partial \mathbf{v}} \cdot \overleftrightarrow{\mathbf{D}} \cdot \frac{\partial}{\partial \mathbf{v}} f_e \ , \tag{1-10}$$

where $\Gamma_e = -\overleftrightarrow{\mathbf{D}} \cdot \partial/\partial \mathbf{v}\ f_e$ is the flux of electrons (in velocity space) induced by rf and $\overleftrightarrow{\mathbf{D}}$ is the quasi-linear diffusion tensor resulting from wave-particle interaction (such as Landau damping).

The diffusion term for the electron Landau damping case is given by

$$L(f_e) = \frac{\partial}{\partial v_{\parallel}} \left[D\delta\left(\frac{\omega}{k_{\parallel}} - v_{\parallel}\right) \frac{\partial f_e}{\partial v_{\parallel}} \right] , \tag{1-11}$$

where $v_{\parallel}$ is the velocity parallel to the magnetic field, the δ function expresses the resonance condition, and D is a constant and proportional to the wave amplitude square, $D \sim E_{\parallel}^2$. Note that the quasi-linear diffusion tensor in Eq. (1-10) has been reduced to only the $\mathbf{v}_{\parallel}\mathbf{v}_{\parallel}$ term, because the current drive mechanism (in this example) utilizes only the resonance at $\omega/k_{\parallel}$, the parallel phase velocity.

For cyclotron heating (ion cyclotron or electron cyclotron),

$$\begin{aligned} L(f_e) &= \frac{1}{v_{\perp}} \frac{\partial}{\partial v_{\perp}} \left[D v_{\perp} \delta\left(\frac{\omega - \Omega}{k_{\parallel}} - v_{\parallel}\right) \frac{\partial f_e}{\partial v_{\perp}} \right] \\ &\sim \frac{\partial}{\partial v_{\perp}^2} \left[D v_{\perp}^2 \delta\left(\frac{\omega - \Omega}{k_{\parallel}} - v_{\parallel}\right) \frac{\partial f_e}{\partial v_{\perp}^2} \right] , \end{aligned} \tag{1-12}$$

where Ω (Ω_e or Ω_i) is the cyclotron frequency ($\Omega = eB/m$), $v_\perp$ is the perpendicular velocity, and, again, D is a constant and proportional to the wave amplitude square, $D \sim |E^+|^2$ or $D \sim |E^-|^2$ with E^+ the left-hand component of the wave field (i.e., the component of the **E** field that rotates in the same sense as ions) and E^- the right-hand component of the wave field (i.e., the component of the **E** field that rotates in the same sense as electrons). Equation (1-12) is for fundamental cyclotron heating.

The current density is given by

$$J = \int e v_\parallel f_e \, d^3v \tag{1-13}$$

and the power dissipated is

$$P = \int \frac{1}{2} m_e v^2 L(f_e) \, d^3v \ , \tag{1-14}$$

where $d^3v \rightarrow v_\perp \, dv_\perp \, dv_\parallel$ and $v^2 = v_\perp^2 + v_\parallel^2$.

Equation (1-9) is a two-dimensional (2-D) nonlinear integro-differential equation in velocity variables $v_\parallel$ and $v_\perp$. In general, this equation has to be solved numerically, except in limiting cases where it can be reduced to a set of one-dimensional (1-D) equations in v. The resulting equations can then be solved analytically (approximately) or numerically (full 1-D), which are considerably simpler than full 2-D equations. Numerical solutions (1-D or 2-D) will not be discussed here; however, we may refer to those results whenever needed (see references).

A compendium of $\hat{J}/\hat{P}$ values (the efficiency factor) calculated for several of the current drive schemes listed in Table 0.1 is displayed in Fig. 1.2 as a function of U_o. Here, U_o is a function of phase velocity for waves, that is,

$$U_o = \frac{\omega/k_\parallel}{v_e} = v_\parallel/v_e \ ,$$

and, for particle injection schemes at velocity V_b, it takes the form

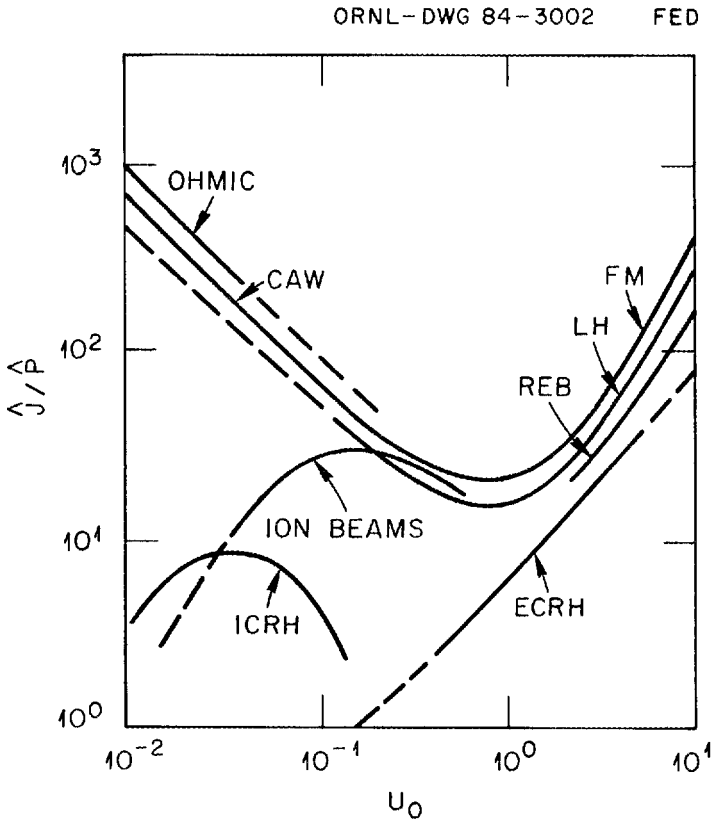

Fig. 1.2. Normalized efficiency factor vs U_o, where $U_o = \omega/k_{\parallel}v_e$ [or $U_o = (\omega - \ell\Omega)/k_{\parallel}v_e$, with Ω the cyclotron frequency] for waves and $U_o = V_b/v_e$ for particle injection at velocity V_b. The abbreviations are as follows (refs. [8,10]):

OHMIC: Self-explanatory
CAW: Compressional Alfvén wave
LH: Lower hybrid
FM: Fast magnetosomic wave
REB: Relativistic electron beams
ECRH: Electron cyclotron resonance heating
ICRH: Ion cyclotron minority heating
Ion beams: Neutral injection.

$$U_o = V_b/v_e \ .$$

Note that for some of the wave schemes U_o is the Doppler-shifted phase velocity, that is,

$$U_o = \frac{\omega - \ell\Omega}{k_{\parallel} v_e} = v_{\parallel}/v_e \quad , \quad \ell = 0,\ 1,\ 2 \ ,$$

where Ω is the cyclotron frequency and ℓ is the harmonic number.

We see from Fig. 1.2 that in the limit of low velocities ($U_o \ll 1$) rf schemes (i.e., compressional and shear Alfvén waves) have a comparable efficiency to ohmic current drive except ion cyclotron minority heating. In the limit of high velocities ($U_o \gg 1$) efficiencies for rf schemes differ by only a factor of 2. Neutral injection and ion cyclotron waves have a somewhat lower efficiency than the other schemes. The reduction in efficiency of the neutral injection scheme at low injection velocities ($U_o \ll 1$) is due to the slowing down of the injected fast ions on the background thermal ions, where the efficiency curve drops off as U_o^2.

The results displayed in Fig. 1.2 do not include relativistic effects, which become important at high velocities. At ultra-relativistic energies where $v_e \sim c$, $\hat{J}/\hat{P}$ no longer scales as U_o^2; instead, it becomes nearly independent of U_o [43].

Another effect not accounted for in Fig. 1.2 is the trapping of electrons in the toroidal field gradient. The results shown in Fig. 1.2 are for a very large aspect ratio ($\epsilon = 0$, where $\epsilon = r/R_o$ is the inverse aspect ratio). For finite aspect ratio, the electrons trapped in the toroidal magnetic field [fraction of trapped particles $\sim (2\epsilon)^{1/2}$] can significantly reduce the current drive efficiency by (a) reducing the number of current-carrying electrons and (b) increasing the frictional drag on the passing electrons (toroidally circulating, current-carrying electrons) through collisions with the trapped electrons. This reduction of current could be particularly significant at low phase velocity (i.e., small U_o) due to the fact that only small increases in perpendicular velocity are required to move electrons from the untrapped (passing) to the trapped region of velocity space. At high phase velocity (large U_o), the wave interacts

mainly with passing particles and so the reduction in current could be modest.

1.3 Reactor Applications

The primary application of driving currents noninductively is the possible continuous operation of a tokamak reactor through the indefinite sustaining of the poloidal magnetic field. In this context, the amount of power required to maintain the current is of crucial importance. Minimizing this power dissipation (minimizing the recirculating power fraction) relies on the excitation of the most favorable waves or particle injection schemes, some of which were discussed in the previous section and are listed in Table 0.1 (see also Fig. 1.2).

Supplying the current necessary to achieve steady-state operation implies that the poloidal magnetic field B_p is completely sustained by the noninductively driven current J. By Ampére's law, the current density J determines the magnetic field B_p, that is,

$$B_p \simeq \mu_o J a/2 \ , \tag{1-15}$$

where a is the plasma radius. The necessary poloidal magnetic field is related to plasma density and temperature through a parameter β_p (poloidal beta) defined by

$$\beta_p = \frac{nk(T_e + T_i)}{B_p^2/2\mu_o} \simeq \frac{4\mu_o nkT}{B_p^2} \ , \tag{1-16}$$

where we assumed, for convenience only, $T_e \simeq T_i = T$. For plasma equilibrium and stability, $\beta_p < A$, where $A = R_o/a$ is the aspect ratio with R_o being the major radius of the torus. Combining Eqs. (1-15) and (1-16), we can write

$$J = \frac{4}{a}\left(\frac{nkT}{\mu_o \beta_p}\right)^{1/2} \ . \tag{1-17}$$

If the operation is achievable at $\beta_p = A$, we have

$$J = 4\left(\frac{nkT}{\mu_o a R_o}\right)^{1/2} \simeq 4.5 \times 10^{-5}\left(\frac{nT}{aR_o}\right)^{1/2} \quad (A/m^2) \tag{1-18}$$

(mks units, T in keV). The normalized J ($\hat{J}$), which we make more frequent use of than the dimensional J, can now be written as

$$\hat{J} = J/nev_e = \frac{4}{a(\beta_p)^{1/2}}\left(\frac{m_e}{ne^2\mu_o}\right)^{1/2} = \frac{4}{a(\beta_p)^{1/2}}\left(\frac{m_e\epsilon_o}{ne^2}\right)^{1/2}\left(\frac{1}{\epsilon_o\mu_o}\right)^{1/2}$$

$$= 4\,\frac{c}{a\omega_{pe}(\beta_p)^{1/2}}\,, \tag{1-19}$$

where c is the speed of light ($c^2 = 1/\epsilon_o\mu_o$) and ω_{pe} is the electron plasma frequency. For $\beta_p = A = R_o/a$, we have

$$\hat{J} = 4\,\frac{c}{\omega_{pe}(aR_o)^{1/2}} \simeq 2.1 \times 10^7\ (naR_o)^{-1/2}\ . \tag{1-20}$$

It is sometimes convenient to express density in units of 10^{20} m^{-3} and temperature in units of 10 keV. Normalizing density and temperature to 10^{20} m^{-3} and 10 keV, respectively, that is,

$$n_{20} = n/10^{20}\ , \quad T_{10} = T/10\ ,$$

we can rewrite Eqs. (1-18) and (1-20) as

$$J \simeq 1.427 \times 10^6 \left[\left(\frac{n}{10^{20}}\right)\left(\frac{T}{10}\right)\frac{1}{aR_o}\right]^{1/2} \qquad A/m^2$$

$$\simeq 1.427 \left(\frac{n_{20}T_{10}}{aR_o}\right)^{1/2} \qquad MA/m^2 \ , \tag{1-21a}$$

$$\hat{J} \simeq 2.1 \times 10^{-3} \left[\left(\frac{10^{20}}{n}\right)\frac{1}{aR_o}\right]^{1/2}$$

$$= 2.1 \times 10^{-3} \left(n_{20}aR_o\right)^{-1/2} \ . \tag{1-21b}$$

Note that Eq. (1-21) is for $\beta_p = A$. For general cases, Eqs. (1-17) and (1-19), similar normalizations can easily be introduced.

A parameter of crucial importance is the recirculating power in a reactor, defined as

$$\epsilon \equiv \frac{1}{Q} = \frac{P_{CD}}{P_{fus}} \ , \tag{1-22}$$

where P_{CD} is the power density required for current drive and P_{fus} is the fusion power density. For a D-T plasma

$$P_{fus} = \frac{n^2 \langle\sigma v\rangle_{DT}}{4} E_{fus} \qquad (W/m^3) \ , \tag{1-23}$$

where $E_{fus} = 17.6$ MeV and $\langle\sigma v\rangle_{DT}$ is fusion reaction rate parameter [$\langle\sigma v\rangle_{DT} \simeq 10^{-22}$ m^3s^{-1} at $T = 10$ keV]. In terms of normalized quantities

$$\epsilon \simeq 18 \frac{\hat{P}/\hat{J}}{(a^2\beta_p)^{1/2}\ (n_{20}T_{10})^{1/2}} \left[\frac{10^{-22}}{\langle\sigma v\rangle_{DT}}\right] \ , \tag{1-24}$$

where $\hat{P}/\hat{J}$ is as given by Eq. (1-6).

For $\beta_p = A$

$$\epsilon \simeq 18 \frac{\hat{P}/\hat{J}}{(aR_o n_{20} T_{10})^{1/2}} \left[\frac{10^{-22}}{\langle\sigma v\rangle_{DT}}\right] . \tag{1-25}$$

In the range of interest to fusion power

$$\langle\sigma v\rangle_{DT} \sim T^2 \qquad 8 < T < 25 \text{ keV} .$$

Toroidal plasma beta β_t is an important reactor design parameter, since the fusion power scales as β_t^2 ($P_{fus} \sim \beta_t^2 B_o^4 \langle\sigma v\rangle_{DT}/T^2$, where B_o is the toroidal magnetic field strength). In terms of toroidal beta.

$$\beta_t = \frac{nk(T_e + T_i)}{B_o^2/2\mu_o} \simeq 0.8 \frac{n_{20} T_{10}}{B_o^2} , \tag{1-26}$$

we can also express the recirculating power fraction as

$$\epsilon \simeq 16.1 \frac{\hat{P}/\hat{J}}{(a^2 \beta_p \beta_t B_o^2)^{1/2}} \left[\frac{10^{-22}}{\langle\sigma v\rangle_{DT}}\right]$$

$$= 16.1 \frac{\hat{P}/\hat{J}}{[\beta_t B_o R_o q_s(a)]} \left[\frac{10^{-22}}{\langle\sigma v\rangle_{DT}}\right] , \tag{1-27}$$

where q_s is the safety factor,

$$q_s(a) = \frac{a}{R_o} \frac{B_o}{B_p} .$$

We should note here that the recirculating power fraction defined by Eq. (1-22) does not include any power conversion efficiencies [i.e., conversion efficiency from thermal to electric power ($\eta_{th} \sim 35\%$), from

electric to beam or rf power ($\eta_{cd} \sim 30$–60%), etc.]. Thus, the actual recirculating power fraction for the overall reactor system is larger (by a factor of 5 to 10, depending on the efficiencies) than that calculated here.

2. CURRENT DRIVE BY NEUTRAL BEAM INJECTION [1,3-13]

The possibility of maintaining a steady-state current in a plasma by the injection of fast ions was first proposed by Ohkawa [1], and experiments on the Culham Levitron [3] and on DITE [7] have confirmed the existence of this current. The simple physical picture of current drive by beams is as follows. The hot ions injected as neutrals are first ionized by the background plasma. They then circulate around the torus, while they slow down on the background plasma, and form a series of stacked, fast ion current loops, thus forming a substantial current. These fast ions, however, push on the background electrons (i.e., this directed flow of the fast ions tends to drag the electrons with it), causing electrons to form a current that is in the opposite direction to the fast ion current. The tendency of fast ions dragging the background electrons is opposed by the electron collisions with the background ions. In some circumstances, this collisionally driven electron current (called the "electron return current" or "back electron current") can completely cancel the fast ion current. This is true, for example, in the classical description of tokamak, where the orbits of trapped electrons are not considered, the return electron current exactly cancels the ion current if the fast ion charge number is equal to the effective plasma charge number (i.e., $Z_f = Z_{eff}$).

If the background plasma contains impurities, such that $Z_{eff} > Z_f$, the frictional force opposing the electron streaming will be increased, with the result that the beam current is not completely compensated for by the electron current. In a toroidal geometry, the trapped elecrons will, similarly, add to the frictional force on the streaming electrons, again leading to a lack of complete compensation of the beam current. When the trapped electron effects are included, even if $Z_f = Z_{eff}$, there can be a significant current.

In general, the injected ions increase the toroidal momentum of the background plasma. This can result in large toroidal plasma flows, especially if there is only one beam whose direction of injection is parallel to the magnetic axis. To keep the total plasma momentum unchanged, beams with opposing directions (one beam parallel and one antiparallel to the magnetic axis) can be injected. This is the scheme proposed by Ohkawa. In this scheme, to avoid increasing the toroidal momentum of the plasma, counter streaming ion beams are injected; a low-energy, high-current beam is injected in the opposite direction to the high-energy beam.

2.1. Simple Calculation of Beam-Driven Current [1,10]

2.1.1 Fast Ion Current

When fast ions are injected into a toroidally confined plasma, the current I_{beam} injected parallel to the magnetic field is multiplied many times by the overlapping of successive ion transits around the torus. The circulating fast ion current I_f satisfies the equation

$$dI_f/dt = I_{beam}/\tau_{circ} - I_f/\tau_f \ , \tag{2-1}$$

where τ_{circ} is the circulation time and τ_f is given by $\tau_f^{-1} = \tau_{fs}^{-1} + \tau_{cx}^{-1}$ in which τ_{fs} is the fast ion slowing-down time on background electrons by Coulomb collisions and τ_{cx} is the charge-exchange time.

In steady state the fast ion current is [from Eq. (2-1)] just the product of the injected beam current and the number of transits a fast ion makes before thermalization:

$$\begin{aligned} I_f &= I_{beam}\left(\frac{\tau_f}{\tau_{circ}}\right) \\ &= I_{beam}\,(V_f\tau_f)/2\pi R_o \ . \end{aligned} \tag{2-2}$$

Here V_f is the fast ion velocity ($\tau_{circ} = 2\pi R_o/v_f$). In most applications $\tau_{cx} >> \tau_{fs}$, in which we can neglect the charge exchange; thus, $\tau_f \simeq \tau_{fs}$.

The product $V_f\tau_{fs}$ has to be calculated using a Fokker-Planck equation for the fast ions if an accurate value is required (see refs. [4,76-79]).

The slowing-down time, which depends on both the fast ion velocity V_f and the electron thermal velocity v_e, is given by

$$\tau_{fs} = \frac{V_f v_e^2}{(1 + m_f/m_e)\, n_e \Gamma_{fe} \psi(V_f/v_e)} \ , \tag{2-3}$$

where

$$\Gamma_{fe} = Z_f^2 e^4 \ \ell n \ \Lambda / 4\pi\epsilon_o^2 m_f^2 \ , \tag{2-4}$$

$$\psi(x) = \frac{\Phi(x) - x\Phi'(x)}{2x^2} \ , \tag{2-5a}$$

with

$$\Phi(x) = \frac{2}{\sqrt{\pi}} \int_o^x e^{-y^2} dy \equiv \mathrm{erf}(x) \ , \tag{2-5b}$$

the error function. If the energy of beam ions is chosen such that

$$E_{beam} > E_{crit} \ ,$$

the beam slows down mainly on electrons and loses its directed momentum (and energy) chiefly to electrons. The critical energy E_{crit} is given by

$$E_{crit} = 14.8 T_e \left[A_f^{3/2} \sum_i \frac{n_i Z_i^2}{n_e} \frac{1}{A_i} \right]^{2/3} \ , \tag{2-6}$$

where A_f and A_i are the atomic weights of the fast beam ion and background plasma ion(s), respectively. This is the energy at which the ion beams heat the plasma electrons and ions at equal rates. When $E_{beam} < E_{crit}$, slowing down is mainly on background ions. In the two extreme limits of $E_{beam} \gg E_{crit}$ and $E_{beam} \ll E_{crit}$, the fast ion current I_f scales as

$$I_f \sim A_f V_f^4 / n_e Z_f^2$$

and

$$I_f \sim A_f V_f T_e^{3/2}/n_e Z_f^2 \sim A_f V_f v_e^3/n_e Z_f^2 \ ,$$

respectively.

Accurate determination of the fast ion current requires the use of the Fokker–Planck equation from which the fast ion distribution function f_{beam} is obtained, and the circulating fast ion current density is calculated from

$$J_f = n_f \langle V_{\parallel f} \rangle eZ_f$$

$$= eZ_f \int v_{\parallel} f_{beam} \, d^3v \ . \qquad (2\text{–}7)$$

Kinetic treatments of both the current carried by the fast ions and the reverse current carried by the electrons are given in refs. [4–6,79].

2.1.2 Electron Return Current

The momentum gained by the electrons as the fast ions slow down is lost by Coulomb collisions with the plasma ions. These in turn slow down by collisions or escape from the confinement system. Thus, both the plasma electrons and ions gain a net drift in the direction of fast ions, and, for simplicity, we assume that they can be represented as Maxwellian distributions shifted by mean velocity $\bar{v}_e$ and $\bar{v}_i$, respectively. The total circulating current in the plasma can be obtained from the force balance equation for the electrons,

$$n_e m_e \frac{dv_e}{dt} = n_f m_f \frac{(V_f - \bar{v}_e)}{\tau_{fs}} - n_i m_i \frac{(\bar{v}_e - \bar{v}_i)}{\tau_i} = 0 \ , \qquad (2\text{–}8)$$

where the notations are obvious: the subscripts f, e, and i represent fast ions, electrons, and plasma ions, respectively; n is the density; m is the mass; and V is the velocity (average). In Eq. (2–8) the first term on the right side is associated with the momentum gained by the electrons (mean velocity $\bar{v}_e$) from the fast ions and the second term

represents the momentum lost by the electrons to the background ions. The time for momentum transfer between plasma ions and electrons is τ_i.

After a few collision times, a net total current density is now given by

$$J = e\left(Z_f n_f V_f + n_i Z_i \bar{v}_i - n_e \bar{v}_e\right) . \tag{2-9}$$

For most tokamak conditions $\bar{v}_e \gg \bar{v}_i$. Noting that $n_f/n_e \ll 1$ and using Eq. (2-8) to eliminate $\bar{v}_e$, Eq. (2-9) can be put in the form

$$J = e n_f Z_f V_f \left(1 - \frac{n_e m_f \tau_i}{n_i m_i Z_f \tau_{fs}}\right) . \tag{2-10}$$

For the ordering $v_i \ll V_f \ll v_e$, the slowing-down times are approximately

$$\tau_i/\tau_{fs} \simeq (m_i/m_f)(Z_f^2/Z_i^2) ,$$

and Eq. (2-10) simplifies to

$$J = e n_f Z_f V_f (1 - Z_f/Z_{eff}) , \tag{2-11}$$

where $Z_{eff} = n_i Z_i^2/n_e$. In terms of fast ion current

$$J = J_f (1 - Z_f/Z_{eff}) \tag{2-12a}$$

or

$$I = I_f \left(1 - \frac{Z_f}{Z_{eff}}\right) . \tag{2-12b}$$

This is the usual expression for current drive by fast ions with I_f given by Eq. (2-2). Thus, we see that if the fast ion charge Z_f is equal to the plasma charge number Z_{eff} there is no current. (Note that for a single ion species $Z_{eff} = Z_i$.)

Equation (2-12) is valid only in the limit $v_e \gg V_f$. If $v_e \sim V_f$, the electron Fokker-Planck equation has to be solved (in this case the assumption of the shifted Maxwellian distribution function does not hold).

2.1.3 Trapped Electron Correction [5,6]

Electron trapping in the toroidal field gradient can significantly reduce the back electron current (a) through reducing the number of current-carrying electrons and (b) by increasing the frictional drag on the current-carrying electrons. A Fokker-Planck treatment of the effect on the current of this electron trapping has been developed [5,6] and the expression for the net current is given by

$$J = J_f\left\{1 - \frac{Z_f}{Z_{eff}}\left[1 - G(Z_{eff},\epsilon)\right]\right\} \tag{2-13a}$$

or

$$I = I_f\left\{1 - \frac{Z_f}{Z_{eff}}\left[1 - G(Z_{eff},\epsilon)\right]\right\} , \tag{2-13b}$$

where the trapped electron correction $G(Z_{eff},\epsilon)$ depends on the inverse aspect ratio $\epsilon = r/R_o$ and on Z_{eff}. For a large aspect ratio tokamak, with calculations correct to order $\epsilon^{1/2}$, $G(Z_{eff},\epsilon)$ is given by

$$G(Z_{eff},\epsilon) \simeq 1.46\ \epsilon^{1/2} A(Z_{eff}) , \tag{2-14a}$$

where $A(Z_{eff})$ is a numerical coefficient, tabulated in Table 2.1 for several values of Z_{eff}. With the aid of Table 2.1, we can approximate G as

$$G(Z_{eff},\epsilon) \simeq 1.46\ \epsilon^{1/2}\left(1 + \frac{0.68}{Z_{eff}}\right) \tag{2-14b}$$

(approximation is in error by $< 2\%$ for $1 < Z_{eff} < 6$). Combining Eqs. (2-13) and (2-14), we have

$$I = I_f \left[1 - \frac{Z_f}{Z_{eff}} + 1.46\, \epsilon^{1/2} \frac{Z_f}{Z_{eff}} \left(1 + \frac{0.68}{Z_{eff}} \right) \right] . \qquad (2\text{-}15)$$

beam current — electron return current — trapped electron

The extra term in Eq. (2-13) [or Eq. (2-15)] from the trapped electrons can give rise to quite a significant current, even when $Z_f = Z_{eff}$.

Table 2.1 Variation of coefficient $A(Z_{eff})$ with Z_{eff} [6]

Z_{eff}	1	2	3	4	5	6
$A(Z_{eff})$	1.68	1.36	1.24	1.18	1.15	1.12

In general, calculations to order $\epsilon^{1/2}$ can over-estimate the trapped electron contribution to net current in a finite aspect ratio tokamak. The finite aspect ratio calculation of $G(Z_{eff},\epsilon)$ can be approximated by [5,13]

$$G(Z_{eff},\epsilon) \simeq 1.46\epsilon^{1/2}A(Z_{eff}) - \epsilon B(Z_{eff})$$

$$\simeq 1.46\ \epsilon^{1/2}\left(1 + \frac{0.68}{Z_{eff}}\right) - \epsilon\left(0.2 + \frac{1.55}{Z_{eff}}\right). \qquad (2\text{-}16)$$

G is sometimes referred to as the neoclassical electron term or electron trapping correction.

To see the effect of ϵ, Z_f, and Z_{eff} on the current, we define a current factor [13]

$$F(Z_f,\ Z_{eff},\ \epsilon) = \frac{I}{Z_f I_f} = \frac{1}{Z_f} - \frac{1}{Z_{eff}}\left[1 - G(Z_{eff},\epsilon)\right], \qquad (2\text{-}17)$$

which is shown in Fig. 2.1. When $Z_f = 1$, the current is carried mainly by the fast ions, and the electron current reduces the beam-driven current. This reduction can be minimized by using $Z_{eff} > 1$ and by taking advantage of the neoclassical electron term (trapped electron term) away from the magnetic axis. (Note that this term is proportional to $\epsilon^{1/2}$ or ϵ, $\epsilon = r/R_o$, and it can have a significant contribution for $r \neq 0$.)

When $Z_f \gg Z_{eff}$, the current is mainly carried by the electrons and is directed opposite the fast ion current. (If the original direction of the current is to be maintained, counterinjection of the beam is required.) In this case, the trapped electron correction reduces the total driven current, and the value of $|F|$ is maximized near the magnetic axis where $G(Z_{eff},\epsilon)$ is small.

The dependence of $F(Z_f,\ Z_{eff},\ \epsilon)$ on Z_f is simply additive; therefore, in Fig. 2.1, F is shown for different Z_{eff} and Z_f by using a set of shifted vertical axes. Note from Fig. 2.1 and Eq. (2-17) that when $Z_f/Z_{eff} \simeq 1\text{-}2$, the magnitude of F (and, thus, the driven current I) is low due to cancellation of terms.

We should note here that, at present, there is uncertainty over the existence of the trapped particle effects (neoclassical correction) since there is as yet no experimental verification of these in tokamaks. At the moment it would be unwise to rely on this effect in any reactor design. In its absence, the classical results, that is, $G = 0$ (see the $\epsilon = 0$ axis of Fig. 2.1), should be used in any reactor

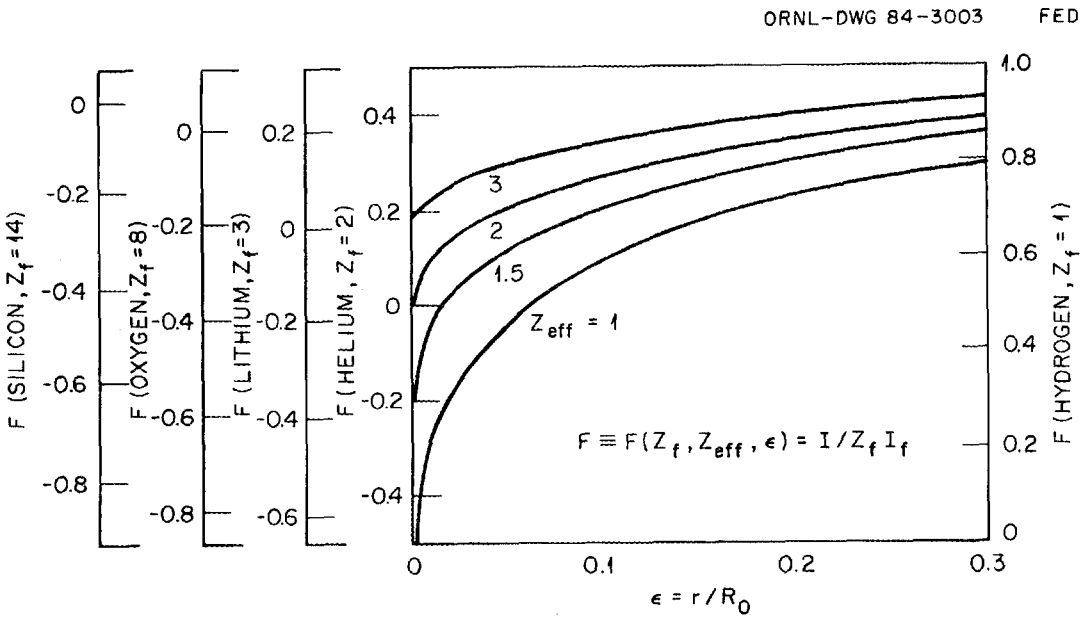

Fig.2.1. Current factor $F(Z_f, Z_{eff}, \epsilon)$ for selected values of fast ion charge Z_f and effective plasma charge Z_{eff}. The vertical axes are labeled with the fast ion (beam) species (ref. [13]).

projections. The removal of the trapped electron correction lowers $|F|$ for deuterium ($Z_f = 1$) and raises $|F|$ for impurity ($Z_f \gg 1$) beams.

2.1.4 Current Drive Efficiency

The efficiency factor J/P can be determined by using Eq. (2-13) and dividing by the power. Using the similar normalization factors introduced in Sect. 1.1, Fig. 2.2 displays the normalized efficiency factor as a function of dimensionless injection energy E_o/T_e (where E_o = injection energy) for three different injected ion beams [deuterium (D), helium (He), and oxygen (O)] into a D-T plasma. It can be seen from Fig. 2.2 that there is an optimum injection energy around $E_o/A_f T_e \sim 30$-50. For example, with $T_e \sim 15$ keV the optimum injection energy for deuterium ion beams is around 1.5 MeV, which requires the use of negative ion beam technology (!). The overall efficiency factor (ratio of the beam-driven current to required beam power) at this optimum energy is (see Fig. 2.2)

$$\frac{I}{P_{beam}} \simeq 0.9 \frac{T_e}{\ell n\, \Lambda} \left(\frac{10^{20}}{n_e}\right) \frac{1}{R_o Z_f} \left(1 - \frac{Z_f}{Z_{eff}}\right) \quad (A/W) \ . \tag{2-18}$$

For a plasma with $n_e \simeq 10^{20}$ m^{-3}, $T_e \simeq 15$ keV, $R_o \simeq 6$ m, and $Z_{eff} \simeq 2$, $I/P \simeq 0.06$ A/W for a deuterium beam. To drive a current of 8 to 10 MA, a power level of order 150 MW is required. Taking into account the electrical power to beam power conversion efficiency, this could lead to a substantial recirculating power fraction in a reactor. The efficiency factor for D beams into D-T plasma can be substantially improved when electron trapping is taken into account.

The power required to drive the current can be reduced by operating at low density; however, this presents a conflict with the need for high density to maximize the fusion power.

2.2. Experiments [3,7]

The first experiment to show the existence of the beam-driven current was the Culham Levitron [3]. The Levitron experiment established the scaling of current with electron temperature for fast ion velocities comparable to the electron thermal velocity. The driven

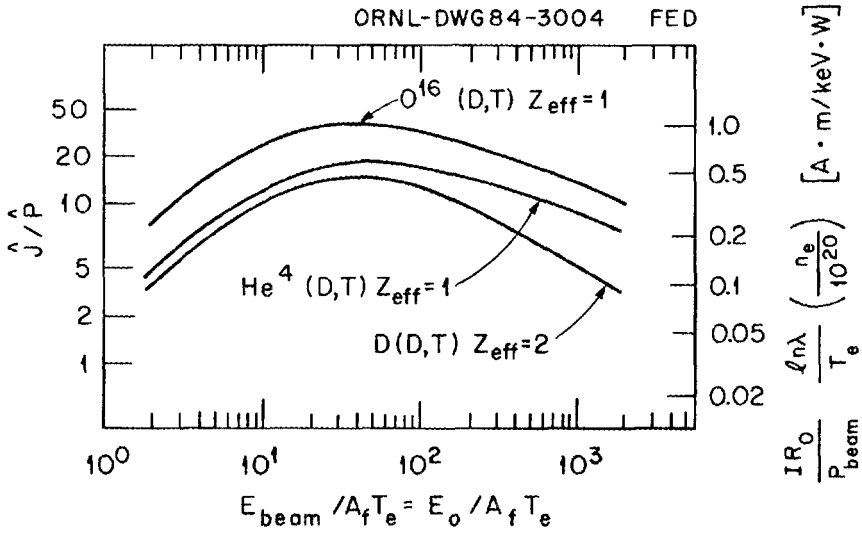

Fig. 2.2. Normalized efficiency factor $\hat{J}/\hat{P}$ vs normalized injection energy $E_{beam}/A_fT_e = E_o/A_fT_e$ (where E_o = beam energy, T_e = electron temperature, and A_f = atomic mass number of fast ion). Three different injection schemes are shown: oxygen into D–T, helium into D–T, and deuterium into D–T with $Z_{eff} = 2$. Shown on the right scale is dimensional quantity $(IR_o/P_{beam})(\ell n\ \Lambda/T_e)(n_e/10^{20})$ (in mks and keV units) (ref. [10]).

current was small; about 1 A of current was driven with about 10 kW of injected beam power. This was a consequence of low electron temperature (~5 eV) and large charge-exchange losses of fast ions. Thus, "demonstration" of temperature scaling was only over a narrow range of a few electron volts.

A more ambitious experiment was later carried out on the DITE (Culham) tokamak [7]. In the DITE experiment, 40% of the plasma current was estimated to be beam driven (about 30 kA out of a total of 80 kA) by the 1-MW beam. The scaling of current with density was observed.

Note that the magnitude of the beam-driven current depends upon the circulating fast ion current, $I \propto I_f$. The fast ion current exceeds the equivalent injected current I_{beam} by the stacking factor $S = V_f \tau_{fs}/2\pi R_o$, as given by Eq. (2-2). For $v_e > V_f$, the slowing-down time τ_{fs} varies as $T_e^{3/2}/n_e$. Thus, for low n_e and high T_e, S is the greatest. One should be cautioned, however, that at low n_e the plasma neutral density could be larger (especially in small devices) and an appreciable fraction of the fast ions could be lost by charge exchange, which we have neglected in our calculations.

No tokamak experiment has yet succeeded in driving its full current by beams and no measurements have yet been made of the effect of electron trapping.

2.3. Future Applications [10-13]

2.3.1 Near-Term Potential

For the present large experiments such as the Tokamak Fusion Test Reactor (TFTR) and the Joint European Torus (JET), it might be possible to drive significant currents by the envisaged injection schemes for these experiments. For example, in TFTR with 10 MW of neutral injection (two 5-MW beam lines with 90-keV H°), $\lesssim$0.5 MA of current could be driven in a plasma of $n_e \sim 3 \times 10^{19}$ m^{-3} and $T_e \sim$ 2-3 keV.

Two highly desirable characteristics of any current drive experiment would be that all the current be driven by the noninductive driver and that there be sufficient time for the current distribution to relax to equilibrium. In operational terms this means that the loop voltage should be reduced to zero (or a slightly negative value) while the total plasma current is held constant and that the loop voltage should remain nonpositive for a current relaxation time.

In TFTR the beam pulse length will probably not be greater than ~1 s (especially in early operations although it could conceivably be extended to 3 to 6 s in later years), which may not be long enough for the current distribution to relax to equilibrium, that is, to produce a constant toroidal electric field.

In JET at a density $n_e \simeq 0.5 \times 10^{20}$ m^{-3}, electron temperature of $T_e \simeq 5$ keV, and $Z_{eff} \simeq 2$, injecting 24 MW of 160-keV deuterium beam into D-T could produce a current of ~2 MA, which can be obtained directly using the results of Fig. 2.2.

2.3.2 Reactor Projections

The neutral beam current drive could be effective enough for use in steady-state tokamak power reactors provided high-efficiency, high-energy (~1 MeV/amu; i.e., ~2 MeV for deuterium) neutral beams were developed to achieve acceptable recirculated power.

A possible optimization scenario for a steady-state reactor driven by beams is discussed in ref. [13]. The essential problem is to optimize the plasma (n, T, β, etc.) and neutral beam (I/P, E_{beam}, Z_f, etc.) simultaneously. It is clear from the current drive efficiency expression (J/P or I/P) that low density and high temperature minimize the power required to drive the current that both compete with the fusion power requirements.

In ref. [13], the cost per unit of electrical power was minimized subject to constraints on plasma β, plasma power balance requirements, fusion power, beam power, driver efficiency, etc. (One can also choose $Q = P_{fusion}/P_{beam}$ to identify the measure of performance and to optimize it, in which case cost may or may not be optimum since a large part of the cost of a reactor is independent of the fusion power.) The resulting optimized cost is shown in Fig. 2.3 as a function of average temperature $T_{av} = (T_e + T_i)/2$ and β for conventional, pulsed tokamak reactors and beam-driven steady-state reactors. For $\beta = 6.7\%$, the optimum beam energy $E_{beam} \gtrsim 1$ MeV with $P_{beam} \simeq 100$ MW, which represents about 15 to 20% recirculating electrical power (engineering $Q_E \sim 5$-6) even at 80% electric-to-beam power conversion efficiency. A steady-state beam-driven reactor scheme is conceivable only if high-efficiency ($\eta > 60\%$) negative ion beams are available.

The main problem with steady-state operation is that it takes a large amount of driven power if the plasma density is high. However, if the plasma density is lowered, then the fusion power and the net

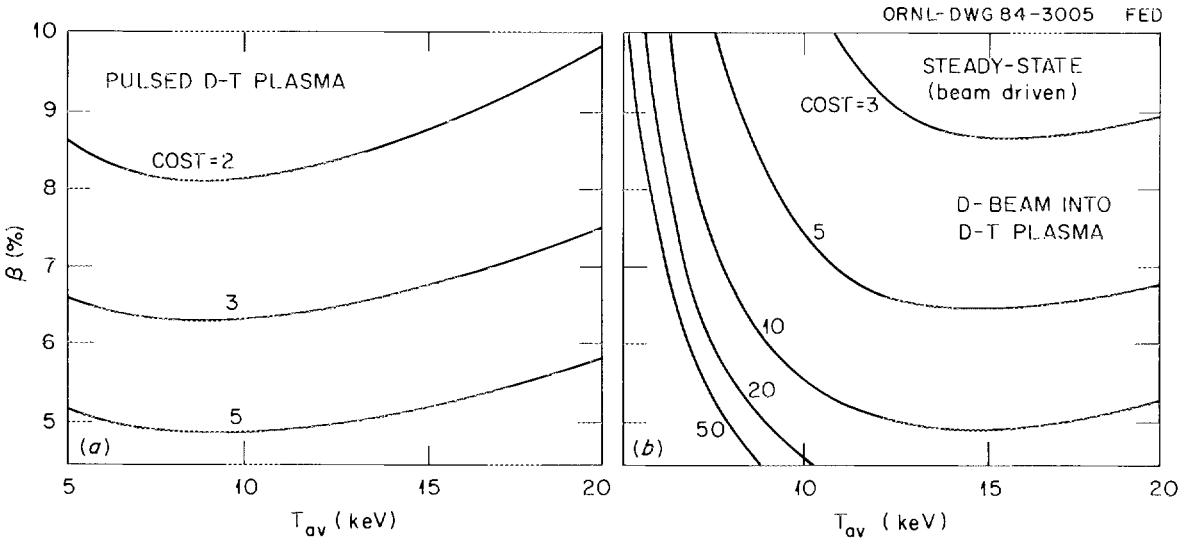

Fig. 2.3. Contours of constant cost per unit power (in arbitrary units) for an INTOR-sized tokamak reactor as a function of beta and average temperature T_{av} for (a) pulsed and (b) beam-driven steady-state operation. For each choice of β and T_{av}, T_e is varied to minimize the cost in (a) and T_e and E_{beam} are varied to minimize the cost in (b). Electrical power to beam power conversion efficiency is assumed to be $\eta_b \simeq 80\%$ in (b) (ref. [13]).

electrical power output drops, and the plant becomes economically unattractive. A possible solution to this problem is cyclic current drive in which plasma parameters, such as density, are modulated to optimize for current drive during the current driving phase and for power production during the high-density burn/power-producing ("coast") phase. This is more attractive than a conventional, normal-pulsed cycle because plasma current is roughly constant and the poloidal field changes less than in the pulsed cycle. Thus, the cyclic part of the out-of-plane forces on the magnets and the fatigue limit are smaller and less severe.

One possible form of cyclic current drive is a combination of noninductive and conventional inductive current drive. This method uses the external transformer to drive current during the high-density (power production) phase to the limit of the OH flux swing; then, while the ohmic heating coil currents are reset to their initial values, beams are used to sustain the current in the low-density drive phase.

Another possibility is the "internal transformer" scheme. The primary current of an internal transformer is the noninductively [11] (beam) driven current inside the plasma. When the fast ion distribution is thermalized and the driven current vanishes after the drive phase is ended, the change in this primary current induces an electric field in the plasma that maintains the total plasma current. As the electric field resistively diffuses away during the power production (coast) phase, the plasma current decreases until intense noninductive current drive restores the current to its initial value, and the cycle begins again. Because the internal transformer method allows the current to rise during the drive phase and to partially decay during the coast phase, a small modulation of current has to be tolerated.

Figure 2.4 compares the relative costs of various current drive options. In the cyclic mode the time-averaged power consumption is lower, and for the internal transformer scheme the beam power requirement is about half that required for the steady-state mode. With cyclic current drive, neutral beams of more modest energy would be adequate. The major disadvantage of cyclic current drive is that it only alleviates the severe cyclic stress problems but does not eliminate them as steady-state current drive does.

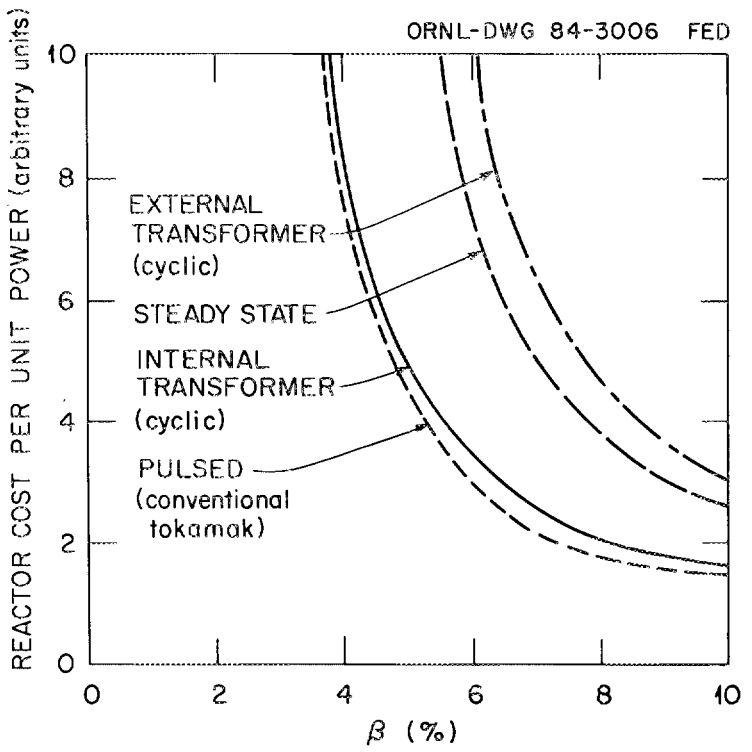

Fig. 2.4. Relative cost per unit power vs beta (β) for various current beam drive options. Conventional pulsed operation is compared with strict steady-state and cyclic (internal and external transformer) beam current drive options (ref. [11]).

3. LOWER HYBRID CURRENT DRIVE [2,9,16–40,66–69,71–74]

The use of rf waves near the lower hybrid (LH) frequency to drive steady-state electron currents in tokamaks was proposed by Fisch [2], and experiments carried out on many tokamaks (see Table 3.1) have observed the LH rf-driven currents, with or without ohmic heating (OH) electric fields.

The LH waves are usually excited by an array of phased waveguides capable of producing a wave spectrum which is broad in $k_{\parallel}$ ($= \mathbf{k} \cdot \mathbf{B}/|\mathbf{B}|$). If the phasing of each guide is $\pi/2$ relative to its neighbor, a traveling wave is launched that carries momentum in the toroidal direction. The LH waves with net parallel momentum transfer momentum to the high-velocity tail of the electron velocity distribution (i.e., to those electrons traveling with the wave parallel phase velocity $\omega/k_{\parallel}$) via Landau damping rather than the particles within the bulk of the distribution. The current is mainly carried by these high-velocity tail electrons (which are resonant with the wave phase velocity $\omega \simeq k_{\parallel} v_{\parallel}$) — superthermal electrons — because they retain momentum longer than bulk thermal electrons. (Note that the dissipation rate of electron momentum by electron-ion collisions varies as $\nu \sim v^{-3} \sim T^{-3/2}$.)

The LH wave exists for

$$\Omega_i^2 \ll \omega^2 \ll \Omega_e^2 ,$$

where Ω_e and Ω_i represent the gyrofrequency (cyclotron frequency) of the electrons and ions, respectively. For plasmas of interest, $\omega_{pi}^2 \gg \Omega_i^2$ and $\omega_{pe} \simeq \Omega_e$ (where $\omega_{pj}^2 = n_j e^2/m_j \epsilon_o$ is the plasma frequency for the jth species), the LH frequency ω_{LH} is on the order of the ion plasma frequency $\omega_{pi} = (m_e/m_i)^{1/2}\omega_{pe}$ and is given by

$$\omega_{LH}^2 = \omega_{pi}^2/(1 + \omega_{pe}^2/\Omega_e^2) \quad . \tag{3-1}$$

If a current is to be excited (rather than heating), the wave frequency should be far from the LH resonance, typically $\omega \gtrsim 2\,\omega_{LH}$. For tokamaks of interest (present or future), $\omega \simeq 0.5$–5.0 GHz.

Table 3.1. Parameters of lower hybrid experiments

	a (cm)	R (cm)	B_{max} (T)	f (GHz)	P_{rf}, max (kW)	I_{rf}, max (kA)	Δt_{rf} (s)	$\eta_{\parallel}$	$\bar{n}_{max}$ (10^{13} cm^{-3})	ω_{pe}^2/Ω_e^2
Steady state										
Alcator C	17	64	10	4.6	600 (1000)	200	0.2	~2	>10	>0.1
PLT	45	132	3.2	0.8	600	420	0.3–4	~2	0.7	0.07
Transient										
FT	20	83	8	2.45	250		0.1	~2	5	0.08→0.3
Wega	15	72	2.3	0.8	50	40	0.02	2, 3, 7	1, 1.3, 1.8	0.2→0.3
T-7	35	122	1.9	0.9	250		0.05	2.5	1.1	0.3
JFT-2	25	90	1.5	0.75	150	35	0.075	2.5, 5.5	0.6	0.3
Versator	13	41	1.5	0.8	150	40	0.02	8	0.6	0.3
WT-2	9	40	1.3	0.92	100	5	0.02			
	20	27	34	41	49	62	73	82	93	107

[Refs: 9, 19–28, 31, 35–40, 62]

As can be seen from Table 3.1, which we discuss later, several tokamak experiments have demonstrated that the toroidal current can be maintained for extended durations by LH waves alone and, in most cases, with high efficiency. As a result, LH current drive was believed to be one of the promising candidates for achieving a steady-state reactor condition for a tokamak. However, at the present, there is no means that appears to be undeniably desirable. With the exception of Alcator-C (and possibly Wega), most LH current drive experiments observe an upper, critical density limit above which the current drive ceases (or diminishes more rapidly than the theoretical scaling $I \propto 1/n_e$). Similar to the case proposed for neutral beams, cyclic current drive approaches can be adopted to improve the reactor current drive efficiency with LH waves. The wave penetration problem is one of the main causes of inefficiency of LH current drive at reactor densities (and temperatures). Here the critical parameter is the parallel wave index $\eta_{\parallel} = ck_{\parallel}/\omega$. In order to resonate with very energetic electrons (high-velocity tail electrons), low-$\eta_{\parallel}$ waves are necessary ($\eta_{\parallel} = ck_{\parallel}/\omega = c/v_{p\parallel} \simeq c/v_{\parallel}$, where $v_{p\parallel}$ is the parallel phase velocity of the wave). Low-$\eta_{\parallel}$ LH waves (the slow wave) can only penetrate to a given plasma density, at which point they undergo mode conversion to "fast waves," which will carry the rf energy back towards the plasma surface.

One of the puzzling aspects of the LH current drive experiments is the observation of far more current than expected. That is, the current carried by a high energy electron tail ($T_e \sim 50$–200 keV in present experiments) contains more particles than predicted. This tail builds up slowly from an initially Maxwellian plasma, which has no preexisting tail before the rf is turned on. This is the so-called problem of spectral gap that revolves around identifying the underlying mechanism for driving electrons from the bulk distribution into the tail. Later in this section, we discuss some of the explanations (theoretical not experimental) offered to explain the process.

In this section we briefly examine the nature of LH waves (propagation, accessibility, choice of frequency, etc.), discuss the quasi-linear theory for current generation, and summarize some of the experimental results. The effectiveness of LH-driven current for reactor applications is discussed in many of the references given, and is not considered here in great length.

3.1. Propagation of LH Wave and Choice of rf Frequency

The frequency range of lower hybrid is intermediate between the electron and ion gyrofrequencies ($\Omega_i^2 \ll \omega^2 \ll \Omega_e^2$). As a result, wave-induced motions of the electrons are described by the guiding-center theory, in which electrons move freely parallel to the magnetic field B_o (toroidal field, in the case of a tokamak) and undergo a combination of the $\mathbf{E} \times \mathbf{B}_o$ drift ($\mathbf{v}_E = \mathbf{E} \times \mathbf{B}_o/B_o^2$) and the polarization drift [$\mathbf{v}_{pol} = -(\Omega_e B_o)^{-1} d\mathbf{E}/dt$] perpendicular to $\mathbf{B}_o$, where $\mathbf{E}$ is the LH wave electric field. The ions respond to $\mathbf{E}$ as if unmagnetized since the wave frequency is much greater than the ion cyclotron (gyro) frequency ($\omega^2 \gg \Omega_i^2$).

The details of wave propagation and dispersion relation for the lower hybrid range of frequencies are discussed elsewhere. Basically, in the cold plasma approximation, the dispersion relation for waves above the LH frequency has two distinct branches: the "fast" wave branch (i.e., large $\omega/k_\perp$) and the "slow" wave branch (i.e., small $\omega/k_\perp$). Both waves have potential for heating and current drive applications. Here, we are interested in current drive. It is the slow wave branch of the dispersion relation that we usually associate with the LH wave. This is an electrostatic wave (as $\omega \to \omega_{LH}$) in that the wave vector $\mathbf{k}$ is parallel to $\mathbf{E}$ ($\mathbf{k} \parallel \mathbf{E}$), and there is no associated rf magnetic field.

The slow waves have the large $E_\parallel$ components needed for effective current drive in single-pass absorption. Fast waves, on the other hand, have relatively small $E_\parallel$ components, so it is likely that (in the event that they are used for current drive) multipass propagation and absorption will be needed for effective current drive. Experiments on present-day tokamaks (see Table 3.1) and future considerations are basically on "slow waves" (also known as LH waves).

3.1.1 Dispersion Relation

The wave propagation is described by a dispersion relation, which we review here briefly. Consider a plasma with a uniform magnetic field in the z direction $\mathbf{B}_o = B_o \hat{\mathbf{e}}_z$ (the toroidal direction in a tokamak) with unperturbed electric field $\mathbf{E}_o = 0$ and unperturbed electron and ion fluid velocities $\mathbf{V}_{eo} = \mathbf{V}_{io} = 0$. The perturbed electric field $\mathbf{E}$, magnetic field $\mathbf{B}$, and current density $\mathbf{J}$ are then described by the Maxwell equations:

$$\nabla \times \mathbf{B} = \mu_o \epsilon_o \frac{\partial \mathbf{E}}{\partial t} + \mu_o \mathbf{J} \ , \tag{3-2a}$$

$$\nabla \times \mathbf{E} = -\frac{\partial \mathbf{B}}{\partial t} \ . \tag{3-2b}$$

Assuming that the wave fields vary as $\exp[i(\mathbf{k} \cdot \mathbf{r} - \omega t)]$, Eqs. (3-2a) and (3-2b) yield the wave equation

$$-\mathbf{k} \times (\mathbf{k} \times \mathbf{E}) = \frac{\omega^2}{c^2}\mathbf{E} + i\omega\mu_o \mathbf{J} \ . \tag{3-3}$$

In the limit of cold plasma, the perturbed current density $\mathbf{J}$ can be expressed as $\mathbf{J} = ne(\mathbf{V}_i - \mathbf{V}_e)$, where $\mathbf{V}_e$ and $\mathbf{V}_i$ are the perturbed fluid velocities of electrons and ions, respectively, determined from two fluid momentum equations (for $T_e = T_i \simeq 0$):

$$\begin{aligned} m_e \frac{d\mathbf{V}_e}{dt} &= -e(\mathbf{E} + \mathbf{V}_e \times \mathbf{B}_o) \ , \\ m_i \frac{d\mathbf{V}_i}{dt} &= e(\mathbf{E} + \mathbf{V}_i \times \mathbf{B}_o) \ . \end{aligned} \tag{3-4}$$

Assuming that $\mathbf{V}_e$, $\mathbf{V}_i$ also vary as $\exp[i(\mathbf{k} \cdot \mathbf{r} - \omega t)]$, we then use Eqs. (3-3) and (3-4) to obtain

$$\mathbf{k} \times (\mathbf{k} \times \mathbf{E}) + \frac{\omega^2}{c^2}\overleftrightarrow{\epsilon} \cdot \mathbf{E} = 0 \ , \tag{3-5a}$$

where $\overleftrightarrow{\epsilon}$ is the cold plasma dielectric tensor

$$\overleftrightarrow{\epsilon} = \begin{bmatrix} \epsilon_1 & -i\epsilon_2 & 0 \\ i\epsilon_2 & \epsilon_1 & 0 \\ 0 & 0 & \epsilon_3 \end{bmatrix} . \tag{3-5b}$$

The components of $\overleftrightarrow{\epsilon}$ are given by

$$\epsilon_1 \equiv \epsilon_\perp = 1 - \sum_j \frac{\omega_{pj}^2}{\omega^2 - \Omega_j^2} ,$$

$$\epsilon_2 = \sum_j \sigma_j \frac{\Omega_j}{\omega} \frac{\omega_{pj}^2}{\omega^2 - \Omega_j^2} \qquad \sigma_j = \begin{cases} +1 \text{ ions} \\ -1 \text{ electrons} \end{cases} , \tag{3-6}$$

$$\epsilon_3 \equiv \epsilon_\parallel = 1 - \sum_j \frac{\omega_{pj}{}^2}{\omega^2} ,$$

where $j = e,i$ and σ_j is the sign of the charge.

We rewrite Eq. (3-5) in matrix form as

$$\begin{bmatrix} \epsilon_1 - \eta_\parallel^2 & -i\epsilon_2 & \eta_\parallel\eta_\perp \\ i\epsilon_2 & \epsilon_1 - \eta^2 & 0 \\ \eta_\parallel\eta_\perp & 0 & \epsilon_3 - \eta_\perp^2 \end{bmatrix} \begin{bmatrix} E_x \\ E_y \\ E_z \end{bmatrix} = 0 , \tag{3-7}$$

where $\mathbf{k} = k_x\hat{\mathbf{e}}_x + k_z\hat{\mathbf{e}}_z = k_\perp\hat{\mathbf{e}}_x + k_\parallel\hat{\mathbf{e}}_z$ $(\mathbf{B} = B_o\hat{\mathbf{e}}_z)$ is used and η is the refractive index

$$\eta^2 = k^2c^2/\omega^2 = \eta_\perp^2 + \eta_\parallel^2 ,$$

$$\eta_\perp = k_\perp c/\omega , \quad \eta_\parallel = k_\parallel c/\omega ,$$

$$k_\perp = k \sin\theta ; \quad k_\parallel = k \cos\theta ,$$

with θ being the angle between $\mathbf{k}$ and $\mathbf{B}_o$.

For a nontrivial solution to exist, the determinant of the matrix [Eq. (3-7)] must vanish. This condition gives the cold plasma dispersion relation:

$$a\eta_\perp^4 - b\eta_\perp^2 + c = 0 , \tag{3-8}$$

where

$$a = \epsilon_1 ,$$

$$b = (\epsilon_1 + \epsilon_3)(\epsilon_1 - \eta_\parallel^2) - \epsilon_2^2 , \tag{3-9}$$

$$c = \epsilon_3[(\epsilon_1 - \eta_\parallel^2)^2 - \epsilon_2^2] .$$

Two solutions to Eq. (3-8) are

$$\eta_\perp^2 = [b \mp (b^2 - 4ac)^{1/2}]/2a . \tag{3-10}$$

For a lower hybrid range of frequencies (i.e., in the limit of $\Omega_e^2 \gg \omega^2 \gg \Omega_i^2$), the elements of the dielectric tensor can be approximated as

$$\epsilon_1 = \epsilon_\perp \simeq 1 + \omega_{pe}^2/\Omega_e^2 - \omega_{pi}^2/\omega^2 \ ,$$

$$\epsilon_2 \simeq \omega_{pe}^2/\omega\Omega_e \ , \tag{3-11}$$

$$\epsilon_3 = \epsilon_\parallel \simeq 1 - \omega_{pe}^2/\omega^2 - \omega_{pi}^2/\omega^2 \simeq 1 - \omega_{pe}^2/\omega^2 \ .$$

The magnitude of terms are such that

$$|\epsilon_3| \gg \epsilon_1, \ \epsilon_2 \ ,$$

which typically yields to $b, c > 0$.

The two branches of Eq. (3-8) [given by Eq. (3-10)] correspond to "slow" and "fast" waves. The slow wave branch (i.e., small $\omega/k_\perp$ or large $\eta_\perp$) corresponds to the plus sign in Eq. (3-10),

$$\eta_\perp^2 \ (\text{"slow"}) = \left[b + (b^2 - 4ac)^{1/2}\right]/2a \ ;$$

and the fast wave branch (i.e., large $\omega/k_\perp$ or small $\eta_\perp$) corresponds to the minus sign in Eq. (3-10),

$$\eta_\perp^2(\text{"fast"}) = [b - (b^2 - 4ac)^{1/2}]/2a \ .$$

We now note a few important features of the dispersion relation of LH waves. (1) There is a cutoff ($\eta_\perp^2 \to 0$) at $c = 0$. For a slow wave this cutoff is at $\epsilon_3 = 0$, $\omega^2 = \omega_{pe}^2$, giving a cutoff density $n_e(\text{cutoff}) \simeq 1.24 \times 10^{16}$ $[f\ (\text{GHz})]^2$, where $f = \omega/2\pi$ is in gigahertz. This density is so low that the slow wave can tunnel through the evanescent layer. (2) The slow wave branch has a resonance (cold plasma resonance) for $a = \epsilon_1 = 0$ (i.e., $\eta_\perp^2 \to \infty$), thus defining the LH frequency $\omega^2 = [\omega_{pi}^2/(1 + \omega_{pe}^2/\Omega_e^2)] \equiv \omega_{LH}^2$. Hence, it is this slow wave branch of the dispersion relation that is typically associated with the

LH waves. (3) The slow and fast wave branches coalesce (mode conversion) when $b^2 - 4ac = 0$. The value of the parallel index of refraction $\eta_{\parallel} = k_{\parallel}c/\omega$ is critical in determining the properties of LH waves, which we will discuss in the next subsection.

Consider a slow wave launched at the edge of the plasma, which propagates well inside the plasma where densities are much greater than those corresponding to the cutoff densities [$n_e > n_e$(cutoff)]. Then, the LH waves are nearly electrostatic ($\eta_{\perp} \gg 1$, $k_{\perp} \gg k_{\parallel}$) inside the plasma. In this case the dispersion relation [Eq. (3-8)] reduces to

$$\epsilon_1\eta_{\perp}^2 + \epsilon_3\eta_{\parallel}^2 = 0 \tag{3-12a}$$

or

$$\epsilon_1 k_{\perp}^2 = -\epsilon_3 k_{\parallel}^2 , \tag{3-12b}$$

which can be rearranged as

$$\omega^2 \simeq \omega_{LH}^2 \left(1 + \frac{k_{\parallel}^2}{k_{\perp}^2}\frac{\omega_{pe}^2}{\omega_{pi}^2}\right) \simeq \omega_{LH}^2 \left(1 + \frac{k_{\parallel}^2}{k_{\perp}^2}\frac{m_i}{m_e}\right) , \tag{3-13}$$

where m_i/m_e is the ion to electron mass ratio. (If the plasma consists of multiple ion species, an effective ion mass can be used as an approximation for m_i.)

Equation (3-12) indicates that LH waves propagate along a localized ray called a "resonance cone" with the cone angle θ with respect to the (static) magnetic field given by

$$\tan^2\theta = k_{\perp}^2/k_{\parallel}^2 = -\epsilon_3/\epsilon_1 \tag{3-14a}$$

$$\simeq -1 + \frac{\omega_{pe}^2/\omega^2}{1 + \omega_{pe}^2/\Omega_e^2} . \tag{3-14b}$$

Equation (3-13) describes propagation of waves at frequencies ω greater than ω_{LH}, a parameter that, in general, increases towards the

plasma center. For the case in which LH energy at a given $k_{\parallel}$ irradiates a plasma slab with density varying in the direction perpendicular to $\mathbf{B}_o$, $k_{\parallel}$ of the waves within the plasma remains constant. This is approximately the case for tokamak geometry. Equation (3-13) then demonstrates a resonance $k_{\perp} \to \infty$ ($\eta_{\perp} \to \infty$), as the density increases to the point where $\omega = \omega_{LH}$ (as mentioned earlier). For current drive purposes, we choose ω to be greater than the maximum LH frequency ($\omega_{LH,max}$) within the plasma so that accessibility of the LH wave to the plasma center is guaranteed (for sufficiently large $k_{\parallel}$ or $\eta_{\parallel}$), but a resonance (which causes heating not current drive) is avoided.

Figure 3.1 shows the group velocity (ray) trajectories, readily obtained from the relation

$$\mathbf{v}_g = \frac{\partial\omega}{\partial\mathbf{k}} = \frac{\partial\omega}{\partial\mathbf{k}_{\parallel}} + \frac{\partial\omega}{\partial\mathbf{k}_{\perp}} . \tag{3-15}$$

From Eq. (3-13) we have

$$\frac{\partial\omega}{\partial k_{\parallel}} = \frac{\omega^2 - \omega_{LH}^2}{\omega k_{\parallel}} , \tag{3-16a}$$

$$\frac{\partial\omega}{\partial k_{\perp}} = - \frac{\omega^2 - \omega_{LH}^2}{\omega k_{\perp}} . \tag{3-16b}$$

Note that the ray (group velocity) trajectories as determined by

$$\frac{\partial\omega/\partial k_{\perp}}{\partial\omega/\partial k_{\parallel}} = - k_{\parallel}/k_{\perp}$$

depend only on wave number through $k_{\parallel}/k_{\perp}$ but from Eq. (3-13) [or Eq. (3-14)] depend only on plasma parameters. Hence, the entire spectrum of $k_{\parallel}(\eta_{\parallel})$ waves excited by the antenna (waveguides) will propagate toroidally within the same rf energy channel, or "resonance cone."

The phase velocity is given by

$$\mathbf{v}_p = \frac{\omega\,\mathbf{k}}{k^2} = \frac{\omega}{k}\hat{\mathbf{k}} \tag{3-17}$$

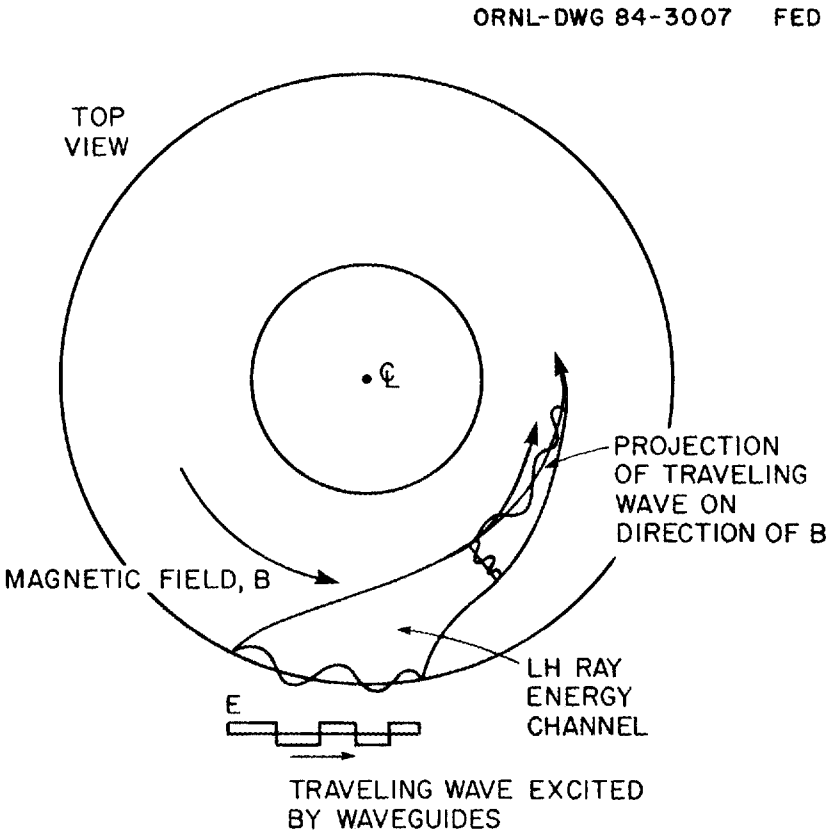

Fig. 3.1. Lower hybrid energy channel as viewed from the top of the torus (ref. [34]).

where $\hat{\mathbf{k}} = \mathbf{k}/k = (k_\perp/k)\hat{\mathbf{e}}_x + (k_\parallel/k)\hat{\mathbf{e}}_z$. We note the group velocity is perpendicular to the wave phase velocity ($\mathbf{v}_g \cdot \mathbf{v}_p = 0$, or $\mathbf{k} \cdot \mathbf{v}_g = 0$).

To describe wave propagation at the LH layer properly, we must consider warm plasma effects. The appropriate dispersion relation in this case is given by [80]

$$- d\eta_\perp^6 + a\eta_\perp^4 - b\eta_\perp^2 + c = 0 \ , \tag{3-18}$$

where a, b, and c are given by Eq. (3-9) and d contains the finite-temperature effects, given by

$$d = 3\,\frac{\omega_{pi}^2}{\omega^2}\,\frac{v_i^2}{c^2} + \frac{3}{4}\,\frac{\omega_{pe}^2}{\Omega_e^2}\left(\frac{\omega\rho_e}{c}\right)^2 \ . \tag{3-19}$$

Here $v_i = (kT_i/m_i)^{1/2}$ is the ion thermal velocity, c is speed of light, and $\rho_e = v_e/\Omega_e$ is the electron Larmor radius [$v_e = (kT_e/m_e)^{1/2}$, electron thermal velocity].

The $\eta_\perp^6$ term represents a new thermal wave branch [called the ion plasma wave or hot ion wave, which does not exist in a cold plasma approximation — Eq. (3-8)]. In a hot plasma, as the waves propagate toward the resonance layer and $\eta_\perp$(i.e., $k_\perp$) increases, thermal effects ($-d\eta_\perp^6$ term) become important. For $\eta_\perp^2 \gg 1$ (electrostatic limit), Eq. (3-18) reduces to

$$- d\eta_\perp^4 + a\eta_\perp^2 - b = 0 \tag{3-20a}$$

or (approximating the coefficients a and b for this limit)

$$(c/\omega)^2 d\ k_\perp^4 + \epsilon_1 k_\perp^2 + \epsilon_3 k_\parallel^2 = 0 \ . \tag{3-20b}$$

Note from Eq. (3-20) that the fast wave branch (which is an electromagnetic wave) has been eliminated.

Two solutions to Eq. (3-20) are

$$\eta_\perp^2 = \frac{a \pm (a^2 - 4bd)^{1/2}}{2d} \tag{3-21a}$$

or

$$\eta_\perp^2 = \frac{-\epsilon_1 \pm (\epsilon_1^2 - 4\epsilon_3\eta_\parallel^2 d)^{1/2}}{2d} \; . \tag{3-21b}$$

The minus sign in Eq. (3-21) corresponds to a slow wave and for small thermal effects (i.e., for $4bd \ll a^2$ or $4\epsilon_3\eta_\parallel^2 d \ll \epsilon_1^2$), we obtain

$$\eta_\perp^2 \simeq b/a \simeq -\epsilon_3\eta_\parallel^2/\epsilon_1 \; , \tag{3-22a}$$

which is the cold plasma LH wave [see Eq. (3-12a)]. The plus sign gives the hot ion plasma wave:

$$\eta_\perp^2 \approx a/d = \epsilon_1/d \tag{3-22b}$$

(again $a^2 \gg 4bd$ is used). Using Eqs. (3-9) and (3-19), we obtain a simplified dispersion relation:

$$\omega^2 \simeq \omega_{LH}^2 \left[1 + 3\frac{k_\perp^2 v_i^2}{\omega^2}\left(1 + \frac{1}{4}\frac{T_e}{T_i}\frac{\omega^4}{\Omega_e^2\Omega_i^2}\right)\right] \; . \tag{3-23}$$

The two branches of Eq. (3-20) will coalesce [i.e., the conversion of the cold, LH wave into the ion plasma wave will occur at $a^2 = 4bd$ ($\epsilon_1^2 = 4\epsilon_3^2\eta_\parallel^2 d$)]. Note that the parallel refractive index $\eta_\parallel$ will determine the spatial location of this ion mode conversion.

For current drive, the wave frequency ω and the parallel refractive index $\eta_\parallel$ must satisfy certain criterion. We discuss them in the following section.

3.1.2 Choice of $\eta_{\parallel}$ and ω

There are limitations on the possibility of using LH waves for current drive. One of the critical parameters is the parallel refractive index $\eta_{\parallel}$.

Low-$\eta_{\parallel}$ waves are necessary to couple energy and momentum to high-energy tail electrons:

$$\eta_{\parallel} = k_{\parallel}c/\omega = c/v_{p\parallel} \simeq c/v_{\parallel} \ ,$$

where $v_{p\parallel} = \omega/k_{\parallel}$ is the parallel wave phase velocity and $v_{\parallel}$ is the parallel velocity of the high-energy tail electrons. As we can see from the simple physical arguments given in Sect. 1, the effectiveness of current generation varies rapidly with the phase velocity of the rf wave ($J/P \sim v_p^2 \sim 1/\eta_{\parallel}^2$). As indicated earlier, the LH current drive scheme is based on the resonant interaction (i.e., $v_{p\parallel} = \omega/k_{\parallel} \simeq v_{\parallel}$). For such waves the current density can be approximated as [Eq. (1-1)]

$$J \simeq n_r e v_r = n_r e v_{\parallel} \simeq n_r e v_p \quad (A/m^2) \ , \tag{3-24a}$$

where n_r is the density of the resonant (high-energy tail) electrons. The power absorbed by the resonant electrons and removed by collision is given by [Eq. (1-2)]

$$P = m_e n_r v_r^2 \nu_r \simeq m_e n_r v_p^2 \nu_r \quad (W/m^3) \ , \tag{3-24b}$$

where ν_r is the collision frequency of the resonant electrons with the bulk plasma electrons of density n

$$\nu_r \simeq \nu_{ee} = \omega_{pe}^4 \ \ell n \ \Lambda/4\pi n v_r^3 \simeq ne^4 \ \ell n \ \Lambda/4\pi\epsilon_o^2 m_e^2 v_p^3 \ .$$

Therefore,

$$J/P \simeq \frac{4\pi\epsilon_o}{e\,\ell n\,\Lambda}\frac{v_p^2}{\omega_{pe}^2} = \frac{4\pi\epsilon_o^2 m_e}{ne^3\,\ell n\,\Lambda}\,v_p^2$$

$$= \frac{4\pi\epsilon_o^2 m_e}{ne^3\,\ell n\,\Lambda}\frac{c^2}{\eta_{\parallel}^2}$$

$$\simeq \frac{197}{\ell n\,\Lambda}\left(\frac{10^{20}}{n}\right)\frac{1}{\eta_{\parallel}^2} = \frac{197}{\ell n\,\Lambda}\frac{1}{n_{20}}\frac{1}{\eta_{\parallel}^2}\,. \tag{3-24c}$$

By volume averaging we find the figure of merit. In practical units the current drive efficiency is

$$\frac{\bar{n}_{20}R_o\ (m)\ I\ (MA)}{P\ (MW)} \simeq \frac{31}{\ell n\,\Lambda}\frac{1}{\langle\eta_{\parallel}^2\rangle}\,, \tag{3-25}$$

where $\bar{n}_{20}$ is the average bulk electron density in units of 10^{20} m^{-3}. This is a rough estimate but is close to that obtained from more detailed calculations (which we will discuss later), and it reflects the general characteristics of current drive effectiveness of LH waves. It is apparent from Eq. (3-25) that small $\eta_{\parallel}$ is required to generate current effectively. However, the minimum $\eta_{\parallel}$ allowed in the plasma is limited by the accessibility criterion of the LH wave. There is also an upper bound on $\eta_{\parallel}$. Let us now examine these limits.

The lower bound $\eta_{\parallel,min}$ comes from the requirement of wave accessibility; that is, the slow wave must satisfy certain accessibility conditions in order not to be converted into the outward propagating fast wave. Suppose that the wave frequency is substantially greater than the maximum LH frequency ($\omega > \omega_{LH,max}$) within the plasma so that the wave accessibility to the plasma center is assured (for sufficiently large $\eta_{\parallel}$) and the wave-ion interactions are minimized; that is,

$$\omega = 2\pi f > \omega_{LH,max}\,,$$

$$\omega_{LH,max} = \left[\omega_{pi}^2/(1 + \omega_{pe}^2/\Omega_e^2)\right]_{max}^{1/2}\,.$$

Then, only waves with sufficiently large $\eta_{\parallel}$ can penetrate to a given plasma density. This limit is approximated by

$$\eta_{\parallel} > \eta_{\parallel,min} \equiv \eta_{\parallel,crit} \simeq (\omega_{pe}/\Omega_e) + (1 + \omega_{pe}^2/\Omega_e^2 - \omega_{pi}^2/\omega^2)^{1/2}$$

$$= (\omega_{pe}/\Omega_e) + \left[(1 + \omega_{pe}^2/\Omega_e^2)(1 - \omega_{LH,max}^2/\omega^2)\right]^{1/2} , \tag{3-26}$$

which is obtained from $b^2 - 4ac = 0$. Figure 3.2 shows the wave propagation characteristics for three different values of $\eta_{\parallel}$. Shown in Fig. 3.2 are $\eta_{\perp}^2$ vs density for given values of $\eta_{\parallel}$ from Eq. (3-18).

Equation (3-26) is the lower bound on $\eta_{\parallel}$ that represents the accessibility condition for a LH (slow) wave.

As the LH wave travels into the hot plasma center, it may suffer mode conversion into heavily-damped, hot-ion waves if $\eta_{\parallel}$ is large enough. (In this case rf energy and momentum is deposited on the ions near the mode conversion point.) The density at which the lower hybrid and hot plasma wave branches coalesce is denoted by N_{MC} in Fig. 3.2. This process (mode conversion into hot-ion wave) may be favorable for the purpose of heating because it effectively transfers wave energy to the ions, but it is clearly unfavorable for current drive. Mode conversion occurs when the rf perpendicular wavelength $\lambda_{\perp} = 2\pi/k_{\perp}$ becomes comparable to the ion gyroradius ρ_i and the wave absorption is via ion Landau damping ($\omega \sim k_{\perp}v_i$). From Eq. (3-23) this can always occur for $\omega < \omega_{LH,max}$. For $\omega > \omega_{LH,max}$, conversion to thermal modes can be avoided if $\eta_{\parallel}$ is less than upper bound, critical value $\eta_{\parallel,max}$:

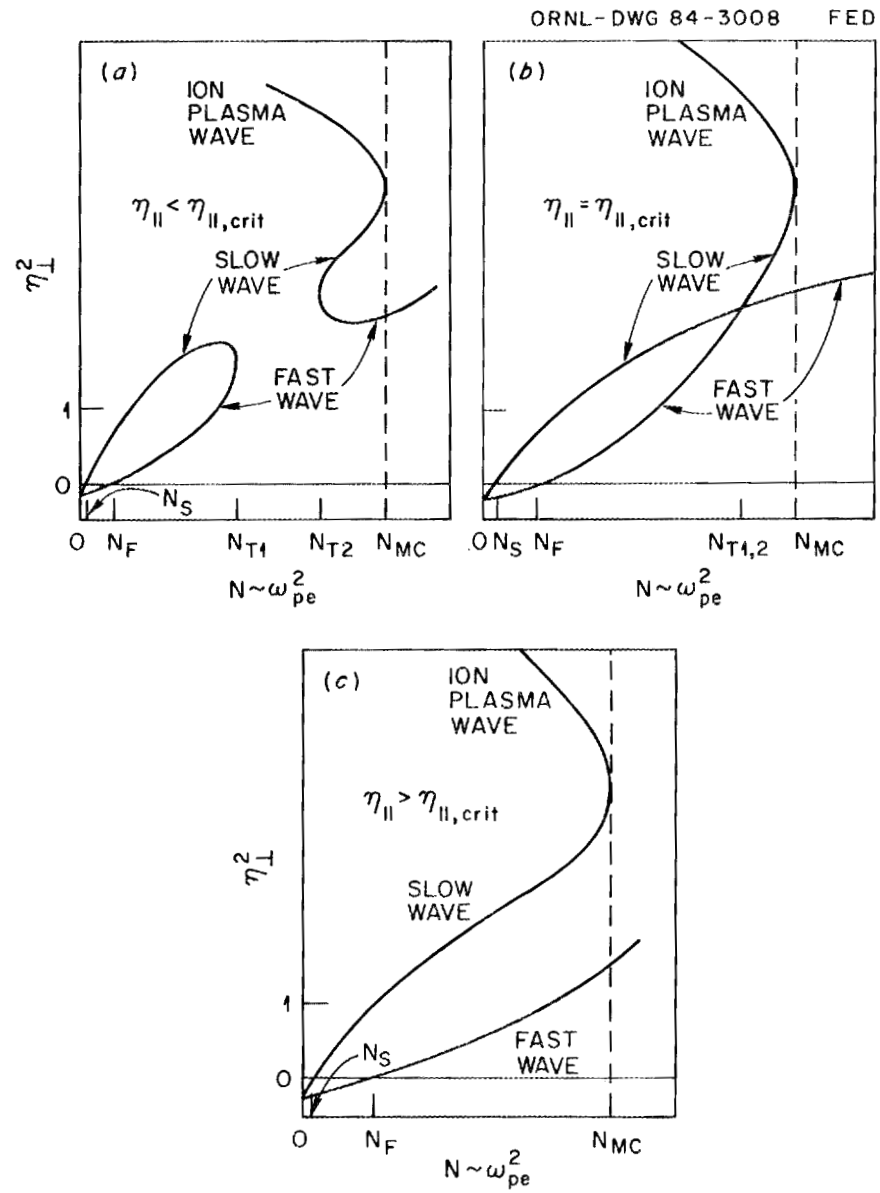

Fig. 3.2. $\eta_{\perp}^2$ vs density $N(\sim \omega_{pe}^2)$ for fixed $\eta_{\parallel}$ from Eq. (3-18). N_S and N_F denote densities correspoding to the slow and fast wave cutoffs. N_{T1} and N_{T2} are the densities corresponding to the mode conversion points $(b^2 - 4ac = 0)$. N_{MC} denotes the density corresponding to the thermal mode conversion point $a^2 - 4bd = 0$ (or $\epsilon_1^2 \simeq 4\epsilon_3^2\eta_{\parallel}^2 d$). (At a given density $\eta_{\parallel,crit}$ is calculated from $b^2 - 4ac = 0$.) (ref. [80]).

$$\eta_{\parallel} < \eta_{\parallel,max} \simeq \frac{\left(\frac{\omega^2}{\omega^2_{LH,max}} - 1\right)}{2\sqrt{3}\left(\frac{v_e}{c}\right)\left(\frac{T_i}{T_e}\right)^{1/2}\left(1 + \frac{1}{4}\frac{T_e}{T_i}\frac{\omega^4}{\Omega_e^2\Omega_i^2}\right)^{1/2}}$$

$$= \frac{\left(\frac{\omega^2}{\omega^2_{LH,max}} - 1\right)\left(\frac{\omega^2_{pi}}{\omega^2}\right)}{\sqrt{3}\left(\frac{v_e}{c}\right)\left(\frac{\omega^2_{pe}}{\Omega_e^2}\right)\left(1 + \frac{4T_i/T_e}{\omega^4/\Omega_e^2\Omega_i^2}\right)^{1/2}} . \tag{3-27}$$

Equation (3-27) is obtained from $a^2 - 4bd = 0$ (i.e., $\epsilon_1^2 = 4\epsilon_3^2\eta_{\parallel}^2 d$), the condition that two branches of Eq. (3-20) (i.e., slow wave and hot ion wave branches) will coalesce.

Satisfying Eqs. (3-26) and (3-27) simultaneously imposes a minimum value on the frequency of the rf (LH) wave (i.e., $\omega > \omega_{min}$). For typical parameters of interest ($n \sim 10^{20}$ m^{-3}, $B \sim 5$ T, and $T \sim 15$ keV), $\omega_{min} \sim 1.5\text{-}1.8\ \omega_{LH,max}$.

An additional consideration in choosing the rf frequency is the necessity to avoid decay of the LH wave via various types of parametric instabilities which would transfer (damp) energy to the ions. Parametric instabilities (which we will not discuss here) would also distort the LH wave spectrum. Such a parametric decay of the LH waves has to be avoided for current generation purposes. Generally, these processes are avoided if $\omega > 2\omega_{LH,max}$.

Expressions given by Eqs. (3-26) and (3-27) are approximations to $b^2 - 4ac = 0$ and $a^2 - 4bd = 0$, respectively. Considering the full expressions, the various regions for wave-plasma interaction described above are depicted in Fig. 3.3. We see in Fig. 3.3 that $\eta_{\parallel,min}$ decreases with increasing magnetic field B whereas $\eta_{\parallel,max}$ decreases with higher T_e. For higher B, $n_{\parallel,max}$ increases (not shown in the figure), thus opening the accessibility window. The effect of density on $\eta_{\parallel}$ can also be deduced from Fig. 3.3. For a given magnetic field B, the lines shown in Fig. 3.3 are essentially for constant $\omega_{pe}^2/\Omega_e^2 \propto n/B^2$. Thus, for a given wave frequency ω/ω_{LH}, $\eta_{\parallel,min}$ increases while $\eta_{\parallel,max}$ decreases with density, resulting in a narrower accessibility window. These characteristics can easily be seen from Eqs. (3-26) and (3-27). Since the electron Landau damping is responsible for current

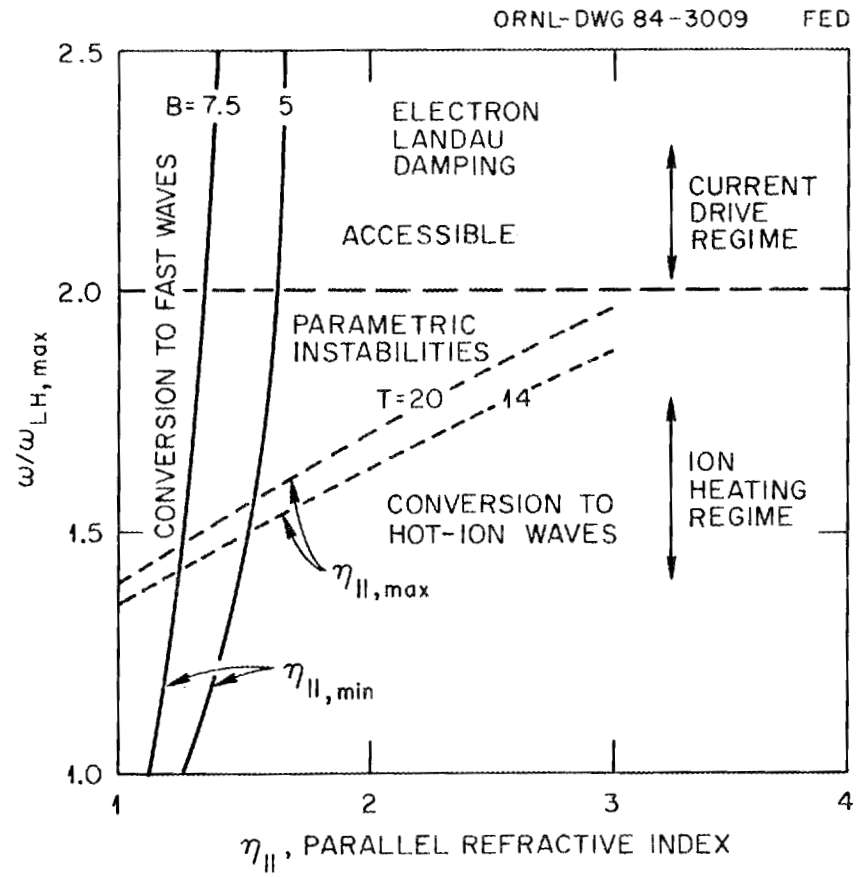

Fig. 3.3. Regions of wave plasma interaction in the parameter space of lower hybrid wave. The solid lines are $\eta_{\parallel,min}$ for $\overline{T}_e$ = 14 keV and B = 7.5 T, 5 T. The dashed lines are $\eta_{\parallel,max}$ for B = 7.5 T and $\overline{T}_e$ = 20, 14 keV. In all cases $\bar{n}_e = 10^{20}$ m^{-3}. [The lines shown represent constant $\omega_{pe}^2/\Omega_e^2 = (m_e/\epsilon_o)(n_e/B^2) = 10.278\ n_{20}/B^2$, where n_{20} is in units of 10^{20} m^{-3}. Thus, $\eta_{\parallel,min}$ lines are for $\omega_{pe}^2/\Omega_e^2 = 0.183$ and 0.41, corresponding to B = 7.5 and 5 T, respectively. $\eta_{\parallel,max}$ lines are for $\omega_{pe}^2/\Omega_e^2 = 0.183$ (or $n_{20}/B^2 \simeq 0.0178$).] (ref. [33]).

generation, one chooses the operating rf frequency to be in that region. Some specific numbers are given in Table 3.2 for hydrogen (H^+) and dueterium (D^+) plasmas. The density and temperature profiles (and central values of n and T) will significantly influence the wave propagation and the accessibility regime shown in Fig. 3.3. If one is not careful, current may be generated near the surface with a profile that may or may not be consistent with MHD equilibrium. Thus, depending on profiles, an additional constraint is imposed on $\eta_{\parallel,max}$ from the desire that only negligible current be generated outside some specified radius.

3.2. Current Generation and Power Absorption

The LH current drive, as mentioned earlier, is based on the damping of high-phase-velocity rf traveling waves. The damping of the waves causes the wave momentum to be given to the (resonant) electrons traveling with the wave parallel phase velocity, resulting in distortion of the electron distribution and formation of a velocity space plateau on the electron distribution function in the region of resonant particles (see Fig. 3.4). Because the wave travels in only one direction (unidirectional wave), the asymmetric electron distribution thus created results in a net current in the direction of the wave's phase velocity. Since these current-carrying electrons (high-energy tail electrons) are mostly traveling at several times the bulk electron thermal velocity, they collide relatively infrequently (i.e., collisionless) and thus retain their current (momentum) for an appreciable time.

The analysis of momentum and energy deposition on the electrons, and their subsequent transfer to the background ions and electrons, is carried out in terms of a Boltzmann equation for the electron velocity distribution. This equation balances the rf-induced quasi-linear diffusion of the electrons against the electron-electron and electron-ion collisional effects, as described by a Fokker-Planck collision operator [Eq. (1-9)]. In this section we describe the calculations and obtain the expressions for current density generated, power density dissipated, and the efficiency factor.

Table 3.2. Lower hybrid frequency at various densities and magnetic fields and corresponding limits on $\eta_{\parallel}$ due to mode conversions ($\overline{T}_e \simeq \overline{T}_i \simeq 15$ keV; $\omega/\omega_{LH,max} = 2.5$ are used)

n_e ($10^{20}m^{-3}$)	B (T)	ω_{pe}^2/Ω_e^2	$\omega_{pi}/2\pi$ H^+ / D^+ (GHz)	$f_{LH}(H^+)$ (GHz)	$f_{LH}(D^+)$ (GHz)	$\eta_{\parallel,min}$ [a]	$\eta_{\parallel,max}$ [b]
	4	0.32	1.48	1.29	0.91	1.62	7.05
0.5	6	0.14		1.38	0.98	1.35	8.26
	8	0.08	1.05	1.42	1.0	1.24	8.62
	4	0.64	2.1	1.64	1.16	1.97	5.61
1.0	6	0.29		1.85	1.3	1.58	7.24
	8	0.16	1.48	1.94	1.4	1.39	8.12
	4	1.28	2.97	1.97	1.39	2.52	4.38
2.0	6	0.57		2.38	1.68	1.9	5.85
	8	0.32	2.1	2.58	1.83	1.62	7.05

[a] Calculated from Eq. (3-26) for $\omega/\omega_{LH} = 2.5$.

[b] Calculated from Eq. (3.27) for $\omega/\omega_{LH} = 2.5$.

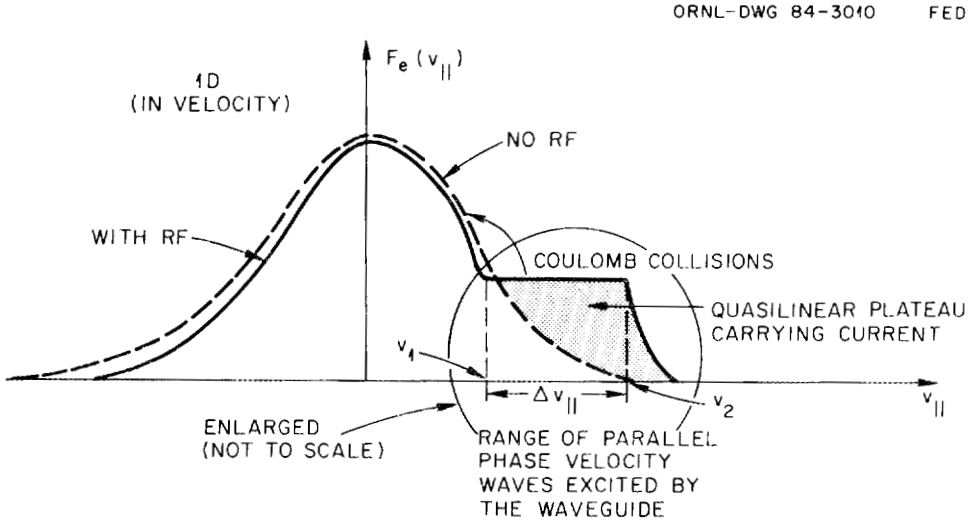

Fig. 3.4. Electron velocity distribution, $F_e(v_{\parallel}) = \int d\mathbf{v}_{\perp} f_e(\mathbf{v})$. The dotted line is the initial Maxwellian distribution (no rf). The solid line shows the distorted distribution formed by the spectrum of LH waves. A velocity space plateau is enlarged to illustrate the process. Region of resonant particles is $v_1 < v_{\parallel} < v_2$; $\Delta v_{\parallel} = v_2 - v_1$ (resonance is defined as $v_{p\parallel} = \omega/k_{\parallel} = v_{\parallel}$ where $v_{p\parallel}$ is parallel wave phase velocity) (ref. [33]).

3.2.1 Electron Distribution Function

We start from the Fokker-Planck equation, Eq. (1-9). The interaction between the plasma electrons and rf wave produces a time development of the electron distribution function, $f_e(\mathbf{v}, t) = f_e(v_\perp, v_\parallel, t)$, which can be represented symbolically as [18]

$$\frac{\partial f_e}{\partial t} = \left(\frac{\partial f_e}{\partial t}\right)_w + \left(\frac{\partial f_e}{\partial t}\right)_{coll} , \tag{3-28}$$

where the first term on the right side is due to the waves (velocity space diffusion caused by the wave) and the second term is due to Coulomb collisions (which describes both parallel and perpendicular velocity scattering). In general, there should be a third term on the right side of Eq. (3-28) that describes the effects of the inductive field, $(\partial f_e/\partial t)_{induct-E}$, a term that is important when rf-driven current replaces only part of the ohmic current. In the steady state, for a pure rf current-driven case, there is no dc electric field.

The LH waves are electrostatic and Landau damped by electrons resonant with the wave $(\omega/k_\parallel = v_\parallel)$. In the event that the waves are uncorrelated, diffusion of the electrons in parallel velocity space results [i.e., only the $\mathbf{v}_\parallel\mathbf{v}_\parallel$ component of the wave diffusion tensor $\overleftrightarrow{\mathbf{D}}$ is nonzero in Eq. (1-10)]:

$$\left(\frac{\partial f_e}{\partial t}\right)_w = \frac{\partial}{\partial v_\parallel} D_w(v_\parallel) \frac{\partial}{\partial v_\parallel} f_e , \tag{3-29}$$

where D_w is the rf quasi-linear diffusion coefficient due to Landau damping, given by

$$D_w(v_\parallel) = \frac{2\pi}{\epsilon_o}\left(\frac{e}{m_e}\right)^2 \frac{k_\parallel}{\omega} W_\parallel(k_\parallel)\Big|_{k_\parallel = \omega/v_\parallel} . \tag{3-30}$$

Here, $W_\parallel$ is the (one-sided) spectral energy density (power spectrum) of the wave, normalized so that

$$\frac{\epsilon_o}{2} E_{\parallel rms}^2 = \frac{\epsilon_o}{2} \langle E_\parallel \rangle^2 = \int_o^\infty dk_\parallel \, W_\parallel(k_\parallel) \ , \tag{3-31}$$

where $E_{\parallel rms} = \langle E_\parallel \rangle$ is the (time-averaged) rms of the applied wave electric field. It is this quasi-linear diffusion that tends to flatten the distribution. The collisions, on the other hand, tend to restore it to a Maxwellian (Fig. 3.4).

The term $(\partial f_e/\partial t)_{coll}$ in Eq. (3-28) is the Fokker-Planck collision operator, which has the following general form:

$$\left(\frac{\partial f_e}{\partial t}\right)_{coll} = \Gamma_{e,j} \left[-\frac{\partial}{\partial v_\alpha}\left(f_e \frac{\partial H}{\partial v_\alpha}\right) + \frac{1}{2}\frac{\partial^2}{\partial v_\alpha \partial v_\beta}\left(f_e \frac{\partial^2 G}{\partial v_\alpha \partial v_\beta}\right)\right] \ , \tag{3-32}$$

where summation over α and β are implied and

$$\Gamma_{e,j} = \frac{e^4 Z_j^2 \, \ell n \, \Lambda}{4\pi\epsilon_o^2 m_e^2} \ ,$$

with j = background particles (e,i). In Eq. (3-32) f_e is the (test-particle) electron distribution (i.e., the distribution of the electrons that carry the current), and H and G are Rosenbluth potentials, which are integrals over the background (field) particle distribution:

$$H(\mathbf{v}) = \frac{m_e}{M} \int \frac{f(\mathbf{v}_j)}{|\mathbf{v} - \mathbf{v}_j|} d\mathbf{v}_j = \frac{m_e}{M} \int \frac{f(\mathbf{v}_j)}{|\mathbf{v} - \mathbf{v}_j|} d^3 v_j \ , \tag{3-33a}$$

$$G(\mathbf{v}) = \int f(\mathbf{v}_j) \ |\mathbf{v} - \mathbf{v}_j| \ d^3 v_j \ , \tag{3-33b}$$

where $M = m_e m_j/(m_e + m_j)$ and j = background particles. Note that in Eq. (3-32) summation over all background particles j should be taken.

When computing $(\partial f_e/\partial t)_{coll}$, it is <u>generally</u> assumed that the background distributions of both ions and electrons are nondrifting, nonevolving Maxwellian distributions. Under this assumption Eq. (3-32) is linearized, and self-collisions among the non-Maxwellian components

of the electron distribution are neglected. (In some specific cases, however, self-collisions (electron-electron) were taken into account using the full Fokker-Planck collision operator, see for example ref. [18.]) In the limit where test particle (tail electron) velocity is much greater than the thermal velocity $v \gg v_e = (kT_e/m_e)^{1/2}$ and the backgound particle velocity v_j is less than or on order of the thermal velocity, Eq. (3-32) is linearized about a Maxwellian and substantially simplified. As a consequence of linearization and the associated assumptions just discussed, Eq. (3-28) becomes

$$\frac{\partial f_e}{\partial \tau} = \frac{\partial}{\partial U_{\parallel}} D(U_{\parallel}) \frac{\partial}{\partial U_{\parallel}} f_e + \frac{Z_i + 1}{4U^3} \frac{\partial}{\partial \xi} (1 - \xi^2) \frac{\partial}{\partial \xi} f_e$$

$$+ \frac{1}{2U^2} \frac{\partial}{\partial U} \left(\frac{1}{U} \frac{\partial}{\partial U} f_e + f_e \right), \tag{3-34}$$

where velocities are normalized to $v_e = (kT_e/m_e)^{1/2}$, time is normalized to ν_o^{-1}, and ξ is the pitch angle variable:

$$U = v/v_e \ , \quad U_{\parallel} = v_{\parallel}/v_e \ , \quad U^2 = U_{\perp}^2 + U_{\parallel}^2 \ ,$$

$$\tau = \nu_o t \ , \quad \nu_o = \ell n \ \Lambda \omega_{pe}^4 / 2\pi n v_e^3 = ne^4 \ \ell n \ \Lambda / 2\pi \epsilon_o^2 m_e^2 v_e^3 \ ,$$

$$\xi = U_{\parallel}/U = v_{\parallel}/v = \cos \theta \ ,$$

$$D(U_{\parallel}) = D_w(v_{\parallel})/(v_e^2 \nu_o) = \text{wave diffusion amplitude.}$$

In Eq. (3-34) symmetry is assumed in the azimuthal direction, with U representing the normalized velocity magnitude in spherical coordinates and θ the polar angle with respect to magnetic field. The first term on the right side of Eq. (3-34) is the quasi-linear rf diffusion term: in (U, ξ) coordinates the $\partial/\partial v_{\parallel}$ operator is expressed as

$$\frac{\partial}{\partial U_{\parallel}} = \xi \frac{\partial}{\partial U} + \frac{(1 - \xi^2)}{U} \frac{\partial}{\partial \xi} .$$

The second term represents pitch angle scattering off ions (with charge Z_i) and electrons. The last term represents energy scattering off electrons.

Equation (3-34) is a 2-D Fokker-Planck equation for the electrons, which can be solved numerically or analytically (under various assumptions and expansions). To gain some insight, we will assume (as is usually done) that the wave amplitude is sufficiently small so that electron distribution f_e is perturbed only sightly. Since the quasi-linear diffusion via the Landau damping causes electron velocity diffusion only parallel to the magnetic field, it is reasonable to assume that the electron velocity distribution remains approximately Maxwellian in the perpendicular direction. Under this assumption Eq. (3-34) is integrated over velocities perpendicular to the magnetic field, resulting in a 1-D quasi-linear equation for an electron distribution function:

$$\frac{\partial}{\partial \tau} F_e(U_{\parallel}) = \frac{\partial}{\partial U_{\parallel}} D(U_{\parallel}) \frac{\partial}{\partial U_{\parallel}} F_e(U_{\parallel}) + \frac{Z_i + 2}{2} \frac{\partial}{\partial U_{\parallel}} \left(\frac{1}{U_{\parallel}^3} \frac{\partial}{\partial U_{\parallel}} + \frac{1}{U_{\parallel}^2} \right) F_e(U_{\parallel}) . \tag{3-35}$$

Here, F_e is the reduced electron velocity distribution

$$F_e(v_{\parallel}) = \int d\mathbf{v}_{\perp} f_e(\mathbf{v})$$

and f_e varies as $\exp(-v_{\perp}^2/2v_e^2)$ with $v_{\perp}$ (the assumption of f_e being Maxwellian in the perpendicular direction).

We are primarily interested in the steady-state solutions to Eq. (3-35). Solving Eq. (3-35) for the steady-state distribution, we obtain

$$F_e(U_{\parallel}) = C \exp\left[- \int^{U_{\parallel}} \frac{U_{\parallel} dU_{\parallel}}{1 + 2U_{\parallel}^3 D(U_{\parallel})/(2 + Z_i)} \right] , \tag{3-36}$$

where C is constant, determined from normalization of the distribution function, $\int_{-\infty}^{\infty} F_e(U_\parallel)dU_\parallel = n_e$.

We see from Eq. (3-36) that in the absence of rf waves (D = 0) the distribution function is Maxwellian, that is,

$$F_e(U_\parallel) = C\ \exp\left(-U_\parallel^2/2\right) = C\ \exp\left(-v_\parallel^2/2v_e^2\right) .$$

The situation of interest for rf heating and especially for current generation is when $D(v_\parallel)$ is very large in a finite velocity interval, for example, $v_1 < v_\parallel < v_2$ (or $U_1 < U_\parallel < U_2$ in terms of normalized velocity), and vanishes elsewhere. We see from Eq. (3-36) that the 1-D solution for the distribution function $F_e(v_\parallel)$ is flat if D is large. This is the mechanism of Landau damping in the region of resonant particles, $v_1 < v_\parallel < v_2$ (Fig. 3.4), that is,

$$v_{p\parallel} - \Delta v_\parallel < v_\parallel < v_{p\parallel} + \Delta v_\parallel/2 \qquad v_{p\parallel} = \omega/k_\parallel , \tag{3-37}$$

where $\Delta v_\parallel \sim (e\Phi/m_e)^{1/2}$ with Φ being the potential field amplitude of the wave $\mathbf{E} = -\nabla\Phi$.

We now return to Eq. (3-30) and try to estimate the diffusion coefficient D_w, which depends on the wave spectrum. In general, the wave spectrum may be of arbitrary shape. Here we will assume a flat wave spectrum in the region of resonance ($v_\parallel = v_{p\parallel} = \omega/k_\parallel$):

$$W_\parallel(k_\parallel) = \begin{cases} W_o & k_2 < k_\parallel = \omega/v_\parallel < k_1 \\ 0 & \text{otherwise} \end{cases} \tag{3-38a}$$

or ($k_1 = \omega/v_1$, $k_2 = \omega/v_2$)

$$W_\parallel(v_\parallel) = \begin{cases} W_o & v_1 < v_\parallel = v_{p\parallel} < v_2 \\ 0 & \text{otherwise} \end{cases} \tag{3-38b}$$

That is, the spectral energy density is centered at $k_{\parallel} = \omega/v_{\parallel}$, corresponding to phase velocity $v_{\parallel} = v_{p\parallel}$ over a narrow width $\Delta k_{\parallel} = k_1 - k_2$ $(\Delta v_{\parallel} = v_2 - v_1)$ of parallel wave numbers (of parallel velocities). Using Eqs. (3-38) and (3-31), we can then approximate Eq. (3-30) as

$$D_w(v_{\parallel}) = \begin{cases} \dfrac{e^2}{m_e^2} \dfrac{\langle E_{\parallel}\rangle^2}{\Delta k_{\parallel}} \dfrac{\pi}{v_{\parallel}} & v_1 < v_{\parallel} < v_2 \\ 0 & \text{otherwise} \end{cases} \tag{3-39a}$$

or, in terms of normalized quantities,

$$D(U_{\parallel}) = D_w(v_{\parallel})/(v_e^2 \nu_o) = \begin{cases} D_o/U_{\parallel} & U_1 < U_{\parallel} < U_2 \\ 0 & \text{otherwise} \end{cases}, \tag{3-39b}$$

where $U_1 = v_1/v_e \left[= (v_{p\parallel} - \Delta v_{\parallel}/2)/v_e\right]$, $U_2 = v_2/v_e$, $U_{\parallel} = v_{\parallel}/v_e$, and

$$D_o = \frac{\pi e^2}{m_e^2} \frac{\langle E_{\parallel}\rangle^2}{\Delta k_{\parallel}} \frac{1}{\nu_o v_e^3} = \frac{2\pi^2 \epsilon_o}{ne^2 \ln \Lambda} \frac{\langle E_{\parallel}\rangle^2}{\Delta k_{\parallel}} . \tag{3-40}$$

Using Eq. (3-39) in Eq. (3-36), the steady-state solution of Eq. (3-35) is given by

$$F_e(U_{\parallel}) = \begin{cases} Ce^{-U_{\parallel}^2/2} & U_{\parallel} < U_1 \\ Ce^{-U_1^2/2} \left(\dfrac{1 + \bar{D}_o U_1^2}{1 + \bar{D}_o U_{\parallel}^2}\right)^{1/2\bar{D}_o} & U_1 \le U_{\parallel} \le U_2 , \\ Ce^{(U_2^2 - U_1^2)/2} \left(\dfrac{1 + \bar{D}_o U_1^2}{1 + \bar{D}_o U_2^2}\right)^{1/2\bar{D}_o} e^{-U_{\parallel}^2/2} & U_{\parallel} > U_2 \end{cases} \tag{3-41}$$

where $\bar{D}_o = 2D_o/(Z_i + 2)$ and the constant C, as mentioned before, is determined by conservation of particles

$$n_e = \int F_e(U_\parallel)\, dU_\parallel \ .$$

If the number density of electrons in the quasi-linear resonance region is small compared to n_e, then C is approximately the usual Maxwellian value, $C = n_e/(2\pi)^{1/2} v_e$.

Equation (3-41) is the solution of Eq. (3-28) in the high-velocity limit and considering only one dimension (parallel velocity). Two-dimensional modeling of the problem is also possible, in which case analytic solutions in limiting cases and numerical solutions by considering the full Fokker-Planck equation can be found in the references given. In order to appreciate the structure of the solution of Eq. (3-28) [which is given by Eq. (3-41) in the 1-D limit considered here], we choose a representative case characterized by the following parameters [16]:

$$Z_i = 1 \ ,$$

$$v_1 = 3\ v_e \qquad (U_1 = 3) \ ,$$

$$v_2 = 5\ v_e \qquad (U_2 = 5) \ ,$$

$$D_w = \frac{1}{2} v_e^2 \nu_o \qquad \left(D = 1/2 \ ; \ \ D_o = \frac{U_\parallel}{2} = \frac{v_\parallel}{2v_e}\right) .$$

Figure 3.5 shows the steady-state solution obtained numerically by solving the 2-D Fokker-Planck equation [16]. In the resonant region ($v_1 < v_\parallel < v_2$), the electrons are approximately plateaued. A significant flattening in the perpendicular direction is also evident in Fig. 3.5, which the 1-D model does not account for (since a Maxwellian perpendicular distribution is assumed in a 1-D model).

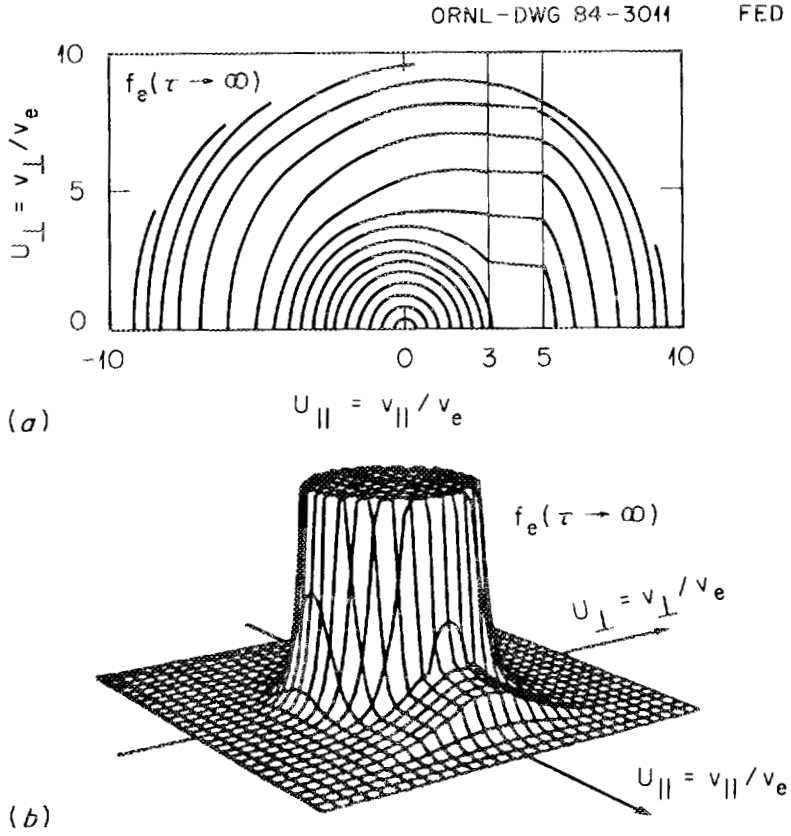

Fig. 3.5. Steady-state distribution function f_e for $Z_i = 1$, $D = 1/2$, $U_1 = 3$, and $U_2 = 5$. (a) Contours of constant $f_e(U_\parallel, U_\perp)$. [Note that for a Maxwellian distribution contours of f_e would be circles.] Notice the deformation of contours near the region of resonance $(U_1 < U_\parallel < U_2)$. (b) The surface $f_e(U_\perp, U_\parallel)$. This is truncated at $f_e(\text{maximum})/50$ in order to show the plateau clearly. In the resonant region plateau in the parallel direction is clearly apparent. There is significant flattening in the perpendicular direction, also (ref. [16]).

By integrating the distribution function shown in Fig. 3.5 over the perpendicular velocity space $[\int f_e \, d\mathbf{v}_\perp = F_e(v_\parallel)]$, we obtain the parallel distribution function $F_e(U_\parallel)$ as shown in Fig. 3.6, which clearly exhibits the current-carrying plateau. Note that $F_e(U_\parallel > U_2)$ drops off more slowly than a Maxwellian distribution with the original temperature would [see analytic solution given by Eq. (3-41) for $U_\parallel > U_2$]. Also note that $F_e(U_\parallel > U_2)$ greatly exceeds the original Maxwellian distribution, a feature that can also be seen from Eq. (3-41).

3.2.2 Current Density

The current density generated can now be obtained from Eq. (3-41) by integrating over velocity space:

$$J = -e \int dv_\parallel \, v_\parallel F_e(v_\parallel) = -ev_e^2 \int dU_\parallel \, U_\parallel F_e(U_\parallel)$$

$$= en_e v_e f_o(U_1) \left\{ -1 + \frac{(1 + \bar{D}_o U_1^2)^{1/2\bar{D}_o}}{(2\bar{D}_o - 1)} \left[(1 + \bar{D}_o U_2^2)^{1-1/2\bar{D}_o} - (1 + \bar{D}_o U_1^2)^{1-1/2\bar{D}_o} \right] + \left(\frac{1 + \bar{D}_o U_1^2}{1 + \bar{D}_o U_2^2} \right)^{1/2\bar{D}_o} \right\} , \qquad (3\text{-}42)$$

where $f_o(U_1) = (2\pi)^{-1/2} \exp(-U_1^2/2)$. When $\bar{D}_o \gg 1$ $(\bar{D}_o U_1^2 \gg 1)$ Eq. (3-42) reduces to

$$J \simeq en_e v_e f_o(U_1) \left(\frac{U_2^2 - U_1^2}{2} \right) = en_e v_e \frac{\exp(-U_1^2/2)}{(2\pi)^{1/2}} \left(\frac{U_2^2 - U_1^2}{2} \right)$$

$$= en_e v_e \frac{\exp\left(-v_1^2/2v_e^2\right)}{(2\pi)^{1/2}} \left(\frac{v_2^2 - v_1^2}{2v_e^2} \right) \qquad (3\text{-}43)$$

$$\simeq 6.72 \times 10^8 n_{20} T_{10}^{1/2} \, f_o(U_1) \left(\frac{U_2^2 - U_1^2}{2} \right) .$$

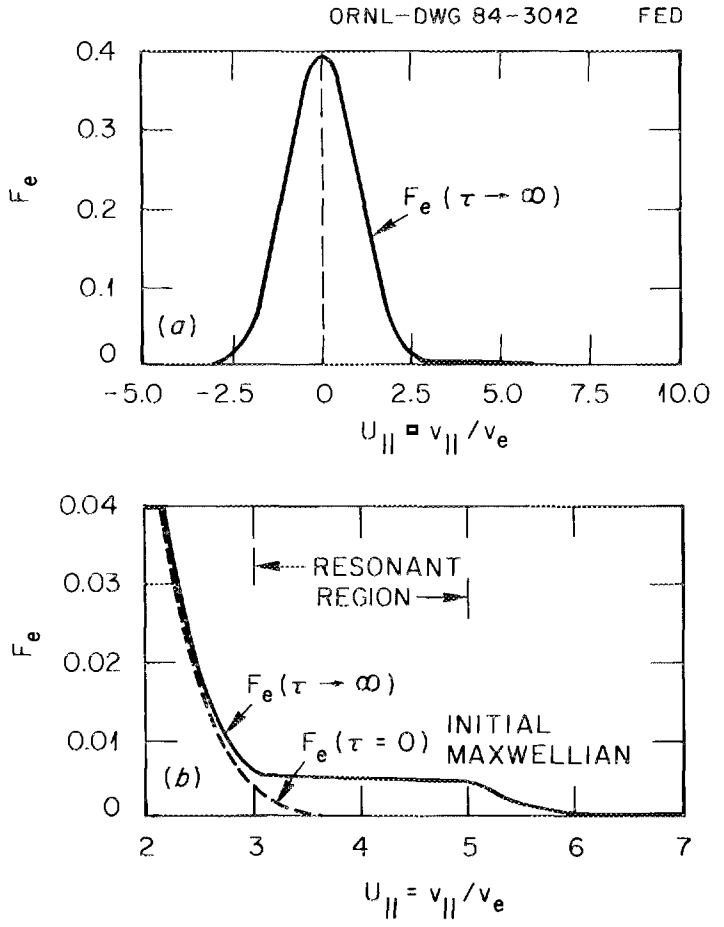

Fig. 3.6. The parallel distribution function $F_e(U_{\parallel})$ for the case shown in Fig. 3.5. In (b) the vertical scale has been magnified tenfold over that in (a). Initial Maxwellian distribution $F_e(\tau \to 0)$ is shown with dashed lines in (b). The current-carrying plateau is clearly seen in (b). Notice that for $U_{\parallel} > U_2$ ($U_{\parallel} > 5$) F_e drops off more slowly than a Maxwellian distribution with the original temperature would. These features can also be seen from Eq. (3-41) (ref. [16]).

Normalized current density is simply

$$\hat{J} = J/en_e v_e = \frac{\exp(-v_1^2/2v_e^2)}{(2\pi)^{1/2}} \left(\frac{v_2^2 - v_1^2}{2v_e^2}\right)$$

$$= f_o(U_1)\left(\frac{U_2^2 - U_1^2}{2}\right). \tag{3-44}$$

We can rewrite Eqs. (3-43) and (3-44) in terms of the parallel refractive index $\eta_{\parallel}$ $(= ck_{\parallel}/\omega)$ as

$$J = \frac{en_e(kT_e/m_e)^{1/2}}{(2\pi)^{1/2}} \left(\frac{m_e c^2}{2T_e}\right) \exp\left[-\left(\frac{m_e c^2}{2T_e}\right)\frac{1}{\eta_1^2}\right] \left(\frac{1}{\eta_2^2} - \frac{1}{\eta_1^2}\right)$$

$$= 2.166 \times 10^{-10} \frac{n_e}{T_e^{1/2}} \exp\left(-\frac{255.5}{T_e\eta_1^2}\right)\left(\frac{1}{\eta_2^2} - \frac{1}{\eta_1^2}\right) \quad (A/m^2) \tag{3-45}$$

$$\simeq 6.85 \times 10^9 \frac{n_{20}}{T_{10}^{1/2}} \exp\left(-\frac{25.6}{T_{10}\eta_1^2}\right)\left(\frac{1}{\eta_2^2} - \frac{1}{\eta_1^2}\right) \quad (A/m^2)$$

and

$$\hat{J} = \frac{1}{(2\pi)^{1/2}} \left(\frac{m_e c^2}{2T_e}\right) \exp\left[-\left(\frac{m_e c^2}{2T_e}\right)\frac{1}{\eta_1^2}\right]\left(\frac{1}{\eta_2^2} - \frac{1}{\eta_1^2}\right) \tag{3-46}$$

$$= \frac{101.93}{T_e} \exp\left(-\frac{255.5}{T_e\eta_1^2}\right)\left(\frac{1}{\eta_2^2} - \frac{1}{\eta_1^2}\right)$$

$$\simeq \frac{10.2}{T_{10}} \exp\left(-\frac{25.6}{T_{10}\eta_1^2}\right)\left(\frac{1}{\eta_2^2} - \frac{1}{\eta_1^2}\right), \tag{3-47}$$

where $\eta_1^2 = c^2k_1^2/\omega^2 = c^2/v_1^2$, $\eta_2^2 = c^2k_2^2/\omega^2 = c^2/v_2^2$, and $v_e = (kT_e/m_e)^{1/2}$ with $m_ec^2 \simeq 511$ keV. (All are in mks units, T_e is in keV, and as before, $n_{20} = n_e/10^{20}$ m^{-3}, $T_{10} = T_e/10$ keV.)

As mentioned earlier and as Eq. (3-41) and Fig. 3.6 show, the electron distribution function at $U_\parallel > U_2$ ($v_\parallel > v_2$ or $\eta_\parallel < \eta_2$) greatly exceeds the original Maxwellian distribution. Thus, current is carried not only by resonant electrons with $v_1 \leq v_\parallel \leq v_2$ but also by tail electrons with $v_\parallel > v_2$. Figure 3.7 shows the fraction of total current carried by resonant electrons under the plateau. For the example considered in Figs. 3.5 to 3.6, more than 90% of the current generated by rf waves is carried by the resonant electrons in the plateau, that is, a case for $U_1 = 3$, $U_2 = 5$. For a high-temperature, reactor-like plasma, (e.g., $T_e \simeq 10$–15 keV), $3 < U_\parallel < 5$ corresponds to $v_\parallel/c \simeq 0.4$–0.8 (or $\eta_\parallel \sim 1.25$–2.5), in which the resonant electrons may become relativistic. For this case, relativistic effects will be more important for tail electrons with $v_\parallel > v_2$ ($> v_1$), which are not included here (some discussion of this will be given later). For moderate values of $U_1 \simeq 2$, $U_2 \simeq 2.5$, we see from Fig. 3.7 that more than half of the current generated by rf waves will be carried by the fast tail electrons.

3.2.3 Power Dissipation

In the steady state, the power dissipated by the waves in the resonant electrons is balanced by the power dissipated in the other particles (bulk electrons and ions) via collisional slowing down of these fast, resonant electrons. Thus, the power density dissipated by the rf wave for maintenance of the quasi-linear distortion of F_e is given by

$$P_{rf} = \int d\mathbf{v}\, \frac{1}{2} mv^2 \left(\frac{\partial f_e}{\partial t}\right)_w \tag{3-48a}$$

$$= \int d^3v\, \frac{1}{2} mv^2 \frac{\partial}{\partial v_\parallel} D_w(v_\parallel) \frac{\partial}{\partial v_\parallel} f_e(v) \tag{3-48b}$$

$$= mv_e^2\nu_o \int d^3U\, \frac{1}{2} U^2 \frac{\partial}{\partial U_\parallel} D(U_\parallel) \frac{\partial}{\partial U_\parallel} f_e(U)$$

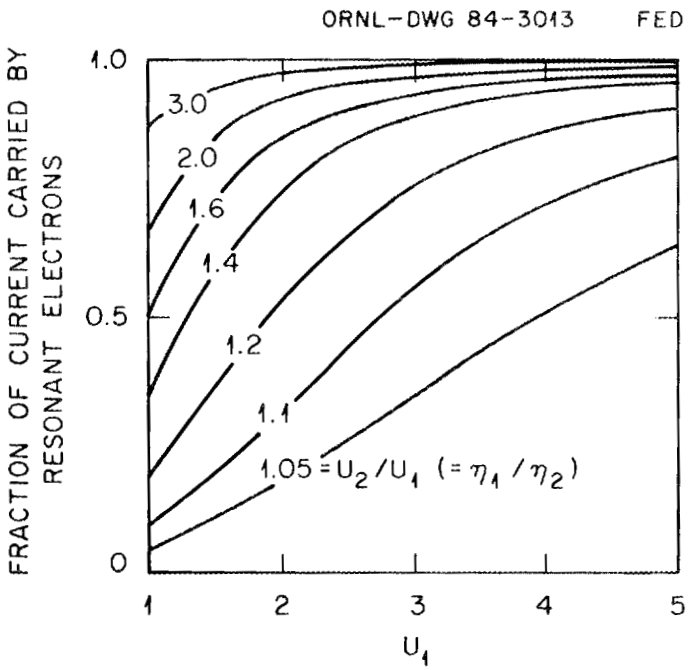

Fig. 3.7. Fraction of rf-generated current carried by resonant electrons ($U_1 < U_{\parallel} < U_2$) is shown as a function of U_1 for various U_2/U_1 ($= \eta_1/\eta_2$) for LH waves (ref. [33]).

$$= - m v_e^2 \nu_o \int_{U_1}^{U_2} dU_\parallel U_\parallel D(U_\parallel) \frac{\partial}{\partial U_\parallel} F_e(U_\parallel) \ , \tag{3-48c}$$

where we used integration by parts in obtaining the last step (other notations are as introduced before). Using Eq. (3-41) in (3-48c) and considering the limit where $DU_\parallel^3 >> 1$ (or $D_o U_\parallel^2 >> 1$), Eq. (3-48c) can be approximated as

$$P_{rf} = \alpha \left(\frac{2 + Z_i}{2}\right) n_e m_e v_e^2 \nu_o f_o(U_1) \ \ell n \left(\frac{U_2}{U_1}\right)$$

$$= \alpha \left(\frac{2 + Z_i}{2}\right) \frac{n_e m_e v_e^2 \nu_o}{(2\pi)^{1/2}} \exp(-U_1^2/2) \ \ell n \left(\frac{U_2}{U_1}\right)$$

$$= \alpha n_e m_e v_e^2 \nu_o \left(\frac{Z_i + 2}{2}\right) \frac{\exp(-v_1^2/2v_e^2)}{(2\pi)^{1/2}} \ \ell n \left(\frac{v_2}{v_1}\right) \quad (W/m^3) \ , \tag{3-49}$$

where α is a correction factor obtained by numerically solving the 2-D Fokker-Planck equation with a quasi-linear term. In general, $\alpha = \alpha(Z_i)$ is a sensitive function of Z_i [16]. For $Z_i = 1$, $\alpha \simeq 0.4$.

Normalized power density is simply

$$\hat{P} = \alpha \left(\frac{Z_i + 2}{2}\right) \frac{1}{(2\pi)^{1/2}} \exp(-v_1^2/2v_e^2) \ \ell n \left(\frac{v_2}{v_1}\right)$$

$$= \alpha \left(\frac{Z_i + 2}{2}\right) \frac{1}{(2\pi)^{1/2}} \exp\left[-\left(\frac{m_e c^2}{2T_e}\right) \frac{1}{\eta_1^2}\right] \ \ell n \left(\frac{\eta_1}{\eta_2}\right)$$

$$= \frac{\alpha}{(2\pi)^{1/2}} \left(\frac{Z_i + 2}{2}\right) \exp\left(-\frac{255.5}{T_e \eta_1^2}\right) \ell n \left(\frac{\eta_1}{\eta_2}\right) . \tag{3-50}$$

In practical units, Eq. (3-49) can be rewritten as

$$P_{rf} = \alpha\left(\frac{Z_i + 2}{2}\right)\frac{n_e^2 e^4 \ \ell n \ \Lambda}{2\pi\epsilon_o^2 m_e^{1/2}(kT_e)^{1/2}}\frac{\exp(-v_1^2/2v_e^2)}{(2\pi)^{1/2}} \ \ell n \left(\frac{v_2}{v_1}\right)$$

$$\simeq 1.11 \times 10^{-31} \ \alpha \left(\frac{Z_i + 2}{2}\right)\frac{n_e^2 \ \ell n \ \Lambda}{T_e^{1/2}}\frac{\exp(-v_1^2/2v_e^2)}{(2\pi)^{1/2}} \ \ell n \left(\frac{v_2}{v_1}\right)$$

$$\simeq 1.32 \times 10^{-30} \ \alpha \frac{n_e^2}{T_e^{1/2}}\left(\frac{\ell n \ \Lambda}{20}\right)\exp(-v_1^2/2v_e^2) \ \ell n \left(\frac{v_2}{v_1}\right) \quad (W/m^3)$$

$$\simeq 4.19 \times 10^{9} \ \alpha \frac{n_{20}^2}{T_{10}^{1/2}}\left(\frac{\ell n \ \Lambda}{20}\right)\exp(-v_1^2/2v_e^2) \ \ell n \left(\frac{v_2}{v_1}\right) \quad (W/m^3)$$

$$\simeq 10^{10} \ \alpha \frac{n_{20}^2}{T_{10}^{1/2}}\left(\frac{\ell n \ \Lambda}{20}\right) f_o(U_1) \ \ell n \left(\frac{U_2}{U_1}\right) \quad (W/m^3) \ ,$$

where $Z_i = 1$ is assumed; n_{20} and T_{10} are in units of 10^{20} m^{-3} and 10 keV, respectively; and $\alpha \simeq 0.4$ is the numerical correction factor.

3.2.4 Efficiency Factor

A crucial parameter by which the practicality of a current drive scheme may be assessed is J/P, the amount of current generated per power dissipated. This is the measure of the efficiency of a current drive scheme (see Sect. 2.1.4). From Eqs. (3-43) and (3-49) we have the following expression for J/P:

$$J/P_{rf} = \left(\frac{2\ \alpha^{-1}}{Z_i + 2}\right) \frac{e}{2m_e v_e^3 \nu_o} \frac{(v_2^2 - v_1^2)}{\ell n\ (v_2/v_1)}$$

$$= \left(\frac{2\ \alpha^{-1}}{Z_i + 2}\right) \frac{\pi \epsilon_o^2 m_e}{n_e e^3\ \ell n\ \Lambda} \frac{(v_2^2 - v_1^2)}{\ell n\ (v_2/v_1)} \tag{3-51a}$$

$$\simeq 2.73 \times 10^3 \left(\frac{2\ \alpha^{-1}}{Z_i + 2}\right)\left(\frac{20}{\ell n\ \Lambda}\right) \frac{1}{n_e} \frac{(v_2^2 - v_1^2)}{\ell n\ (v_2/v_1)}\ . \tag{3-51b}$$

For $Z_i = 1$, $\alpha = 0.4$, and in terms of refractive index we have

$$J/P_{rf} \simeq 4.08 \times 10^{20} \left(\frac{20}{\ell n\ \Lambda}\right) \frac{1}{n_e} \left(\frac{1}{\eta_2^2} - \frac{1}{\eta_1^2}\right)\left(\ell n\ \frac{\eta_1}{\eta_2}\right)^{-1}$$

$$= \frac{4.08}{n_{20}} \left(\frac{20}{\ell n\ \Lambda}\right) \frac{\eta_2^{-2} - \eta_1^{-2}}{\ell n\ (\eta_1/\eta_2)}\ . \tag{3-52}$$

Expression (3-51) [or (3-52)] shows us that J/P_{rf} is independent of T_e, is inversely proportional to n_e, and varies rather rapidly with the phase velocity of the rf wave. In terms of normalized quantities,

$$\hat{J}/\hat{P} = \left(\frac{2\ \alpha^{-1}}{Z_i + 2}\right) \frac{(U_2^2 - U_1^2)/2}{\ell n\ (U_2/U_1)} = \left(\frac{2\ \alpha^{-1}}{Z_i + 2}\right) \frac{(v_2^2 - v_1^2)/2v_e^2}{\ell n\ (v_2/v_1)} \tag{3-53a}$$

$$= \left(\frac{2\ \alpha^{-1}}{Z_i + 2}\right) \langle U_{\parallel}^2 \rangle\ , \tag{3-53b}$$

where we defined

$$\langle U_{\parallel}^2 \rangle \equiv \left\langle \left(\frac{v_{\parallel}}{v_e}\right)^2 \right\rangle \equiv \frac{1}{2}\frac{U_2^2 - U_1^2}{\ell n\ (U_2/U_1)} = \frac{\Delta U_{\parallel}}{2}\frac{U_1 + U_2}{\ell n\ (U_2/U_1)}$$

$$\simeq \frac{U_1^2 + U_2^2}{2}\left[1 + 0\left(\frac{\Delta U_{\parallel}}{U_1}\right)^2\right] . \tag{3-54}$$

Here $\Delta U_{\parallel} = U_2 - U_1 = \Delta v_{\parallel}/v_e$. For a narrow spectrum $\langle U_{\parallel}^2 \rangle \approx U_1^2$. For $\alpha \simeq 0.4$ and $Z_i = 1$, we have

$$\hat{J}/\hat{P} \simeq 1.7\langle U_{\parallel}^2 \rangle \simeq 1.7\,\frac{(U_2^2 - U_1^2)/2}{\ell n\ (U_2/U_1)} . \tag{3-55}$$

In terms of the amount of current generated, we have from Eq. (3-51) [or (3-52)]

$$\frac{n_{20}R_o(m)\ I(MA)}{P_{rf}(MW)} \simeq 7.8\left(\frac{2\ \alpha^{-1}}{Z_i + 2}\right)\frac{1}{\ell n\ \Lambda}\frac{(\eta_2^{-2} - \eta_1^{-2})}{\ell n\ (\eta_1/\eta_2)}$$

$$\simeq \frac{26}{\ell n\ \Lambda}\frac{1}{\langle \eta_{\parallel}^2 \rangle} = 1.3\left(\frac{20}{\ell n\ \Lambda}\right)\frac{1}{\langle \eta_{\parallel}^2 \rangle} , \tag{3-56}$$

where we defined

$$\frac{1}{\langle \eta_{\parallel}^2 \rangle} \equiv \frac{1}{2}\frac{1}{\ell n\ (\eta_1/\eta_2)}\left(\frac{1}{\eta_2^2} - \frac{1}{\eta_1^2}\right)$$

$$= \frac{\langle U_{\parallel}^2 \rangle}{(c/v_e)^2} = \left(\frac{v_e}{c}\right)^2 \langle U_{\parallel}^2 \rangle = \left(\frac{T_e}{511}\right)\langle U_{\parallel}^2 \rangle . \tag{3-57}$$

It is apparent from these expressions that small $\eta_{\parallel}$ is required to generate current effectively. Figure 3.8 plots J/P for various

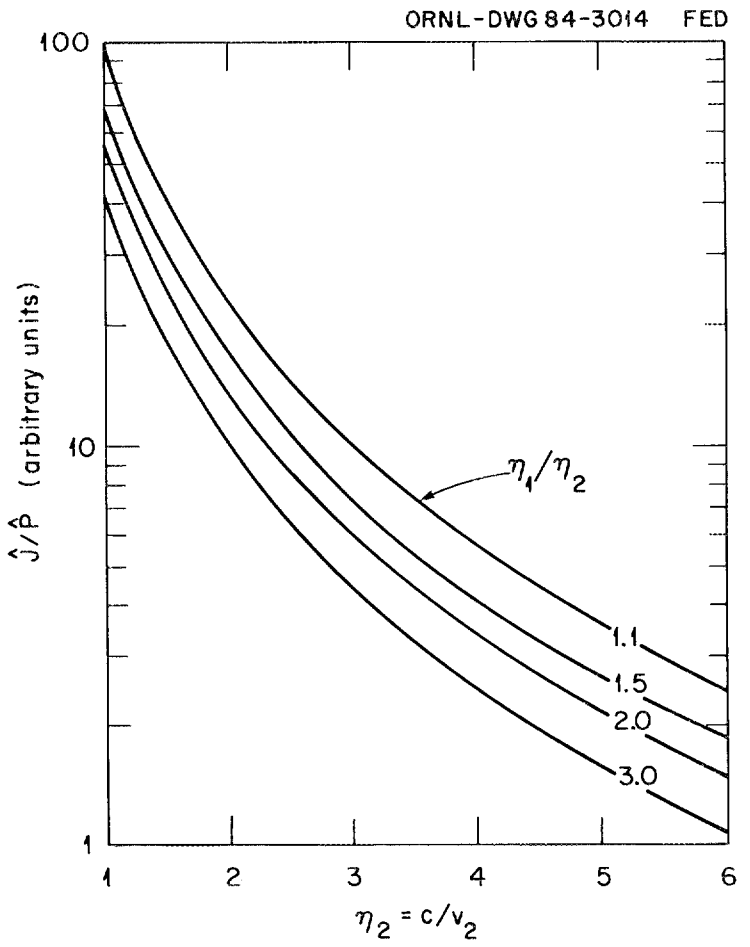

Fig. 3.8. Effectiveness of current drive by LH waves as a function of parallel refractive index of LH waves.

$\eta_1 (= c/v_1)$ and $\eta_2 (= c/v_2)$. As we discussed in Sect. 3.1.2, the minimum $\eta_\parallel$ (η_2) allowed in the plasma is limited by the accessibility criterion of the LH wave (among other constraints).

For resonant electrons ($v_1 < v_\parallel < v_2$), we choose $\eta_\parallel$ such that

$$\eta_2 < \eta_\parallel < \eta_1$$

with

$$\eta_2 \geq \eta_{\parallel,min} , \qquad \eta_1 \leq \eta_{\parallel,max} ,$$

where $\eta_{\parallel,min}$ and $\eta_{\parallel,max}$ are given by Eqs. (3-26) and (3-27), respectively. To obtain reasonable efficiencies (Fig. 3.8) a fairly narrow spectral width would be required, that is,

$$\Delta\eta_\parallel/\eta_\parallel \doteq (\eta_1 - \eta_2)/\eta_\parallel \simeq 0.2 .$$

3.3. **Experiments** [19-28,31,35-40]

By far the most experimentally used method of driving currents in tokamaks has been the use of LH waves. These include the following tokamaks: Princeton Large Torus (PLT) at Princeton [19-21,27,38], Alcator-C at Massachusetts Institute of Technology (MIT) [22,26,31,36], Frascati Tokamak (FT) in Frascati [28,37], Wega at Grenoble [23,30], T-7 at Kurchatov [40], JFT-2 at JAERI [35], Versator II at MIT [26,36], WT-2 [25,39], and several others. A summary of the parameters of these experiments is given in Table 3.1. One of the principal achievements has been the maintenance of the current with rf power alone for extended durations in Alcator-C and PLT (listed as "steady-state" in Table 3.1, where "steady state" refers to the fact that both the magnitude and profile of the current do not change, that is, no redistribution of current). In both of these experiments the OH current has been terminated, and the plasma current produced by rf has been kept constant (flat top) for periods longer than the L/R time (where L is the total inductance of the plasma and R is the plasma

resistance), a necessary condition for eliminating transient currents and unambiguously demonstrating rf current drive. This is shown in Fig. 3.9 for the longest pulse generated in PLT. In the following we discuss some of the results observed from these experiments: (1) demonstration of current drive, (2) current drive efficiency, (3) density limit, (4) spectral gap, (5) current ramp up, etc.

3.3.1 Demonstration of Current Drive

In a toroidal system the current flow can be strongly influenced by electric fields induced by changes in the poloidal magnetic field. Demonstration of rf current drive can be decided by examining the power flow relationship [20]:

$$I_p^2 R + \frac{d}{dt}(LI_p^2/2) = I_p(M_{OH}dI_{OH}/dt + M_v dI_v/dt) + P_{rf} , \qquad (3\text{-}58)$$

where I_p is the plasma current; R is the plasma resistance; $L = \mu_o R_o[\ell n\ (8R_o/a) - 2 + \ell_i/2]$ is the total inductance of the plasma; a and R_o are the minor and major radii; $\mu_o R_o \ell_i/2$ is the internal inductance; M_{OH} and M_v are the mutual inductances between the plasma current and the OH primary and vertical (equilibrium) field coils, respectively; and P_{rf} is the rf power driving the current. To demonstrate rf, current drive conditions have been produced in the experiments such that the I^2R_p and P_{rf} terms of Eq. (3-58) are the only dominant ones:

$$P_{rf} \simeq I^2 R_p .$$

A typical current drive shot in the PLT tokamak with and without rf power is shown in Fig. 3.10. Here the waveguides are phased 90° ($\Delta\phi = \pi/2$), and 130 kW of rf power (f = 0.8 GHz) is applied for a period of up to 1 s after the primary ohmic current is terminated. The plasma current was maintained at 240 kA during the rf pulse. The average density is initially $\bar{n} \simeq 7 \times 10^{12}$ cm^{-3} (to suppress runaways); then, it is maintained flat at $\bar{n} \simeq 3.5 \times 10^{12}$ cm^{-3}. A long-pulse current drive on PLT is shown in Fig. 3.9 in which a plasma current of

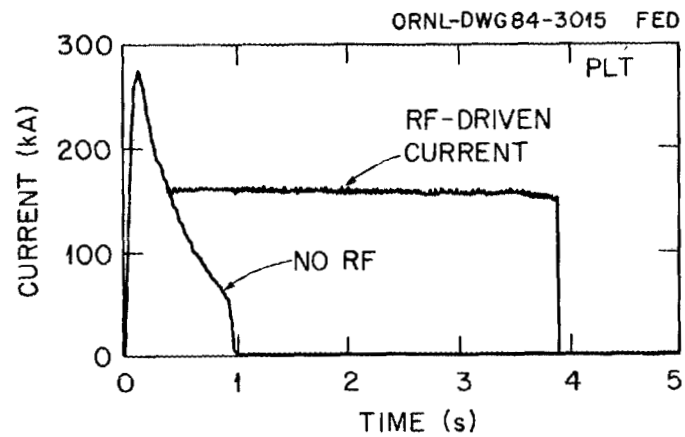

Fig. 3.9. Long-pulse current drive on PLT. The plasma is formed by the OH system, which was turned off at the current peak. Lower hybrid power P_{rf} = 70 kW, B_o = 2.3 T, and $\bar{n}_e \simeq 3 \times 10^{18}$ m^{-3} (refs. [19, 20, 27]).

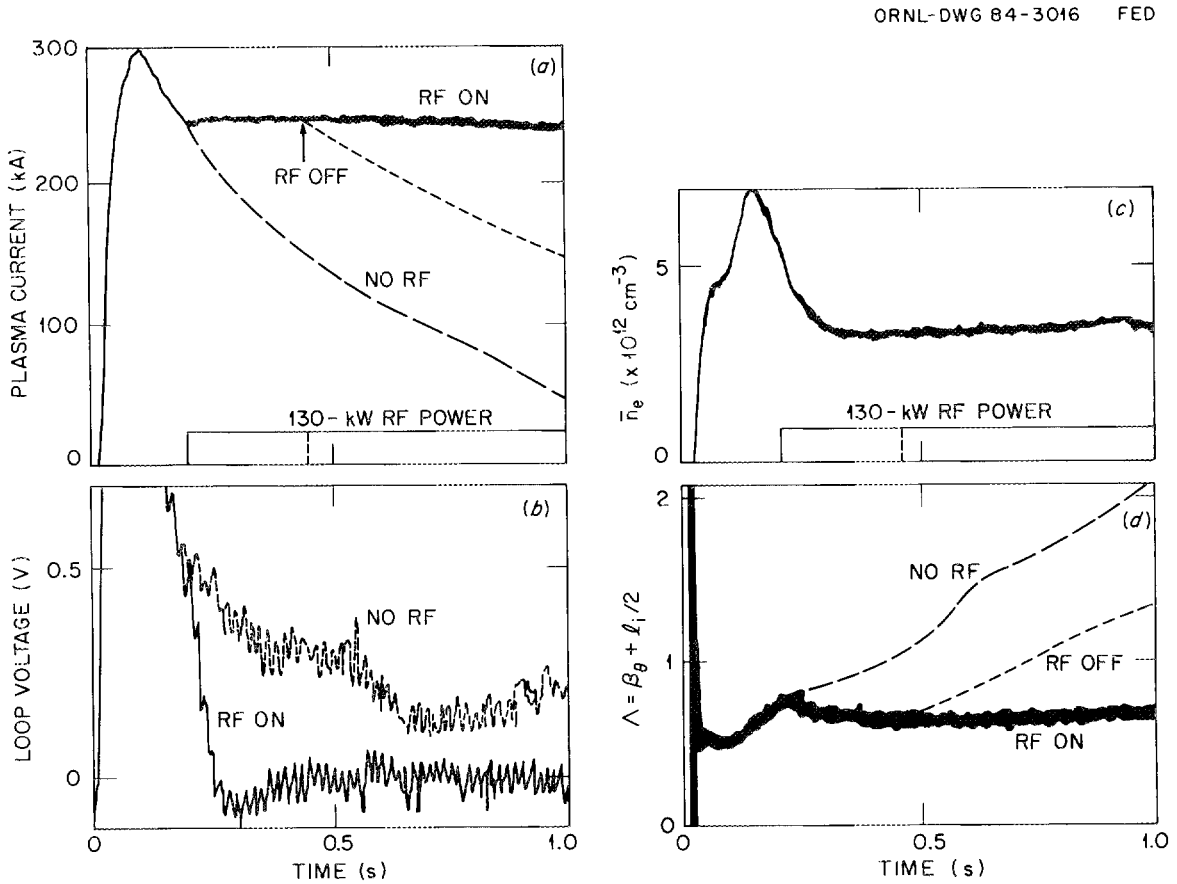

Fig. 3.10. A typical current drive shot in the PLT tokamak with (solid lines) and without (dashed lines) rf-power: (a) plasma current, (b) loop voltage, (c) average plasma density, and (d) $\beta_\theta + \ell_i/2$ (β_θ = poloidal beta) (ref. [20]).

165 kA was maintained for ~3.5 s. Although results shown in Figs. 3.9 and 3.10 were obtained at relatively low densities, similar results were obtained on the Alcator-C tokamak at higher densities ($\bar{n} \simeq 3 \times 10^{13}$ cm^{-3}), as shown in Fig. 3.11.

3.3.2 Current Drive Efficiency

As we have seen, the current drive efficiency may be written in the following form:

$$\frac{R_o\ (m)\ n_{20} I\ (MA)}{P\ (MW)} = 0.015 \left(\frac{20}{\ell n\ \Lambda}\right) T_{10} \frac{\hat{J}}{\hat{P}}\ , \tag{3-59}$$

where $\hat{J}/\hat{P}$ is the normalized current drive efficiency for LH waves, given in Sect. 3.2.4 [see Eqs. (3-51)-(3-56)],

$$\frac{\hat{J}}{\hat{P}} = \left(\frac{2\alpha^{-1}}{Z_i + 2}\right) \langle U_{\parallel}^2 \rangle \simeq 1.7\ \langle U_{\parallel}^2 \rangle$$

or

$$\frac{\hat{J}}{\hat{P}} = \left(\frac{2\alpha^{-1}}{Z_i + 2}\right) \left(\frac{c}{v_e}\right)^2 \frac{1}{\langle \eta_{\parallel}^2 \rangle} \simeq \frac{85.2}{T_{10}} \frac{1}{\langle \eta_{\parallel}^2 \rangle}\ ,$$

with $\alpha \simeq 0.4$ and $Z_i \simeq 1$ and $\langle U_{\parallel}^2 \rangle$ and $\langle \eta_{\parallel}^2 \rangle$ given by Eqs. (3-54) and (3-57), respectively. For LH waves $\hat{J}/\hat{P}$ is expected to vary from 10 to 60 (with smaller values may be resulting in the reactor regimes). As we have seen, in order to have as large $\hat{J}/\hat{P}$ as possible, a wave spectrum should be rich with high values of the phase velocity (i.e., low values of $\eta_{\parallel}$, $\eta_{\parallel} = ck_{\parallel}/\omega = c/v_p$, $v_p \simeq v_{\parallel}$). This is possible only if $\omega_{pe}^2/\Omega_e^2 \ll 1$ so that low values of $\eta_{\parallel}$ are accessible [see Eq. (3-26)]. In most present experiments $\omega_{pe}^2/\Omega_e^2 \simeq 0.1$ (see Table 3.1), whereas in a reactor we expect $\omega_{pe}^2/\Omega_e^2 > 0.5$. Shown in Fig. 3.12 is the current drive efficiency [Eq. (3-59)] vs T_e in various LH current drive tokamak experiments listed in Table 3.1. We see from Fig. 3.12 that in most experiments to date $\hat{J}/\hat{P} \simeq 30$-$50$ (except in JFT-2, where high values of $\eta_{\parallel}$ result in lower efficiencies). For example, for

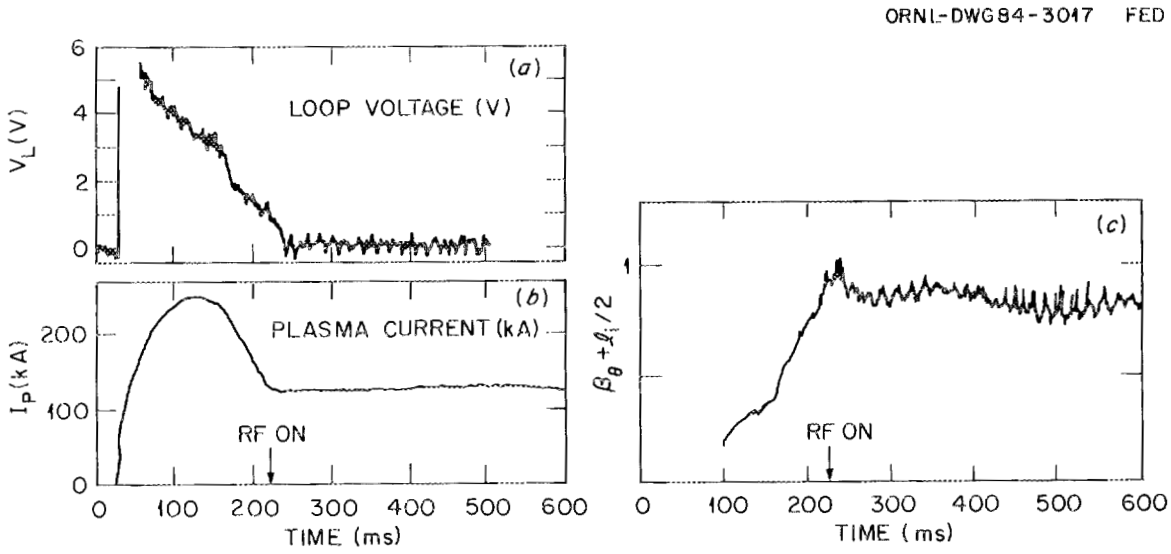

Fig. 3.11. Current drive shot in Alcator-C at $\bar{n} \simeq 3.5 \times 10^{13}$ cm^{-3}, $P_{rf} \simeq 615$ kW, $f = 4.6$ GHz, and $B_o = 8$ T (refs. [22, 36]).

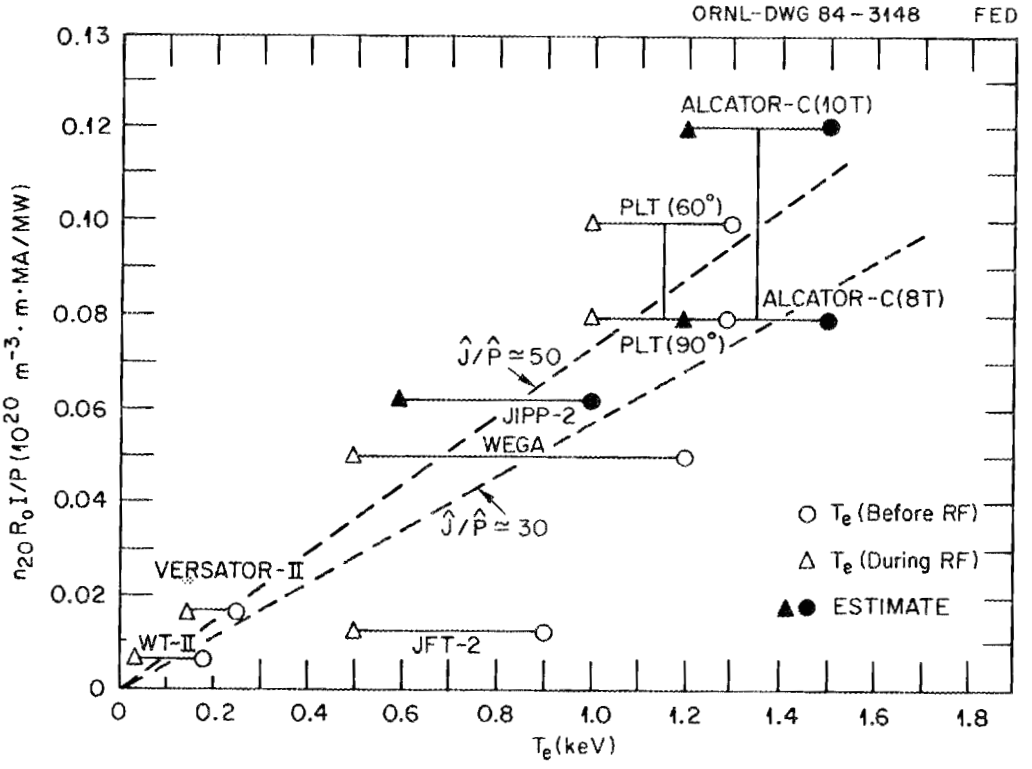

Fig. 3.12. Current drive efficiency vs T_e for a number of LH current drive tokamak experiments. Data are given in Table 3.1. For a reference, $\hat{J}/\hat{P}$ = 30 and 50 are shown (dashed lines) (refs. [22, 71]).

Alcator-C, $n_{20}I$ (MA) R_o (m)/P (MW) $\simeq 0.08\ T_e$ (keV) at $B_o = 8$ T. At $B_o = 10$ T, this efficiency is of order $0.12\ T_e$. Power and density dependence of the efficiency are shown in Figs. 3.13(a) and (b) for Alcator-C, $B_o = 10$ T.

3.3.3 Density Limit

In most of the experiments a critical density limit was observed. Above this critical density, current drive effects disappear (i.e., current drive ceases or diminishes more rapidly than the 1/n scaling, Fig. 3.13). The exception is Alcator-C (and possibly Wega), where $I/P \sim 1/n_e$ (Fig. 3.13) up to the highest density ($\bar{n} \sim 10^{14}$ cm^{-3}) used. At present Alcator-C is believed to be power limited.

The critical density in any given experiment appears to be relatively insensitive to variations in plasma parameters; however, a well-defined correlation is apparent from Fig. 3.14 between the density limit and frequency of the rf source ($n_{crit} \sim f^2$). Thus, one of the speculations is that the observed critical density has its origin in the choice of the wave frequency (f = 800 MHz in PLT whereas f = 4.6 GHz in Alcator-C). It is, however, fair to note that the mechanism responsible for the "critical density" limit is not well understood at the present, although a number of possible explanations have been proposed. Some of them are related to propagation effects. For examaple, in PLT, ray-tracing calculations indicate reduced accessibility of the waves to the plasma center at higher densities with low values of $\eta_{\parallel}$, which are responsible for the high-energy tail. PLT has a relatively small aspect ratio ($A = R_o/a = 3$) as compared to Alcator-C ($R_o/a = 4$), and calculations indicate that the critical density is dependent on aspect ratio and that rapid decrease in current drive efficiency is much more pronounced at lower aspect ratios [38].

Also associated with lack of accessibility, results from both PLT and Alcator-C show a decrease in current-drive efficiency with a decrease in magnetic field (Fig. 3.15). These results, however, differ somewhat from those obtained in FT where the density cutoff is found to be insensitive to magnetic field [37].

Other possible explanations are related to the onset of parametric decay instabilities [JFT-2, Ref. 35], to the onset of a strong interaction of LH waves with the ions (which involve absorption of part of the rf power by the ions rather than the fast electrons), to the

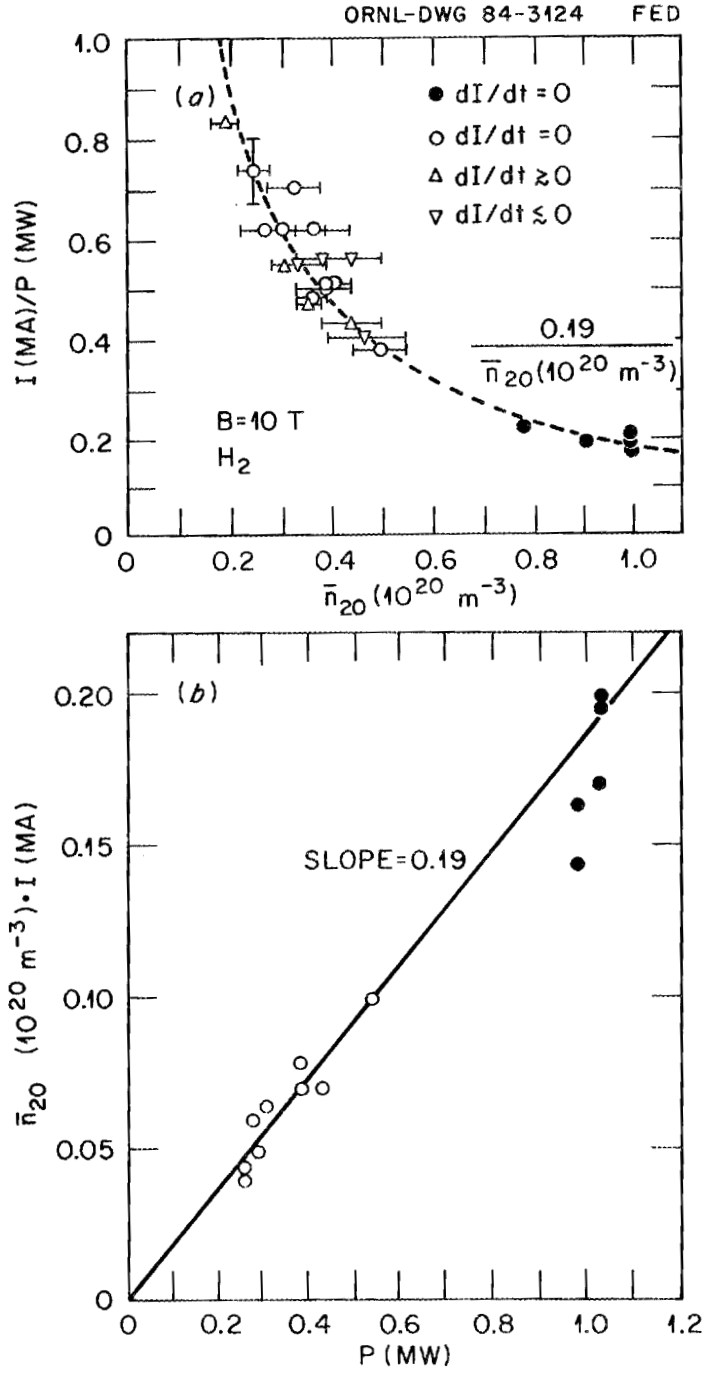

Fig. 3.13. Alcator-C lower hybrid current drive at B_o = 10 T, H_2 gas: (a) I/P vs $\bar{n}_e$ and (b) $\bar{n}_e I$ vs P. Solid dots correspond to 50-ms pulse length (which is less than L/R time). At densities of $\bar{n} \leq 5 \times 10^{19}\ m^{-3}$, flattop currents of $I \simeq 200$ kA were produced. At higher densities, this level of current requires $P \gtrsim 1$ MW, which has a pulse length limit. Proportionality of $P \sim n$ implies that principal energy losses are due to collisions (refs. [31, 36]).

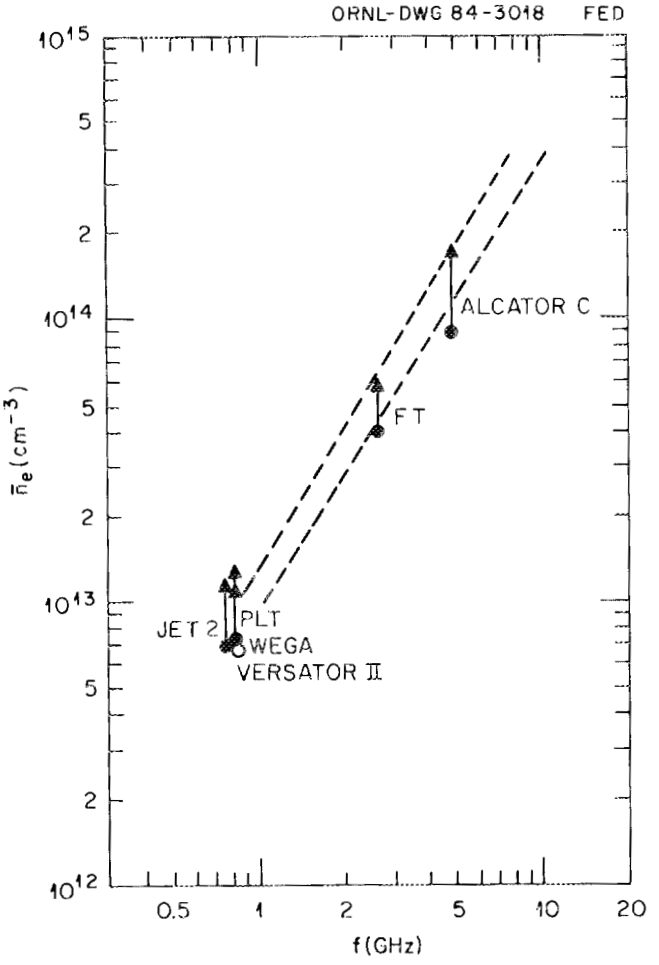

Fig. 3.14. Possible scaling of observed density limit with frequency in several LH current drive tokamak experiments (ref. [37]).

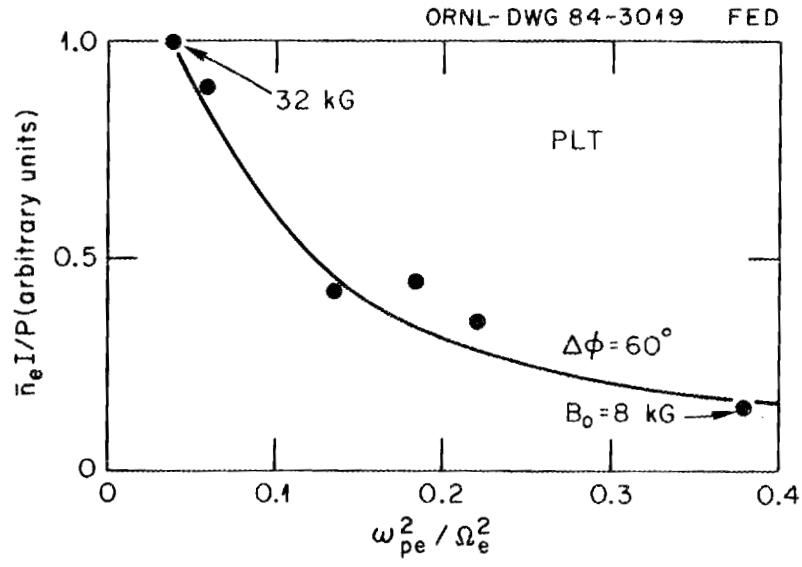

Fig. 3.15. Current drive efficiency degrades with decreasing magnetic field in PLT. Solid line represents the predictions of model (ray tracing) calculations. Relative phasing of waveguides $\Delta\phi = 60°$ and $\bar{n}_e \simeq (2\text{–}4) \times 10^{12}$ cm^{-3} (ref. [38]).

occurrence of ponderomotive effects at large $\eta_\perp$ (i.e., at high density), etc.

3.3.4 Spectral Gap

As discussed previously, the observed current drive efficiency (Fig. 3.12) in many experiments (especially in Alcator-C and PLT) has a value $n_{20}IR_o/PT_e \sim 0.1$, which is in reasonable agreement with the theoretical predictions. In these experiments, X-ray measurements indicate that the current is carried by a high-energy electron tail (with energies up to 200 keV for $T_e \sim 1$ keV) produced by the rf power (Fig. 3.16). Measurements also indicate that the fast electron component constitutes about a few percent of the total electrons. However, at a plasma temperature of $T_e \lesssim 1$ keV, energies around 30 to 200 keV should produce a negligibly small value of the electron distribution function in the plateau region $f_e(30\text{ keV}) \rightarrow f_e(0)\exp(-30)$. With this value, the current predicted from quasi-linear theory [Eq. (3-43)] is many orders of magnitude smaller than experimental observation.

One of the principal questions that arises in these experiments has to do with the explanation of the mechanism by which the high-energy (superthermal) electrons are generated by high-phase-velocity (low-$\eta_\parallel$) waves in a relatively cold plasma with no preexisting tail before the rf is turned on. Specifically, how is the gap (the so-called "spectral gap") bridged between the electron thermal velocity v_e and v_1, the low velocity end of the applied wave spectrum (where $v_1 = c/\eta_1$, $\eta_2 < \eta_\parallel < \eta_1$, see Fig. 3.4)? A number of theoretical models have been proposed to explain the mechanism that would bridge the gap between the wave phase velocity $v_\parallel = \omega/k_\parallel = c/\eta_\parallel > 5v_e$ and v_e.

One possibility is the toroidal upshift in the $k_\parallel$ (or $\eta_\parallel$) spectrum due to reflection of waves around the torus. The large $\eta_\parallel$ waves can then interact with bulk electrons and a significant quasi-linear plateau extending over a wide energy range could be formed [69]. This enhanced tail of electron distribution function extending almost from v_e to v_2 (upper end of wave spectrum, c/η_{min}) can account reasonably well for the magnitude of the current generated. However, the results are somewhat sensitive to the allowed number of bouncing of the waves around the torus [69]. Another possibility of broadening and upshifting of the $\eta_\parallel$-spectrum is claimed to be associated with the ponderomotive effects [81].

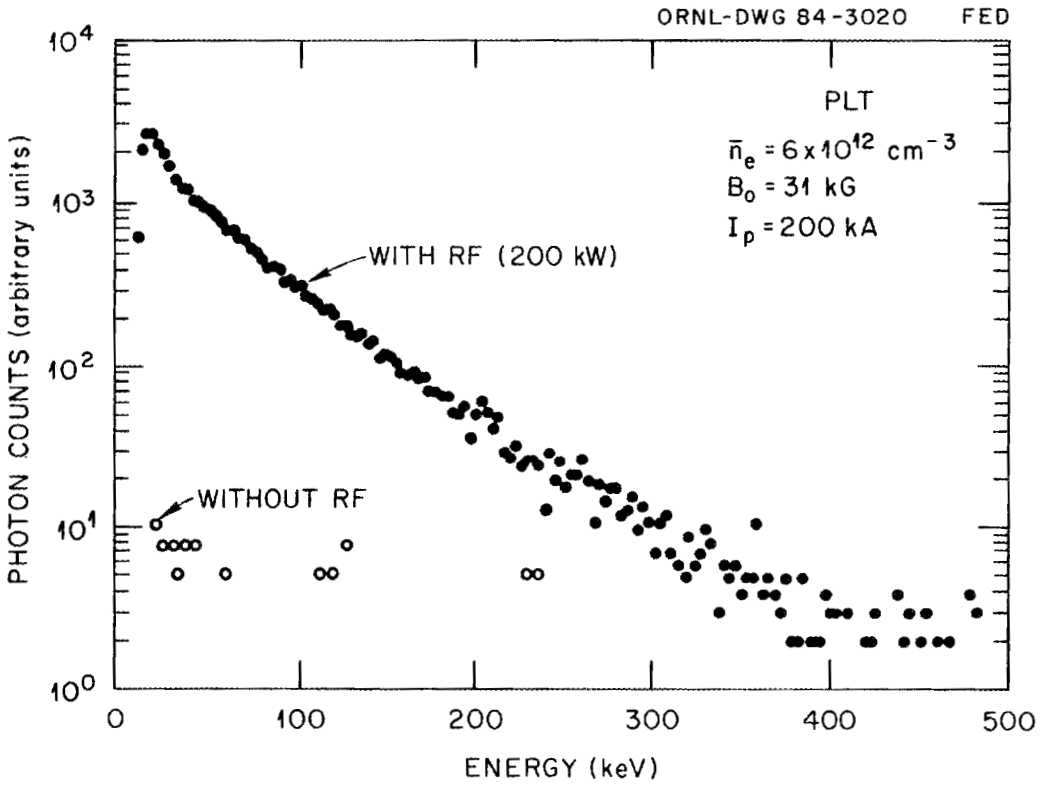

Fig. 3.16. X-ray spectrum in PLT without and with rf. Note that target plasma (without rf) contains relatively few X rays (refs. [20, 21]).

Another possibility is the anomalous Doppler interaction [73, 74]. Basically, the electron distribution function sustained by LH waves in current drive experiments exhibits an anisotropy $T_{\parallel} > T_{\perp}$ for the tail population. This anisotropy drives an instability via anomalous Doppler resonance $\omega + \Omega_e = k_{\parallel} v_{\parallel}$. This is a Parail and Pogutse [82] type "fan" instability [74], which is a magnetized plasma oscillation with $\omega = \omega_{pe} k_{\parallel}/k$. This instability then transfers momentum from high-phase-velocity LH waves to lower-phase-velocity plasma waves and increases the perpendicular tail temperature by wave pitch angle scattering. Both of these contribute to a large energetic electron population, leading to significant current sustainment.

At present, experiments have yet to provide any insight into this question. There are some measurements of instabilities. In all the transient experiments (Table 3.1), both microwave radiation and X-ray measurements show relaxation oscillations (instabilities). This instability converts electron parallel momentum into perpendicular momentum. As a result, this instability is thought to be that of the Parail and Pogutse mode, which is driven by $T_{\parallel} > T_{\perp}$ anisotropy. In WT-2 and Versator this instability was shown to quench by application of electron cyclotron resonance heating (ECRH). Note that ECRH increases the perpendicular energy and thus reduces the disparity between $T_{\parallel}$ and $T_{\perp}$. During steady-state (flat top) operation of PLT and Alcator-C, however, no such oscillations were observed.

4. ELECTRON CYCLOTRON CURRENT DRIVE [9,18,41-53,84]

Electron cyclotron current drive relies on creating an asymmetric plasma resistivity rather than on transfering momentum to the electrons (as in the Landau damping scheme). This mechanism is proposed by Fisch and Boozer [41].

Despite their low momentum content, electron cyclotron waves could drive currents with similar efficiencies to other noninductive schemes (see Fig. 1.2). To create an asymmetric resistivity, it is necessary to alter the plasma collisionality in such a way that electrons moving in one direction (e.g., to the left) collide more frequently with the ions than electrons moving in the opposite direction (e.g., to the right). As a result, a net electric current would be produced with ions moving to one direction (to the left) and electrons, on average, moving in the opposite direction (to the right). The means of accomplishing this is to preferentially heat the electrons that are moving in one direction along the magnetic field lines (i.e., in this example, those electrons moving to the right), so that being hotter they collide less. An electron cyclotron wave is an obvious candidate for this selective heating, which can be achieved by tuning the wave frequency ω such that the Doppler shift due to the electron velocity along the magnetic field ($v_{\parallel}$) synchronizes the wave frequency and the electron cyclotron frequency (Ω_e) or one of its harmonics. Thus, for nonrelativistic electrons, the resonance condition is

$$\omega - \ell\Omega_e - k_{\parallel}v_{\parallel} = 0$$

or

$$\omega - \ell\Omega_e = k_{\parallel}v_{\parallel} \ , \qquad (4\text{-}1)$$

where ℓ is the harmonic number. Resonance is achieved for all perpendicular velocities provided the parallel velocity $v_{\parallel}$ satisfies Eq. (4-1). We see from Eq. (4-1) that the electron cyclotron wave couples only to electrons with one sign of $v_{\parallel}$ on one side of the resonance. That is, electrons moving parallel (antiparallel) with the wave will be in resonance if the wave frequency ω is greater (less) than $\ell\Omega_e$. In the inhomogeneous field of a tokamak, the frequency difference ($\omega - \ell\Omega_e$) changes sign across the resonance layer so that the current flows in opposite directions on opposite sides of the

resonance. For a weakly damped wave these opposing currents are about of equal amplitude, which results in no net current flow. Thus, this immediately shows that for this method to be successful strong wave damping is required such that the wave is extinguished before it passes through the resonance. This requirement is modified when relativistic corrections to the resonance condition [Eq. (4-1)] are included.

As the electrons become relativistic the electron cyclotron frequency develops a velocity dependence due to the relativistic mass increase:

$$\Omega_e(\text{relativistic}) = eB/m_o\gamma = \Omega_e(1 - v^2/c^2)^{1/2} \ , \tag{4-2}$$

where $m_o\gamma$ is the relativistic electron mass, γ is the relativistic factor $\gamma = (1 - v^2/c^2)^{-1/2}$, and Ω_e is the nonrelativistic cyclotron (gyro-) frequency $\Omega_e = eB/m_o$, with electron rest mass m_o. In a weakly relativistic plasma ($v^2/c^2 \ll 1$), the resonance condition [Eq. (4-1)] is changed to

$$\omega - k_{\parallel}v_{\parallel} - \ell\Omega_e\left(1 - \frac{1}{2}\, v^2/c^2\right) = 0 \ . \tag{4-3}$$

It is clear from Eq. (4-3) that a change in sign of $(\omega - \ell\Omega_e)$ across the resonance layer no longer simply produces a change in sign of $v_{\parallel}$. Thus, in a tokamak the currents on opposite sides of the cyclotron resonance layer have different amplitudes and do not cancel each other in the case of weak damping (absorption).

The progress on current drive by asymmetric ECRH has been largely in the theoretical calculations although two experiments have been carried out on the Culham Levitron and TOSCA (a small tokamak) devices. Both of these devices demonstrated the existence of ECRH-driven currents through asymmetric resistivity, which we will briefly discuss later.

The resonance surface is accessible to electron cyclotron waves provided the plasma is underdense, that is, $\omega > \omega_{pe} \equiv (n_e^2/m_e\epsilon_o)^{1/2}$. These waves can be injected into the plasma through small waveguide apertures. In this respect, wave launching structures are advantageously simple compared to other rf schemes in which

accessibility to the plasma requires launching a wave spectrum with proper parallel wave number, thus necessitating design of the launching structure. The main problem in generating current by ECRH is the power requirement, both in terms of the magnitude of the recirculated power in a tokamak reactor and the costs of the microwave equipment at these frequencies ($f > 100$ GHz in a reactor). Efficient continuous wave (cw) gyrotrons for this range of frequencies are yet to be developed. Assuming that these sources can be developed, minimal power dissipation requires the absorption of the wave by only the fastest electrons, which are the most collisionless and hence retain their directed current longest. In this respect, the ECRH scheme is similar to the technique of current generation by LH waves (though electron cyclotron waves do not have a high parallel momentum content).

In this section we give a brief description of the ECRH current drive mechanism based on single-particle treatment (heuristic derivation) and then discuss the various approaches used to calculate the driven current and power absorbed. The effect of trapped electrons and the role of relativistic correction to the resonance condition will also be considered. We will summarize some of the experimental results and discuss the effectiveness of ECRH current drive for reactor applications.

Before considering any of these, some general observations are in order. First, once again, the aims of current drive are different from those of bulk heating since currents are most effectively generated by coupling of the wave to superthermal electrons and detaching them from the bulk electrons. Second, the collisions between the electrons and ions are responsible for the current generation, whereas electron-electron collisions will tend to remove the asymmetry. Third, electron cyclotron waves increase the perpendicular energy of the resonant electrons (i.e., increase the perpendicular energy of those electrons moving in the same direction as the wave via Doppler-shifted cyclotron damping). This means that resonant electrons continue in resonance (Eq. (4-1)] while increasing their perpendicular energy.

4.1. Basic Mechanism of Current Generation [41]

Here we follow the analysis of Fisch and Boozer [41], called the Fisch-Boozer mechanism, that is based on a single-particle approach.

Consider the displacement in velocity space of a small number, δf, of electrons from region 1 to region 2 (see Fig. 4.1) due to rf heating. That is, assume that the rf power will heat a particle with energy W_1 and collision frequency ν_1 to a higher energy W_2 and lower collision frequency ν_2. The energy required to do this is

$$\Delta W = (W_2 - W_1)\delta f \ . \tag{4-4}$$

Because electrons in different regions of velocity space scatter at different rates (i.e., $\nu_1 \neq \nu_2$), a current is generated. The current density (in the direction parallel to the magnetic field) generated is given by

$$j_{\parallel}(t) = e\delta f\left[v_{1,\parallel}\exp(-\nu_1 t) - v_{2,\parallel}\exp(-\nu_2 t)\right] \ . \tag{4-5}$$

The time average of $j(t)$ over an interval Δt that is long compared to $1/\nu_1$ ad $1/\nu_2$ (i.e., $\Delta t \gg 1/\nu_1;\ 1/\nu_2$) is

$$J \equiv \frac{1}{\Delta t}\int_0^{\Delta t} j_{\parallel}(t)dt \simeq e\,\frac{\delta f}{\Delta t}\,(v_{1,\parallel}/\nu_1 - v_{2,\parallel}/\nu_2) \ . \tag{4-6}$$

The dissipated rf power over this time interval can be approximated as

$$P_{rf} \simeq \frac{\Delta W}{\Delta t} \simeq (W_2 - W_1)\,\frac{\delta f}{\Delta t} \ . \tag{4-7}$$

From Eqs. (4-6) and (4-7) we find the expression for current drive efficiency:

$$J/P_{rf} = -\,e\,\frac{v_{1\parallel}/\nu_1 - v_{2\parallel}/\nu_2}{W_1 - W_2} \ . \tag{4-8a}$$

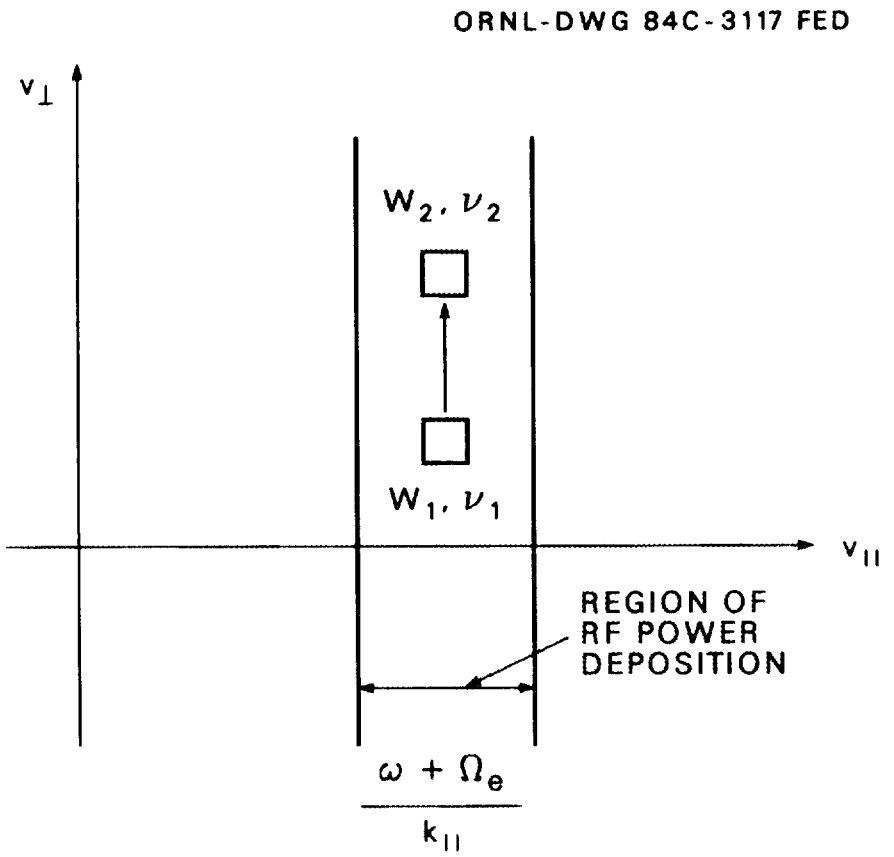

Fig. 4.1. Schematic picture of power deposition in velocity space for ECRH.

In the limit $\mathbf{v}_1 \to \mathbf{v}_2$, the locations 1 and 2 are separated infinitesimally (in the velocity space), and J/P_{rf} reduces to

$$J/P_{rf} \xrightarrow[\lim \mathbf{v}_1 \to \mathbf{v}_2]{} -e \frac{\hat{\mathbf{s}} \cdot \nabla_v (v_{\parallel}/\nu)}{\hat{\mathbf{s}} \cdot \nabla_v W} , \tag{4-8b}$$

where $\hat{\mathbf{s}}$ is the unit vector in the direction of velocity displacement and ∇_v is the del operator in velocity space.

Without any detailed discussion of the collision processes, several results can be obtained from Eq. (4-8). Assuming that the collision frequency varies as

$$\nu \propto v^{-3} ,$$

where v is the velocity of the resonant electrons, the form of J/P can be immediately obtained. For example, for LH waves (discussed in Sect. 3), velocity displacement is in the parallel direction $\hat{\mathbf{s}} = \mathbf{v}_{\parallel}/v_{\parallel}$ (or $\hat{\mathbf{s}} \parallel \hat{\mathbf{e}}_z$, where $\mathbf{B} = B_0 \hat{\mathbf{e}}_z$); we have

$$J/P_{rf} \propto \frac{\partial}{\partial v_{\parallel}} (v_{\parallel}/\nu) / \frac{\partial}{\partial v_{\parallel}} W$$

$$\propto \frac{1}{v_{\parallel}} (v_{\perp}^2 + v_{\parallel}^2)^{3/2} + 3v_{\parallel} (v_{\perp}^2 + v_{\parallel}^2)^{1/2} . \tag{4-9}$$

For resonant electrons, the effective current drive regime (with LH waves) is $v_{\parallel}^2 \gg v_{\perp}^2$. In this limit the term arising from the energy input [second term in Eq. (4-9)] is three times larger than the term arising from the momentum input [first term in Eq. (4-9)]. This implies that for successful current drive it is not necessary for waves to have net (large) momentum content. The wave with low momentum content, such as electron cyclotron waves, can in principle have similar current drive efficiencies to LH waves, which carry much more momentum. For electron cyclotron waves, $\hat{\mathbf{s}}$ is parallel to $v_{\perp}$ and $J/P_{rf} \propto \partial/\partial v_{\perp}(v_{\parallel}\nu^{-1})/\partial W/\partial v_{\perp}$, which results in

$$J/P_{rf} \propto 3v_{\parallel}(v_{\perp}^2 + v_{\parallel}^2)^{1/2} \ . \tag{4-10}$$

Comparison of Eqs. (4-9) (for LH waves) and (4-10) (for ECRH) in the limit $v_{\parallel}^2 \gg v_{\perp}^2$ indicates that J/P_{rf} for ECRH would be about three-fourths of the value for lower hybrid.

We will now determine the collision frequency ν to be used in Eq. (4-8). In the high-velocity limit $v \gg v_e$, the Fokker-Planck equation contains two collisional scattering rates (see Sect. 3.2.1): a slowing-down rate

$$\nu_s = \nu_o/2U^3 \tag{4-11}$$

and a momentum destruction rate

$$\nu_m = \frac{2 + Z_i}{2U^3} = (2 + Z_i)\nu_s \ , \tag{4-12}$$

where $U = v/v_e$, $\nu_o = \omega_{pe}^4 \ln \Lambda/2\pi n v_e^3$, $v_e = (kT_e/m_e)^{1/2}$, and Z_i is the ion charge state. Consider a test electron (i.e., a resonant electron with speed $v \gg v_e$) that slows down energetically. In Ref. [41] diffusion in energy is ignored, but the slowing down in energy causes both collision rates (ν_s and ν_m) to vary. The slowing-down equation is given by

$$dU/dt = -\nu_s U \ . \tag{4-13}$$

The current carried by the electron is

$$j_{\parallel}(t) = j_{\parallel}(t = 0)\exp\left[\int_0^t - \nu_m(t)\ dt\right] \ . \tag{4-14a}$$

With the use of Eqs. (4-12) and (4-13), Eq. (4-14a) becomes

$$j_{\parallel}(t) = j_{\parallel}(t = 0)\left[U(t)/U(t = 0)\right]^{2 + Z_i} , \tag{4-14b}$$

where $U(t = 0) \equiv U_o$ is the initial normalized electron velocity. Note that the background electrons, as well as the ions, contribute to the current destruction.

Using Eq. (4-13), we write the time-integrated current as

$$\int_0^{\infty} j_{\parallel}(t)dt = -j_{\parallel}(t = 0) \int_{U_o}^{0} \left(\frac{U}{U_o}\right)^{2 + Z_i} \frac{dU}{\nu_s U}$$

$$= \frac{j_{\parallel}(t = 0)}{\nu_o} \frac{2U_o^3}{5 + Z_i} , \tag{4-15}$$

where we have used Eq. (4-12). It follows that the correct ν to be used in Eqs. (4-5)-(4-8) is given by

$$\nu = \nu_o \frac{5 + Z_i}{2U^3} . \tag{4-16}$$

Using Eq. (4-16) in Eq. (4-8b) and normalizing velocities to v_e, current J to $-env_e$, and dissipated power to $m_e n v_e^2 \nu_o$, we can write the normalized efficiency factor as

$$\hat{J}/\hat{P} = \frac{-J/env_e}{P_{rf}/m_e n v_e^2 \nu_o} = \frac{\hat{s} \cdot \nabla_v (U_{\parallel} U^3)}{\hat{s} \cdot \nabla_v (U^2)} \frac{4}{5 + Z_i} , \tag{4-17}$$

where $U_{\parallel} = v_{\parallel}/v_e$.

The range of application of Eq. (4-17) is limited to situations where the location in velocity space of electrons that absorb energy from a wave is known, which is obtained from the resonance condition [Eq. (4-1)]. Note that the resonance condition ($\omega - k_{\parallel}v_{\parallel} = \ell\Omega_e$, or $\omega - \ell\Omega_e = k_{\parallel}v_{\parallel}$) for LH waves is $\ell = 0$ whereas for electron cyclotron waves it is $\ell = \mp 1$ for fundamental resonance ($\ell = \mp 2$ for second harmonic). The precise perpendicular velocity of the electrons is

immaterial to Eq. (4-17), unless it becomes comparable to the parallel velocity.

Electron cyclotron waves induce velocity space diffusion primarily in the perpendicular direction, so that the perpendicular flattening of the electron distribution should be expected to be more pronounced than when excited by LH waves.

Accessibility constraints of the electron cyclotron waves, especially in high-beta plasmas, is somewhat less stringent than for LH waves. For the current to be generated in a single direction, it is necessary that all the power be absorbed before the cyclotron layer. Thus, launching from the high-field side may be necessary to control the absorption.

In the next section we discuss the experiments that rely on the Fisch-Boozer mechanism for producing a current by electron cyclotron waves and then introduce the results from detailed treatments of the nonrelativistic and relativistic theories.

4.2. Experiments [47,48,52]

Two experiments have been carried out on the Culham Levitron [47] and TOSCA [48] experiments to verify the theory of ECRH driven current produced by the Fisch-Boozer mechanism.

Experiments on the superconducting Levitron have established the existence of such a current, although only in a low-temperature, low-density plasma ($3\ \mathrm{eV} < T_e < 18\ \mathrm{eV}$; $10^{11}\ \mathrm{cm}^{-3} < n_e < 3 \times 10^{11}\ \mathrm{cm}^{-3}$) where a 10-GHz microwave source of approximately 120 W was used. Current reversal on either side of the cyclotron resonance was also demonstrated. Figures 4.2(a) and 4.2(b) show the amplitude of the rf-driven current as a function of microwave power (indicating the overall efficiency of net current drive) and nI/P vs T_e, respectively. As can be seen from Fig. 4.2(a) the efficiency of current drive is about 0.03 A/W.

On TOSCA (a small air-cored tokamak with $R_o = 30$ cm, $a \lesssim 8.5$ cm, and no conducting shell), ECRH experiments at the second harmonic have been performed where a 28-GHz gyrotron with up to 85 kW was used. The current drive efficiency is claimed to be as high as 0.02 A/W. A variation of 1 kA in plasma current is observed as the resonance is moved across the plasma. The driven current was at a maximum when the resonance layer was on the high-field side (inside the geometric axis). A sharp falloff in current drive efficiency was observed as the

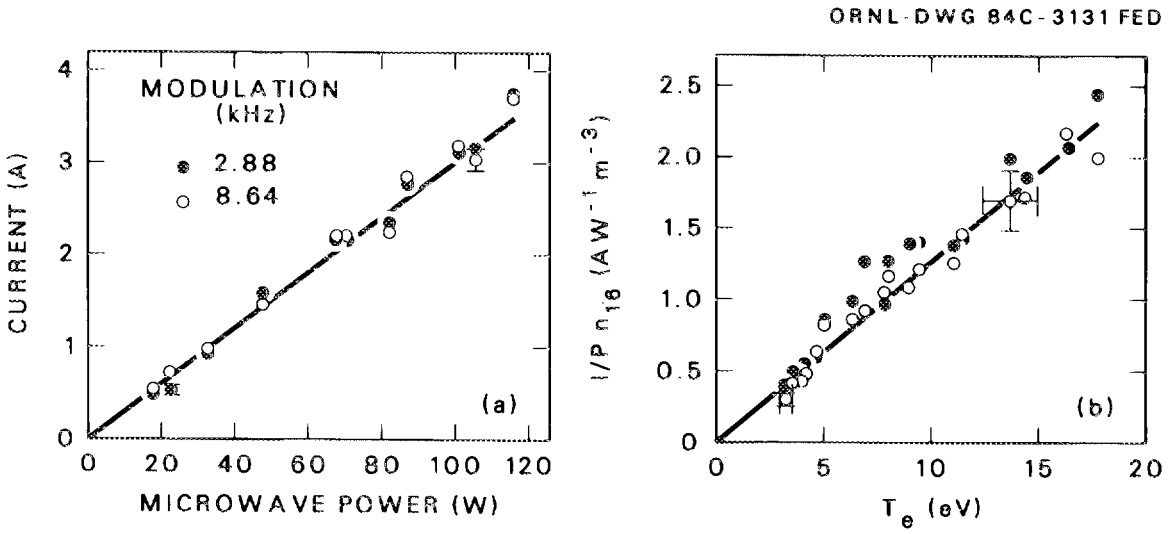

Fig. 4.2. (a) ECRH driven current vs microwave power in Levitron, and (b) current per unit power times density (in units of 10^{16} $m^{-3}AW^{-1}$ vs electron temperature (in eV) (ref. [47]).

resonance was moved outside the geometric axis (low-field side), where trapped electrons were present, suggesting that trapped electrons significantly reduce any driven current. This is shown in Fig. 4.3 where the resonance position was varied by changing the value of the toroidal field.

4.3. Propagation and Wave Absorption of Electron Cyclotron Waves

The electron cyclotron waves are electromagnetic waves. The electromagnetic waves, when propagating perpendicular to the confining magnetic field ($\mathbf{k} \perp \mathbf{B}_o$), can be divided into two linear polarizations: the ordinary ($\mathbf{E} \parallel \mathbf{B}_o$) and the extraordinary ($\mathbf{E} \perp \mathbf{B}_o$), where $\mathbf{E}$ is the wave electric field and $\mathbf{B}_o$ is the static confining field (i.e., toroidal magnetic field in tokamak). These waves are labeled O- and X-waves, respectively. The effective propagation of each mode is obtained only if the electron density remains below a certain plasma cutoff value. The dispersion relation and resonance and cutoff conditions for these waves can easily be obtained from Eq. (3-7) [or Eq. (3-8)]. Note that when propagation is along the magnetic field ($\mathbf{k} \parallel \mathbf{B}_o$), there exist right- and left-hand circularly polarized waves, denoted as R- and L-waves, respectively.

4.3.1 Dispersion Relation and Polarization

In the frequency range of interest (i.e., $\omega \gg \Omega_i$), we approximate components of the dielectric tensor [Eq. (3-6)] as follows:

$$\begin{aligned} \epsilon_1 &\simeq 1 - \omega_{pe}^2/(\omega^2 - \Omega_e^2) \ , \\ \epsilon_2 &\simeq -(\Omega_e/\omega)\omega_{pe}^2/(\omega^2 - \Omega_e^2) \ , \\ \epsilon_3 &\simeq 1 - \omega_{pe}^2/\omega^2 \ . \end{aligned} \tag{4-18}$$

With these substitutions, the cold plasma dispersion relation [Eq. (3-8)] yields two polarizations of electromagnetic waves that satisfy

$$\eta^2 = \frac{k^2c^2}{\omega^2} = 1 - \frac{2(\omega_{pe}^2/\omega^2)(1 - \omega_{pe}^2/\omega^2)}{2(1 - \omega_{pe}^2/\omega^2) - (\Omega_e^2/\omega^2)\sin^2\theta \pm \Delta(\Omega_e^2/\omega^2)} \ , \tag{4-19}$$

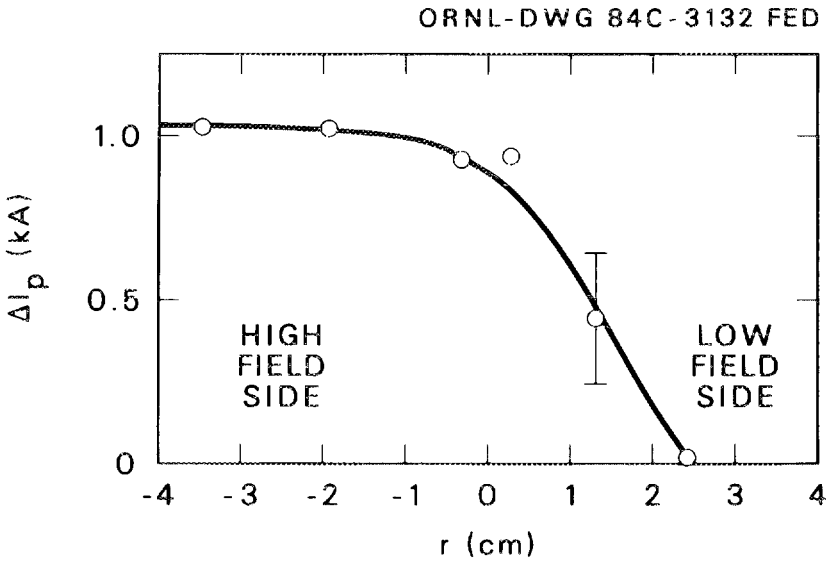

Fig. 4.3. Plasma current in TOSCA driven by ECRH as a function of resonance position. The current drive efficiency is about 0.01 A/W of injected power in this case (refs. [48, 52]).

where θ is the angle between $\mathbf{k}$ and $\mathbf{B}_o$ and

$$\Delta = \left[\sin^4\theta + 4(\omega^2/\Omega_e^2)(1 - \omega_{pe}^2/\omega^2)\cos^2\theta\right]^{1/2} . \tag{4-20}$$

Equation (4-19) is for the general case of oblique propagation. For the special case of $\theta = \pi/2$ ($\mathbf{k} \perp \mathbf{B}_o$, $k = k_\perp$), we have the ordinary (+ sign) and extraordinary (- sign) modes: that is, for the O-wave

$$\eta^2 = \eta_\perp^2 = \epsilon_3 \quad \text{or} \quad \frac{k_\perp^2 c^2}{\omega^2} = 1 - \frac{\omega_{pe}^2}{\omega^2} , \tag{4-21}$$

and for the X-wave

$$\eta^2 = \eta_\perp^2 = (\epsilon_1^2 - \epsilon_2^2)/\epsilon_1 \tag{4-22}$$

or

$$\frac{k_\perp^2 c^2}{\omega^2} = 1 - \frac{\omega_{pe}^2}{\omega^2} \frac{(\omega^2 - \omega_{pe}^2)}{[\omega^2 - (\omega_{pe}^2 + \Omega_e^2)]} .$$

For the special case of $\theta = 0$ ($\mathbf{k} \parallel \mathbf{B}_o$, $k = k_\parallel$), we have the right (+ sign) and left (- sign) circularly polarized waves; that is, for the R-wave

$$\eta^2 = \eta_\parallel^2 = \epsilon_1 + \epsilon_2 \quad \text{or} \quad \frac{k_\parallel^2 c^2}{\omega^2} = 1 - \frac{\omega_{pe}^2/\omega^2}{1 - \Omega_e/\omega} \tag{4-23}$$

and for the L-wave

$$\eta^2 = \eta_\parallel^2 = \epsilon_1 - \epsilon_2 \quad \text{or} \quad \frac{k_\parallel^2 c^2}{\omega^2} = 1 - \frac{\omega_{pe}^2/\omega^2}{1 + \Omega_e/\omega} . \tag{4-24}$$

Equation (3-7) relates the phases and magnitudes of the electric field of the waves. From the y-component of Eq. (3-7), we write

$$\frac{iE_x}{E_y} = \frac{\eta^2 - \epsilon_1}{\epsilon_2} . \tag{4-25}$$

If $iE_x/E_y = +1$ the electric field is right-hand circularly polarized and if $iE_x/E_y = -1$ it is left-hand circularly polarized, corresponding to the sense in which electrons and ions gyrate about the magnetic field, respectively. For $\theta = 0$ (i.e., for waves propagating along the magnetic field), the electric field has circular polarization for $R(iE_x/E_y = 1)$ and $L(iE_x/E_y = -1)$ waves. For $\theta = \pi/2$, the electromagnetic waves are plane polarized (O-wave, $E_x = E_y = 0$, $E_{\parallel} \neq 0$) and elliptically polarized (X-wave). For other angles (oblique propagation), both O- and X-waves have elliptical polarization.

4.3.2 Accessibility

From the cold plasma dispersion relation for the O-wave [Eq. (4-21)], we see that the wave propagation is possible only if

$$\omega_{pe}^2 < \omega^2$$

(i.e., $k_\perp^2 > 0$). As ω_{pe} approaches ω the propagation of this mode is cut off (i.e, $k_\perp^2 \to 0$). Since the wave becomes evanescent if $\omega_{pe}^2 > \omega^2$ (i.e., $k_\perp$ is purely imaginary so that the wave is damped exponentially), the accessibility to $\omega = \ell\Omega_e$ exists only for densities such that $\omega_{pe} < \ell\Omega_e$; namely,

$$n_e < n_{cutoff} \equiv 1.24 \times 10^{16} [f\ (\mathrm{GHz})]^2 \quad (\mathrm{m}^{-3})$$

$$\equiv 9.7 \times 10^{18} \ell^2 [B\ (\mathrm{T})]^2 \quad (\mathrm{m}^{-3}) \ , \tag{4-26}$$

where $f = \omega/2\pi$ is the wave frequency and ℓ is the harmonic number. For the ordinary mode, in the special case of $k_{\parallel} = 0$, there is no resonance (i.e., $k_{\perp} \to \infty$) condition. However, direct wave absorption at $\omega = \Omega_e$ occurs due to finite temperature effects (which must be calculated from the Vlasov equation) and due to Doppler broadening at the cyclotron resonance layer. When the resonance condition Eq. (4-1) is satisfied, cyclotron damping by electrons takes place with the resonance zone (absorption zone) being accessible from both the high- and low-field sides of the tokamak.

For purely perpendicular propagation the dispersion relation for the X-wave is given by Eq. (4-22), which can be rearranged as

$$\frac{k_{\perp}^2 c^2}{\omega^2} = \frac{(\omega^2 - \omega_R^2)(\omega^2 - \omega_L^2)}{\omega^2 [\omega^2 - (\omega_{pe}^2 + \Omega_e^2)]} \ . \tag{4-27}$$

The X-mode will propagate ($k_{\perp}^2 > 0$) provided either

$$\omega > \omega_R = (\Omega_e/2) + (\Omega_e^2 + 4\omega_{pe}^2)^{1/2}/2$$

or

$$\omega_L < \omega < \omega_{UH} \ ,$$

where $\omega_L = -(\Omega_e/2) + (\Omega_e^2 + 4\omega_{pe}^2)^{1/2}/2$ and $\omega_{UH} = (\omega_{pe}^2 + \Omega_e^2)^{1/2}$, known as the upper hybrid (UH) frequency. The wave is resonant ($k_{\perp} \to \infty$) as $\omega \to \omega_{UH}$ (known as UH resonance) and it is cut off ($k_{\perp} \to 0$) as $\omega = \omega_R$ and $\omega = \omega_L$ (known as the right- and left-hand cutoff frequencies, respectively). Just as in the case of the O-mode, X-mode absorption at $\omega = \ell\Omega_e$ is due to Doppler broadening (and relativistic effects).

The X-mode can mode convert at the UH layer, $\omega = \omega_{UH} = (\omega_{pe}^2 + \Omega_e^2)^{1/2}$ into electron Bernstein waves, which are absorbed through electron Landau damping. Bernstein waves are electrostatic waves, which propagate perpendicular to the magnetic field near $\omega \simeq \ell\Omega_e$.

In the presence of a finite $k_{\parallel}$ it is possible for a wave of one polarization (e.g., the O-mode) to convert to a wave of the other polarization. This occurs if a surface is encountered on which discriminant Δ [Eq. (4-20)] vanishes. As a result of this effect it is possible to launch an O-mode from the low-field side, which subsequently mode-converts to an X-wave and then transfers its energy to the Bernstein waves via UH mode conversion.

For the purpose of current drive (not for bulk heating), Bernstein waves appear to be the most efficient because they are strongly damped as the cyclotron resonance layer is approached, especially the strength of the damping at very high temperatures. The efficiency of current drive [Eq. (4-17)] is very sensitive to the Doppler-shifted resonance velocity $[(\omega - \Omega)/k_{\parallel}]$. The larger is this velocity, the larger is the efficiency.

4.4. Nonrelativistic Calculations [18,45-46,50]

4.4.1 Resonance Condition

The cyclotron interaction is a resonant diffusion in velocity space, and heating occurs when Eq. (4-1) is satisfied:

$$\omega - \ell\Omega_e - k_{\parallel}v_{\parallel} = 0 \ ,$$

known as the resonance condition. A distinction should be made between electron cyclotron heating (ECH) in a uniform magnetic field and that in a toroidal geometry, where the magnetic field varies as 1/R (here, R is the major radius $R = R_o + r \cos\theta$; see Fig. 4.4 for the coordinate system). In a uniform magnetic field (considered in Sect. 4.1), only electrons with $v_{\parallel} = V_o$, where $V_o \equiv (\omega - \ell\Omega_e)/k_{\parallel}$ is a constant, can resonate with the wave. In a toroidal geometry V_o is no longer a constant because $\Omega_e = \Omega_e(r)$ varies on a flux surface. As a result, more particles can take part in wave-particle interaction. Figure 4.5 illustrates the difference in the resonance region in velocity space

ORNL-DWG 84-3133 FED

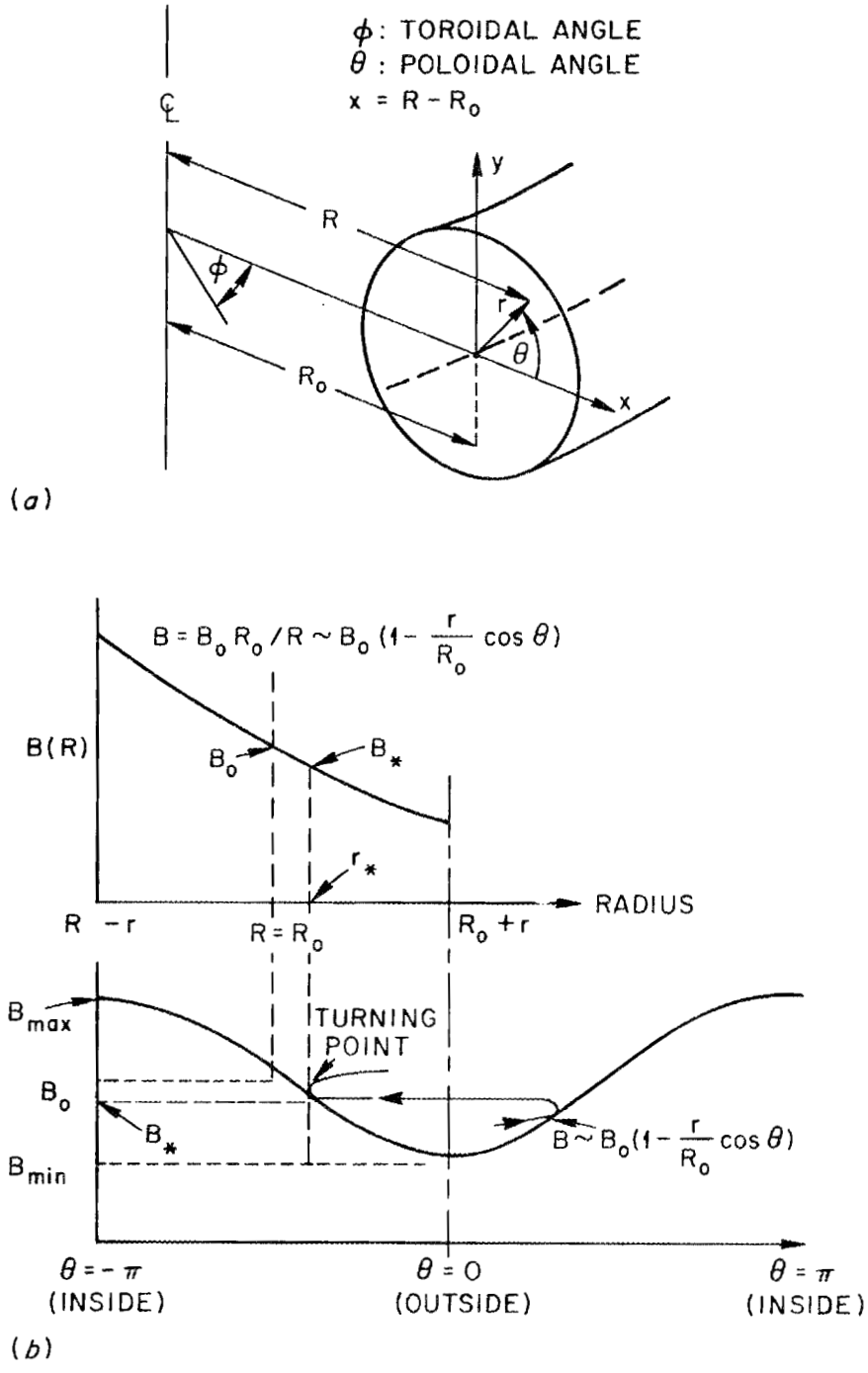

Fig. 4.4. (a) Toroidal coordinate system, and (b) variation of magnetic field as a function of radius (top) and along a field line (bottom).

ORNL-DWG 84C-3134 FED

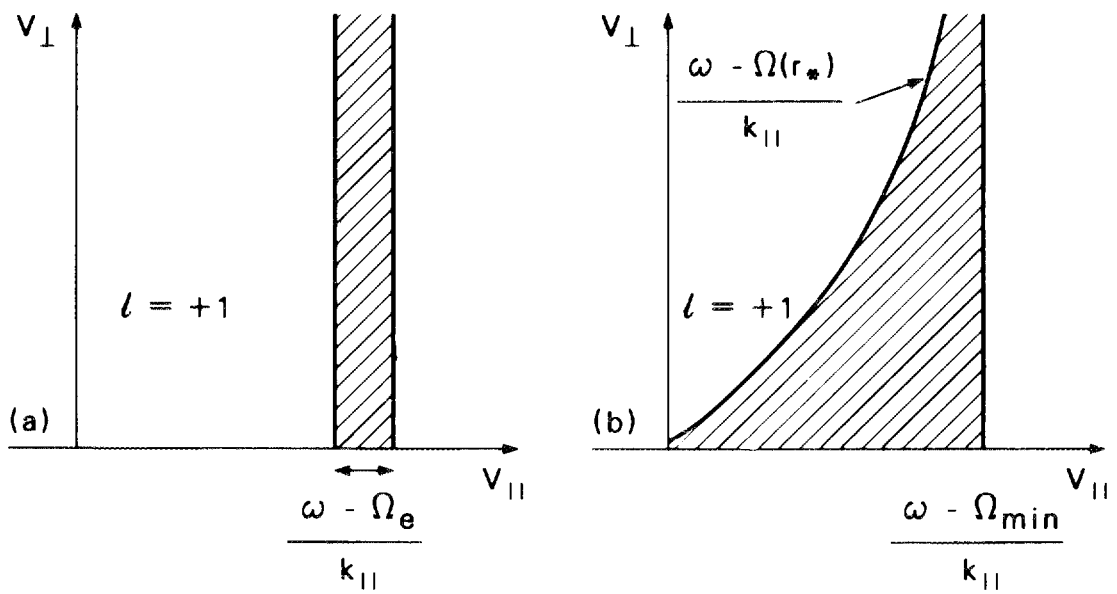

Fig. 4.5. Resonance region in velocity space (shaded area) for (a) uniform magnetic field and (b) toroidal magnetic field, where $\Omega_{min} = eB_{min}/m_e$ [see Fig. 4.4(b)] and $r = r_*$ is the turning point. In both figures $\ell = +1$ (fundamental resonance) is considered.

for a uniform magnetic field and a toroidal field. The reference plane for Fig. 4.5(b) is at the bottom of the magnetic well, corresponding to $B = B_{min}$ in Fig. 4.4(b). An important point to note is that both large and small $v_{\parallel}$ particles will participate in the heating. Since slower electrons are less efficient to heat for generating currents, it becomes critical that the electron cyclotron wave damps completely before $v_{\parallel}$ becomes too small.

4.4.2 Fokker-Planck Equation

The effect of ECRH is to increase primarily the perpendicular velocity of the resonant electrons. Considering the wave-particle interaction as a diffusive process, only the $\mathbf{v}_{\perp}\mathbf{v}_{\perp}$ compnent of the wave diffusion tensor $\overleftrightarrow{\mathbf{D}}$ [Eq. (1-10)] is nonzero for electron cyclotron waves. The electron Fokker-Planck equation, in a symbolic form, is given by Eq. (3-28), where the wave contribution is now given by

$$\left(\frac{\partial f_e}{\partial t}\right)_w = \frac{1}{v_{\perp}}\frac{\partial}{\partial v_{\perp}}\left[D v_{\perp}^{2\ell-1}\delta(\omega - \ell\Omega_e - k_{\parallel}v_{\parallel})\frac{\partial f_e}{\partial v_{\perp}}\right] , \tag{4-28}$$

where D is the quasi-linear wave diffusion coefficient due to cyclotron damping and the δ function expresses the resonance condition. For the X-mode D is independent of velocity space variables and is given by

$$D = \pi\left(\frac{e}{2m_e}\right)^2 |E^-|^2 , \tag{4-29}$$

where $E^- = E_x - iE_y$ is the right-hand circularly polarized component of the $\mathbf{E}$ field in the plane perpendicular to the magnetic field ($\mathbf{B}_o = B_o\hat{\mathbf{e}}_z$, $\mathbf{k} = k_{\perp}\hat{\mathbf{e}}_x + k_{\parallel}\hat{\mathbf{e}}_z$). Without distinguishing between the O- or X-modes,

$$D = \pi\left(\frac{e}{2m_e}\right)^2 \left|E^- + \frac{k_{\perp}v_{\parallel}}{\Omega_e}E_{\parallel}\right|^2 . \tag{4-30}$$

Implied in the use of Eqs. (4-28) through (4-30) is the assumption of monochromatic wave spectrum. In practice there is a spread in wave

numbers that can simply be introduced in Eq. (4-28) as an integral over the $k_{\parallel}$ spectrum, as is done for LH waves (see Sect. 3.2.1).

Considering only the X-mode and $\ell = +1$,

$$\left(\frac{\partial f_e}{\partial t}\right)_w = \frac{1}{v_\perp}\frac{\partial}{\partial v_\perp}\left[\frac{\pi e^2}{4m_e^2}\frac{|E^-|^2}{k_\parallel} v_\perp \delta\left(\frac{\omega - \Omega_e}{k_\parallel} - v_\parallel\right)\frac{\partial f_e}{\partial v_\perp}\right] . \tag{4-31}$$

To simplify the calculations, the wave amplitude is usually assumed to be small, and, as such, it produces a small perturbation of the electron distribution function

$$f_e = f_o + f_1 ,$$

where f_o is the unperturbed Maxwellian distribution and f_1 is the perturbation of the electron distribution function away from the Maxwellian. As a result, the Fokker-Planck equation can be linearized, giving in steady state

$$\frac{1}{v_\perp}\frac{\partial}{\partial v_\perp}\left(D_w v_\perp \frac{\partial f_o}{\partial t}\right) + \left(\frac{\partial f_1}{\partial t}\right)_{coll} = 0 , \tag{4-32}$$

where $(\partial f_1/\partial t)_{coll} = C_{ee}(f_o, f_1) + C_{ei}(f_1, f_o)$ is the collision term and

$$D_w = D\frac{1}{k_\parallel}\delta\left(\frac{\omega - \Omega_e}{k_\parallel} - v_\parallel\right)$$

$$\simeq \left(\frac{e}{2m_e}\right)^2 |E^-|^2 \frac{\pi}{v_\parallel \Delta k_\parallel} , \tag{4-33}$$

with $\Delta k_\parallel$ the finite (but small) $k_\parallel$ spectrum within the resonance region.

Equation (4-32) can be solved analytically and/or numerically to obtain f_1, which will not be given here (see references), from which the driven current

$$J = -e \int v_{\parallel} f_1 \, d^3v \tag{4-34a}$$

and absorbed (or dissipated) rf power

$$P_{rf} = \int \frac{1}{2} m_e v^2 \left(\frac{\partial f_e}{\partial t}\right)_w d^3v \tag{4-34b}$$

can be obtained. It turns out that a simple analytic theory (based on a single-particle approach and discussed in Sect. 4.1 [41]) and the expression for the efficiency factor given by Eq. (4-17) give a very accurate approximation to a full Fokker-Planck code. Such a comparison is shown in Fig. 4.6, where normalized efficiency $\hat{J}/\hat{P}$ is plotted as a function of $\langle U_{\parallel}^2 \rangle$, and the average is computed with a Maxwellian weighting; that is,

$$\langle U_{\parallel}^2 \rangle = \left\langle \left(\frac{v_{\parallel}}{v_e}\right)^2 \right\rangle = \frac{\int_{U_1}^{U_2} U_{\parallel}^2 f_o(U_{\parallel}) \, dU_{\parallel}}{\int_{U_1}^{U_2} f_o(U_{\parallel}) \, dU_{\parallel}} \tag{4-35}$$

is the normalized parallel velocity of the resonant electrons. For the results shown in Fig. 4.6, the diffusion coefficient D_w is assumed to be small and localized in velocity space:

$$D_w = \begin{cases} D & U_1 < U_{\parallel} < U_2 \quad \text{and} \quad U_{\perp} < 1 \\ 0 & \text{otherwise} \end{cases}$$

As can be seen from Fig. 4.6, there is excellent agreement between the numerical results (circles) and the analytical predictions (lines) for the selected parameter range $\Delta U_{\parallel} = U_2 - U_1 = 1$ and $\mathbf{D} = D_w/v_e^2\nu_o = 10^{-3}$ (normalized D). As a comparison, results for the LH case are also shown that indicate the efficiency ratio of 4/3 in favor of lower hybrid, as predicted by Eq. (4-17).

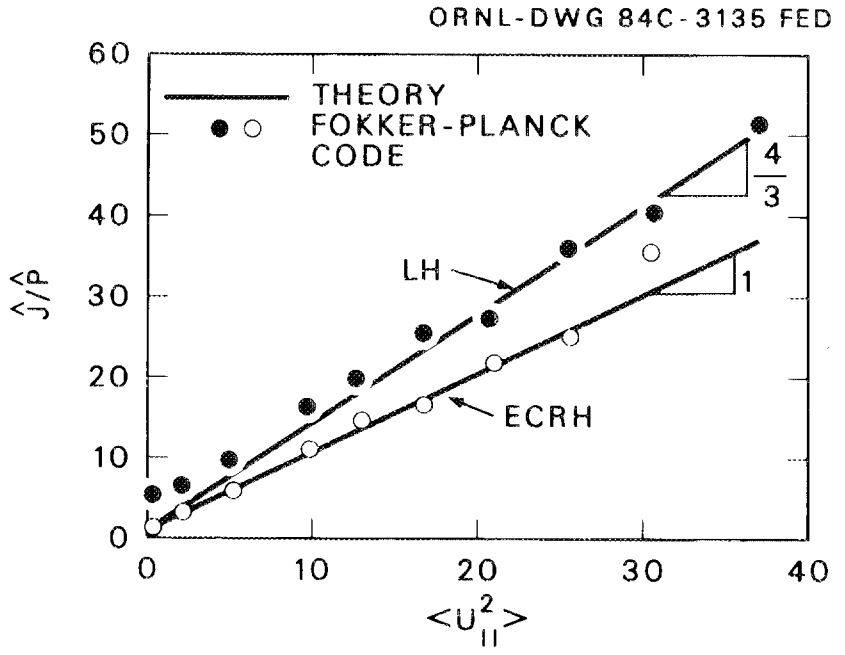

Fig. 4.6. $\hat{J}/\hat{P}$ for small D_w as a function of $\langle U_{\parallel}^2 \rangle$, where $D_w/v_e^2\nu_o = 10^{-3}$ and $\Delta U_{\parallel} = U_2 - U_1 = 1$. The waves exist only for $U_{\perp} = v_{\perp}/v_e < 1$. Open circles denote cyclotron damping and closed circles Landau damping. Lines show the theoretical predictions of Eq. (4-17), that is, $\mathbf{s} = \mathbf{v}_{\perp}/v_{\perp}$ for cyclotron damping (ECRH) and $\mathbf{s} = \mathbf{v}_{\parallel}/v_{\parallel}$ for Landau damping (LH) (ref. [45]).

4.4.3 Projections of Efficiency Factor

The efficiency factor is given by Eq. (4-17):

$$\frac{\hat{J}}{\hat{P}} = \frac{\hat{\mathbf{s}} \cdot \nabla_v (U_\parallel U^3)}{\hat{\mathbf{s}} \cdot \nabla_v (U^2/2)} \frac{2}{5 + Z_i} .$$

For electron cyclotron waves $\hat{\mathbf{s}} = \mathbf{v}_\perp / v_\perp$,

$$\frac{\hat{J}}{\hat{P}} = \frac{2}{5 + Z_i} 3U_\parallel U \simeq \frac{6}{5 + Z_i} U_\parallel^2 = \frac{6}{5 + Z_i} U_o^2 , \tag{4-36}$$

where we assume $U_\parallel \simeq U$ and $U_o \equiv U_\parallel = (\omega - \Omega_e)/k_\parallel v_e$ is the Doppler-shifted resonance velocity normalized to v_e. For $Z_i = 1$, $\hat{J}/\hat{P} = \langle U_\parallel^2 \rangle \simeq U_o^2$ is plotted in Fig. 4.6.

Clearly the efficiency is very sensitive to U_o, which is determined not so much by the parallel wave number spectrum launched but by how strongly a particular mode is damped at a given U_o. As previously discussed, the farther away the cyclotron resonance layer a mode is completely absorbed, the larger are U_o and the efficiency. The first step in the calculation is to find out if the waves can deposit their energy in the central plasma region. This is necessary to obtain reasonable current profiles. These calculations are carried out by tracing a set of rays that emit from the waveguide through the plasma and calculating the power deposition along each ray trajectory. In general, a single-pass absorption is desirable in the inhomogeneous field of a tokamak in order to eliminate the cancelling effects of currents on opposite sides of the resonance. In a Maxwellian plasma at high-temperature conditions when single-pass absorption is achieved, it is possible to achieve

$U_o \gtrsim 1.5$ for O- and X-waves ,

$U_o \gtrsim 3.0$ for Bernstein waves .

In terms of practical units, Eq. (4-36) gives

$$\frac{I}{P_{total}} = \frac{n_e v_e}{m_e n v_e^2 \nu_o} \frac{\hat{J}}{\hat{P}} \frac{1}{2\pi R_o} = \frac{\epsilon_o^2 m_e v_e^2}{ne^3 \ \ell n \ \Lambda} \frac{1}{R_o} \frac{6}{5 + Z_i} U_o^2$$

$$\simeq 0.3 \frac{T_{10}}{n_{20} R_o \ \ell n \ \Lambda} \frac{6}{5 + Z_i} U_o^2 \qquad (A/W) \ . \tag{4-37}$$

Assuming $U_o \sim 3$, $Z_i \simeq 1$, and $\ell n \ \Lambda \simeq 18$, the efficiency becomes

$$\frac{I \ (MA)}{P \ (MW)} \simeq 0.15 \frac{T_{10}}{R_o n_{20}} \ , \tag{4-38}$$

where T_{10} is in units of 10 keV and n_{20} is in units of 10^{20} m^{-3}. Thus, for a reactor with parameters $R_o \simeq 5$ m, $n \simeq 10^{20}$ m^{-3}, and $T_e \simeq 20$ keV, $I/P \simeq 0.06$ MA/MW. To drive a current of 8 to 10 MA, power level on the order of 150 MW is required.

Consideration of trapped electron effects would reduce the current drive efficiency (as much as a factor of 2 to 3 depending on the location where the power is deposited). Nonlinear effects, on the other hand, can enhance $\hat{J}/\hat{P}$ (I/P).

4.4.4 Trapped Electron Effects [18,46]

The effect of electrons trapped in the toroidal magnetic field on the current drive efficiency has been considered in refs. [18] and [46]. The neoclassical trapped particle effect and the anisotropic resistivity tend to oppose each other. The degree of cancellation depends on where the microwave power is being deposited.

Results from a Fokker-Planck code are shown in Fig. 4.7, where the current drive efficiency is plotted as a function of inverse aspect ratio $\epsilon = r/R_o$. Figure 4.7 clearly shows the cancellation of the two effects, leading to a reduction of J/P and eventually to a reversal of the current for larger r/R_o. There is only a minimal reduction in the current drive efficiency if the power is deposited near the center of the plasma ($r \simeq 0$). To expand this point, Fig. 4.8 shows the variation of the ECRH-driven current density profile with a minor radius. It can

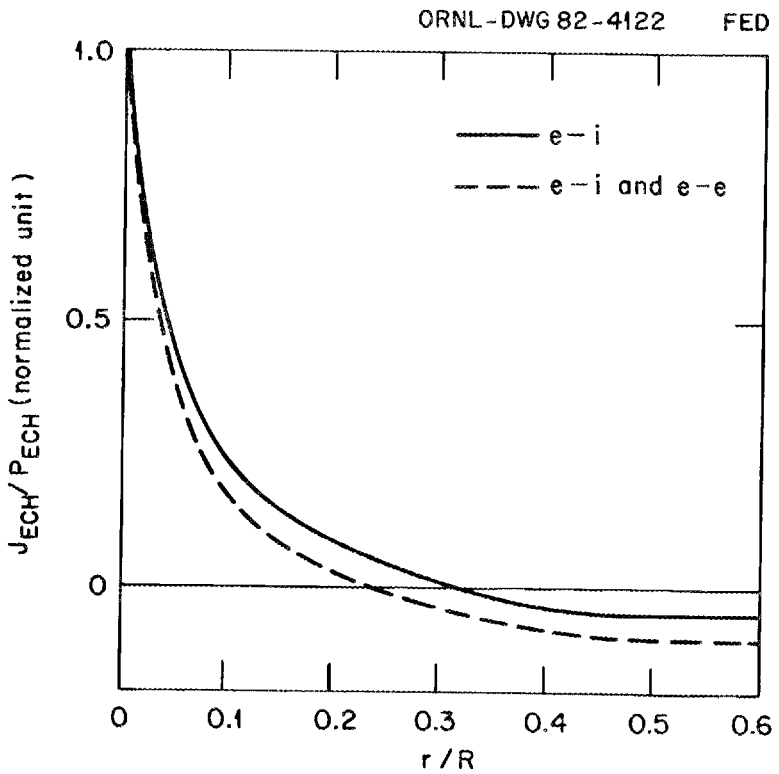

Fig. 4.7. ECH-driven current density per unit power as a function of $\epsilon = r/R_0$ with electron-ion collisions only (solid line) and with electron-ion and electron-electron collisions (dashed line) (refs. [46, 71]).

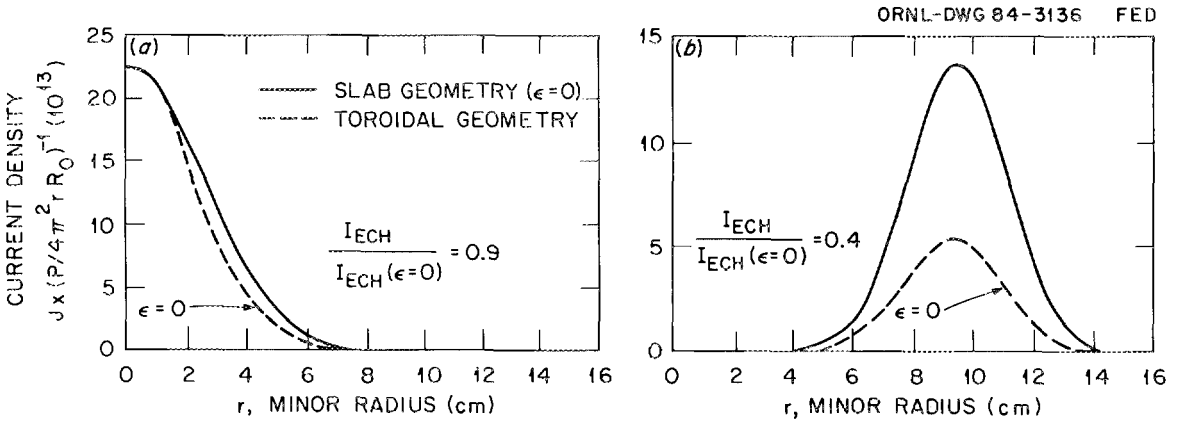

Fig. 4.8. ECRH-driven current density profile with power deposition (a) near the plasma center and (b) away from the plasma center without (solid lines) and with (dashed lines) toroidal corrections. Results are for an X-mode launched from the high-field side of a tokamak with parameters R_o = 140 cm, a = 30 cm, $n_o = 2.5 \times 10^{13}$ cm^{-3}, T_o = 1 keV, $\omega = 2\pi \times 60$ GHz, and $\eta_{\parallel} = ck_{\parallel}/\omega = 0.7$ (n and T profiles are assumed to be parabolic) (ref. [46]).

be seen that trapped electron effects produce only a small (~10%) reduction in the ECRH-induced current when the power is deposited (i.e., the current is centered) near the magnetic axis [Fig. 4.8(a)]. On the other hand, when the power is deposited away from the magnetic axis (i.e., when the current is flowing away from the center), a significant modification of the current profile occurs and the current drive efficiency is reduced to about one-third the value it has when trapped electrons are ignored [Fig. 4.8(b)]. This effect is claimed to be observed on TOSCA (see Fig. 4.3).

4.5. Relativistic Calculations [43,49,51,53,]

4.5.1 Resonance Condition

The electron cyclotron resonance condition for mildly relativistic electrons is given by Eq. (4-3):

$$\omega - k_{\parallel} v_{\parallel} - \ell\Omega_e \left(1 - v^2/2c^2\right) = 0$$

or

$$\omega - k_{\parallel} v_{\parallel} - \ell\Omega_e \left(1 - \frac{v_{\perp}^2 + v_{\parallel}^2}{2c^2}\right) = 0 \ ,$$

where $v^2/c^2 \ll 1$ and $\Omega_e = eB/m_o$, the nonrelativistic cyclotron frequency. In terms of normalized velocity space coordinates, $v_{\parallel}/v_e$ and $v_{\perp}/v_e$, the resonance condition is a semicircle,

$$\left(\frac{v_{\perp}}{v_e}\right)^2 + \left(\frac{v_{\parallel}}{v_e} - \frac{1}{2S}\right)^2 = \frac{1 - 4U_oS}{4S^2} \ , \qquad (4\text{-}39)$$

with a radius of $(1 - 4U_oS)^{1/2}/2S$ centered on the $v_{\perp}/v_e = 0$ axis at $v_{\parallel}/v_e = 1/2S$, where $U_o = (\omega - \ell\Omega_e)/k_{\parallel}v_e$ and $S = \ell\Omega_e v_e/2k_{\parallel}c^2$. In the nonrelativistic limit the resonance becomes the straight line $v_{\parallel}/v_e = U_o$, if the magnetic field is uniform, corresponding to Fig. 4.5(a).

Several resonance curves for positive values of S are shown in Fig. 4.9 for $U_o = 1$ and $U_o = -1$. For $S > 0$, positive values of U_o correspond to absorption on the low-field side of the electron cyclotron resonance in a tokamak. In this case the mass increase (due to relativistic effects) serves to increase the difference between the wave frequency ω and the cyclotron frequency Ω_e (or $\ell\Omega_e$), leading to resonant values of $v_\parallel$ that are always positive and greater than the nonrelativistic value. For $S > (1/4U_o)$, the frequency difference cannot be recovered by the Doppler shift for any value of $v_\parallel$; thus, a cutoff in wave absorption occurs. At the cutoff $v_\parallel/v_e = 2U_o$, $v_\perp/v_e = 0$.

On the high-field side of the electron cyclotron resonance the cyclotron frequency exceeds the wave frequency ($\ell\Omega_e > \omega$) for nonrelativistic electrons, and the resonance condition is satisfied by negative values of $v_\parallel$. For energetic electrons, on the other hand, the mass increase can cause the cyclotron frequency to fall below the wave frequency ($\ell\Omega_e/\gamma < \omega$, where γ is the relativistic factor), giving rise to positive values of $v_\parallel$ at resonance, as shown in Fig. 4.9(b). Thus, on the high-field side, electrons moving both parallel and antiparallel to the wave can absorb power.

For pure perpendicular propagation ($k_\parallel = 0$), all directionality disappears (as expected) and the wave is absorbed by isoenergetic electrons ($v_\perp = v_\parallel = v$). The resonance curve is a semicircle $v^2 = 2c^2(\ell\Omega_e - \omega)/\ell\Omega_e$ centered at $v_\parallel = v_\perp = 0$.

Further insights into the effects of finite temperature, $k_\parallel$ spectrum (or $\eta_\parallel = ck_\parallel/\omega$), spatial variation of magnetic field, etc., on the resonance condition may be obtained by solving Eq. (4-3) and writing it in a slightly different form than that given by Eq. (4-39) near the resonance layer:

$$\frac{v_\parallel}{c} = \eta_\parallel \pm \left(\eta_\parallel^2 - \frac{v_\perp^2}{c^2} - \frac{2\Delta_o}{\ell\Omega_e}\right)^{1/2} , \tag{4-40}$$

where $\Delta_o = \omega - \ell\Omega_e$. [In terms of the variables of Eq. (4-39), $2\Delta_o/\ell\Omega_e = (U_o/S)(v_e^2/c^2)$.] The magnetic field varies as $1/R$ ($B = B_oR_o/R$), and within the region of the electron cyclotron resonance, we assume a linear field profile with

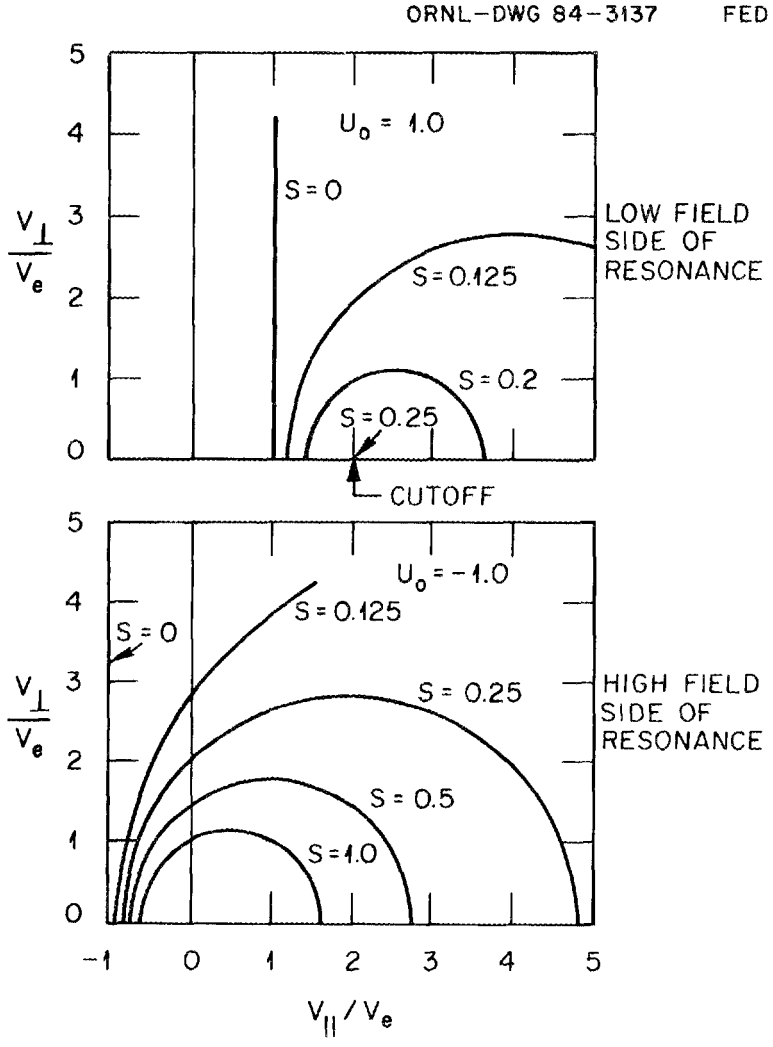

Fig. 4.9. Electron cyclotron resonance contours in velocity space for (a) $U_o = 1$ and (b) $U_o = -1$ for several values of S, which parameterizes the relativistic effect. Here $U_o = (\omega - \ell\Omega_e)/k_{||}v_e$ is the Doppler-shifted resonance velocity normalized to v_e and $S = \ell\Omega_e v_e/2k_{||}c^2$. $S = 0$ is the nonrelativistic limit. Note the cutoff for $U_o = 1$ as S reaches the value 0.25 (the cutoff condition is given by $S = 1/4U_o$). (a) Values of $U_o > 0$ correspond to absorption on the low-field side of the resonance, and (b) values of $U_o < 0$ correspond to absorption on the high-field side of the resonance (ref. [49]).

$$\frac{\omega - \ell\Omega_e}{\ell\Omega_e} \simeq \frac{x}{R_o} , \tag{4-41}$$

where x is the distance measured from the resonance. Note that the low-field side of the resonance corresponds to $x > 0$ and the high-field side corresponds to $x < 0$. The dependence of $v_\parallel$ on $\eta_\parallel$, $v_\perp$, and $\Delta_o/\ell\Omega_e$ (or x/R_o) is shown in Fig. 4.10. Plotted as a function of $\Delta_o/\ell\Omega_e$, the resonant values of $v_\parallel$ for fixed $v_\perp$ lie on a parabola, as illustrated in Figs. 4.10(a) and (b) for $\eta_\parallel = 0.1$ and 0.2, respectively. The nonrelativistic limit corresponds to a line that is tangential to the $v_\perp = 0$ parabola at the origin (resonance location), independent of $v_\perp$. It is clear from Fig. 4.10 that even at nonrelativistic temperatures ($T_e \sim 1$-10 keV) relativistic corrections to the resonance condition are important, in that the resonant values of $v_\parallel$ are no longer antisymmetric about the resonance.

We see from Eq. (4-40) that there are no resonant particles if x/R_o ($\equiv \Delta_o/\ell\Omega_e$) $> \eta_\parallel^2/2$. This condition determines a point on the low-field side for which there is neither power absorption nor current drive.

4.5.2 Strong Relativistic Limit ($v \sim c$) [43]

In the absence of relativistic corrections, the current drive efficiency $\hat{J}/\hat{P}$ increases without bound as $P_\parallel^2$, the square of the toroidal momentum. [In the nonrelativistic limit $P_\parallel = mv_\parallel$ and Eq. (4-36) scales as $\hat{J}/\hat{P} \sim P_\parallel^2$.] However, as the velocity of the resonant electrons (i.e., the current carriers) approach the speed of light, the previous statement becomes invalid and the inclusion of relativistic dynamics to the Fisch-Boozer single-particle model shows a bound on the limits of current drive efficiency [43].

In the strongly relativistic limit, Fig. 4.11 exhibits the results of ref. [43] both for lower hybrid and ECRH. Note that the normalization constants for current and the dissipated power are somewhat different than those used earlier. In Fig. 4.11, J is normalized to $-enc$ (not $-env_e$) and P is normalized to $\nu nm_o c^2$ (not $\nu_o nm_e v_e^2$), where $\nu = \nu_o(v_e/c)^3$ and m_o is the rest mass of electrons. In terms of conventional normalizations used earlier,

$$\hat{J}/\hat{P} \rightarrow (\hat{J}/\hat{P})_c (c^2/v_e^2) ,$$

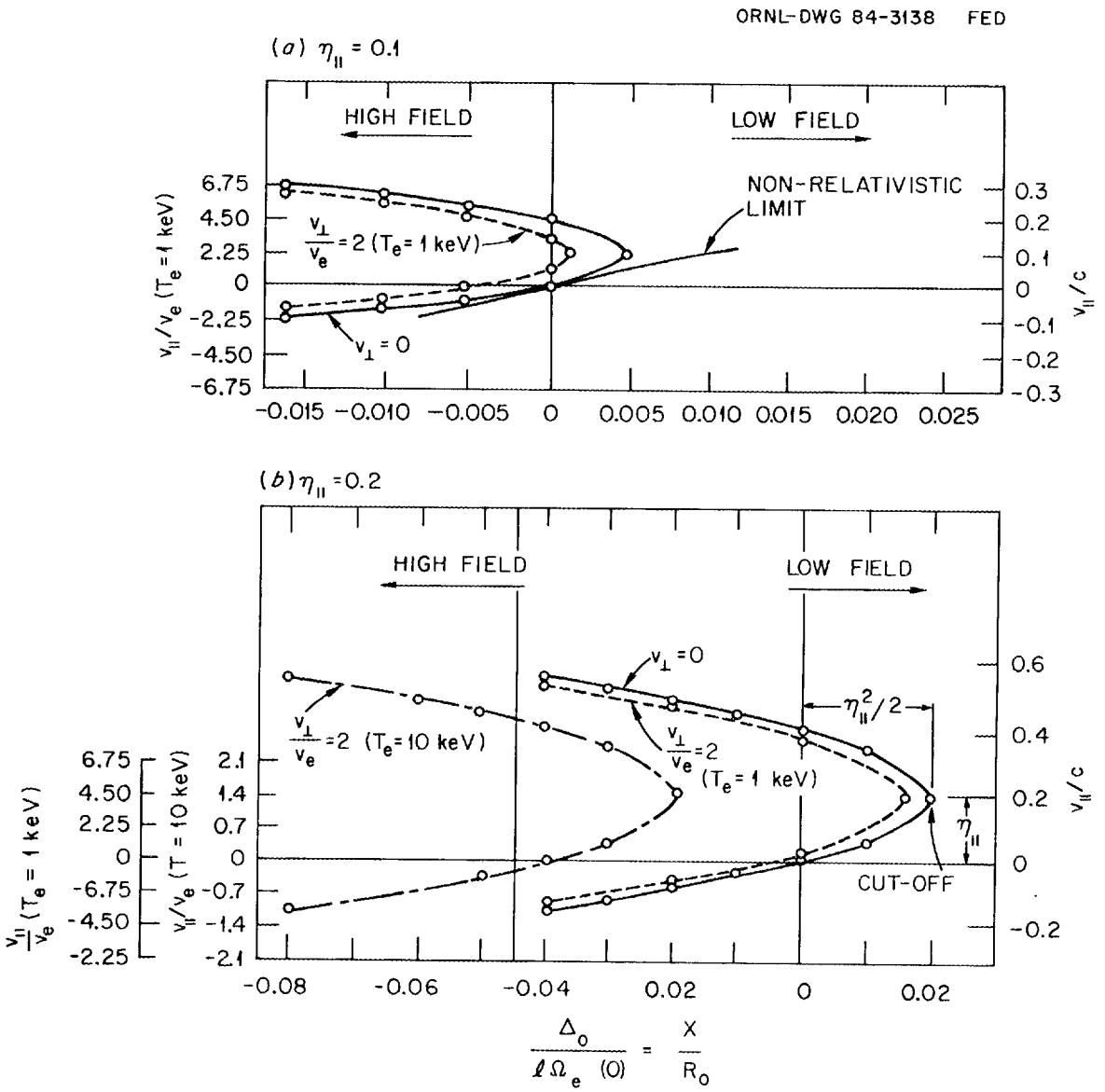

Fig. 4.10. $v_\parallel/c$ as a function of $\Delta_o/\ell\Omega_e$ ($= x/R_o$) with $v_\perp/v_e$ as a parameter: (a) $\eta_\parallel = 0.1$, and (b) $\eta_\parallel = 0.2$. Note that there is no resonance for $x/R_o > \eta_\parallel^2/2$. Here, $\Delta_o = \omega - \ell\Omega_e(x)$ and x is measured from the resonance. (Based on a similar figure from ref. [53]).

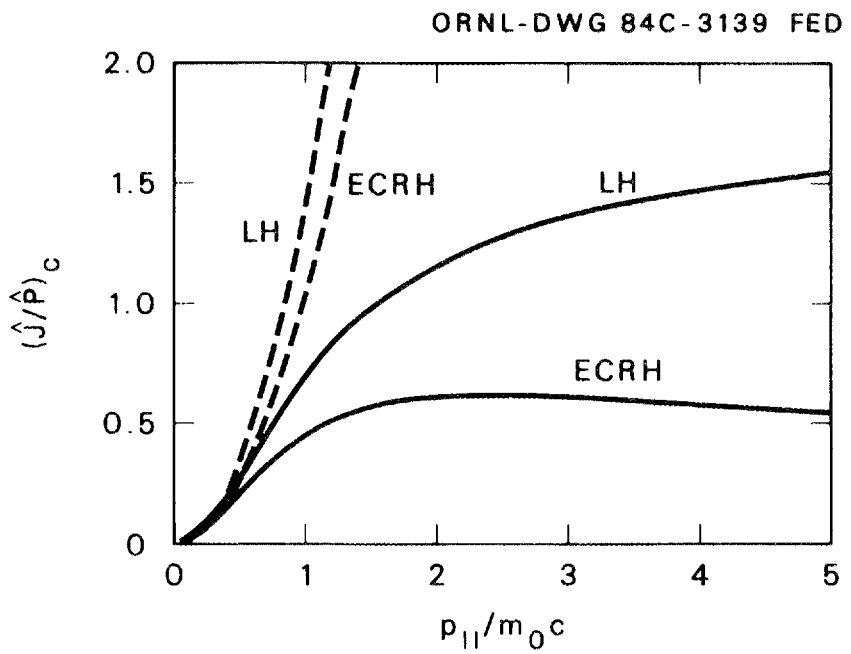

Fig. 4.11. $(\hat{J}/\hat{P})_c$ vs normalized parallel momentum $p_{\parallel}/m_0c$. The dashed lines indicate the nonrelativistic treatment. Here $Z_i = 1$ and $p \simeq p_{\parallel} (\gg p_{\perp})$ are assumed. Note that in $(\hat{J}/\hat{P})_c$ J is normalized to $-enc$ and p to $\nu n m_0 c^2$, where $\nu = \omega_{pe}^4 \ln \Lambda / 2\pi n c^3$. Efficiency of current drive increases nonrelativistically (dashed lines) with increasing momentum of the resonant electrons. However, there is a bound to the efficiency due to relativistic dynamics (solid lines) in the limit $v \sim c$ (ref. [43]).

where $(\hat{J}/\hat{P})_c$ is the numerical factor to be taken from Fig. 4.11. In terms of practical units

$$\frac{I}{P_{total}} \simeq \frac{15.65}{n_{20}R_o \ \ell n \ \Lambda} \left(\frac{\hat{J}}{\hat{P}}\right)_c \quad (A/W) \ . \tag{4-42}$$

Equation (4-42) applies explicitly to the strongly relativistic regime, where the electron velocity $v \sim c$. However, as seen in the previous section, the relativistic effects are important even when $v_e \ll c$.

4.5.3 Weak Relativistic Limit ($v^2/c^2 \ll 1$)

For mildly relativistic electrons ($v^2/c^2 \ll 1$), one might neglect the relativistic dynamics of fast particles and consider only the relativistic correction to the resonance condition arising from the velocity dependence of the electron cyclotron frequency. These calculations are given in refs. [49,53]. To calculate the effect of electron cyclotron waves on the particle distribution, the linearized, steady-state Fokker-Planck equation is used. The wave contribution is of the form given by Eq. (4-28) with the relativistic correction included only in the cyclotron frequency in the δ-function, which expresses the resonance condition. Here, we present a few results to illustrate the effects of the relativistic resonance condition on the driven current.

In Fig. 4.12 we show representative current profiles obtained from nonrelativistic and relativistic theories for a tokamak with $T_e = 1$ keV, $R_o = 1.2$ m with a wave frequency $f = 60$ GHz, and a density such that $\omega_{pe}^2/\omega^2 = 0.75$. Figure 4.12 represents the wave incident from the low-field side of the resonance in the O-mode with an angle of incidence such that $\eta_{\parallel} = 0.1$. From this figure we see the effect of the sharp cutoff on the low-field side. We also note that according to the nonrelativistic theory the current density changes sign at the origin, whereas in the relativistic case the current does not reverse in going through the origin (with the origin refering to the resonance location where $x = 0$). This nonreversal of current is much more pronounced for small values of $\eta_{\parallel}$, where relativistic effects are very important. This is because for small $\eta_{\parallel}$ (i.e., small $k_{\parallel}$) the Doppler shift component in the resonance condition plays only a minor role compared to the mass increase.

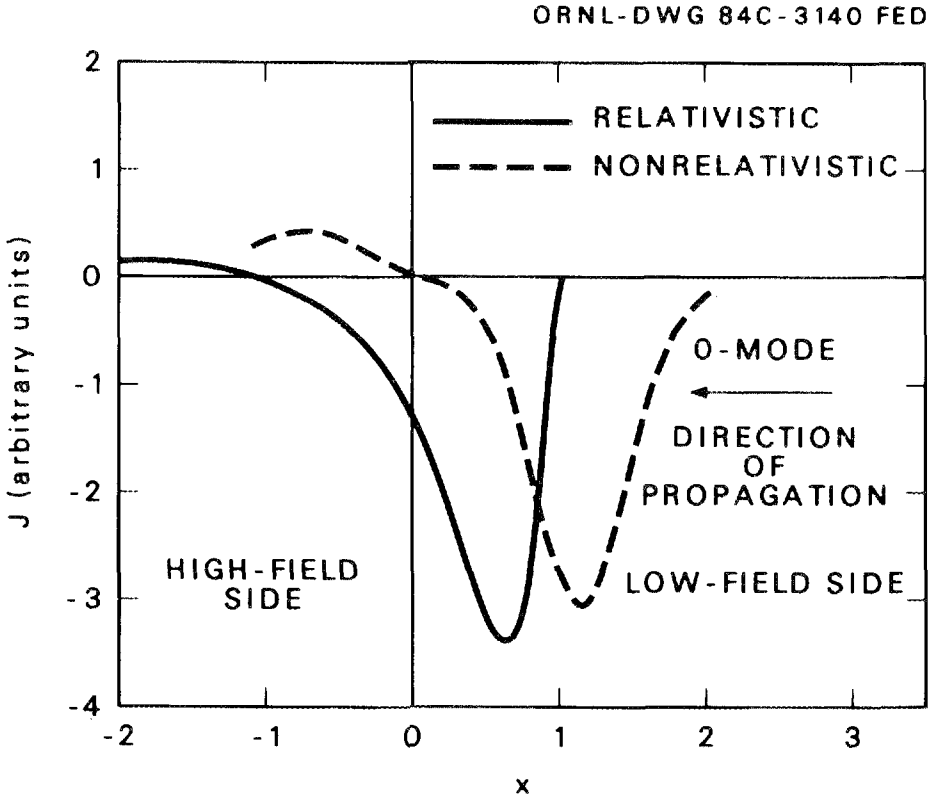

Fig. 4.12. Current profile for O-mode incident from the low-field side for relativistic (solid line) and nonrelativistic (dashed line) resonance conditions for $\ell = 1$. Representative tokamak parameters are $T = 1$ keV, $R_o = 1.2$ m, with $f = 60$ GHz, $\omega_{pe}^2/\omega^2 = 0.75$, and $\eta_{\parallel} = 0.1$. Here x is the distance measured from the resonance ($x > 0$ corresponds to low-field side and $x < 0$ corresponds to the high-field side). A negative current density is in the opposite direction to the $k_{\parallel}$ vector of the wave. (Based on similar figures from refs. [50, 53]).

When the wave is incident from the high-field side (in which case the resonance is accessible by either O- or X-mode), absorption may occur (and thus the current drive may start) far from the cyclotron resonance. Note from Fig. 4.10 that the resonant velocities get smaller as the resonance is approached and absorption and current drive can begin as soon as there are a sufficient number of resonant electrons to produce a significant effect. If the plasma is sufficiently hot, strong absorption could be possible well before the wave reaches the cyclotron resonance. Such an example is illustrated in Fig. 4.13, which shows the current profile produced by the O-mode (incident from the high-field side). Representative parameters are $T_e = 5$ keV, $R_o = 5$ m, $f = 150$ GHz, $\omega_{pe}^2/\omega^2 = 0.75$, and $\eta_{\parallel} = 0.1$. The current profile for the X-mode, incident from the high-field side, is very similar.

4.6. Comments

The basic mechanism of current drive by electron cyclotron waves is well established theoretically (Sect. 4.1), and there is some experimental evidence that such currents exist (Sect. 4.2). However, more detailed experiments (particularly in large, hot, and dense plasmas) are necessary before a definitive conclusion can be reached about the viability of ECRH current drive for practical applications.

On the theoretical side, nonrelativistic and relativistic treatments are used. The calculations in the first category (Sect. 4.4) are more elaborate where the full Fokker-Planck model has been solved including the effects of trapped electrons and toroidal geometry. However, in most calculations the wave amplitude is assumed to be small so that the electron distribution function is perturbed only slightly. Also assumed in these calculations is a constant quasi-linear wave diffusion coefficient (independent of velocity space variables). The only nonlinear calculation (not discussed here) is given in ref. [45], where the diffusion coefficient is taken large enough to perturb the electron distribution significantly. The calculations, however, use the nonrelativistic resonance condition and neglect the trapped particle effects.

Relativistic effects are important for description of energetic electrons in reactor-like plasmas. Relativistic corrections to the resonance condition change the whole picture of ECRH current drive even at modest temperatures (few kiloelectron volts) for small $k_{\parallel}$

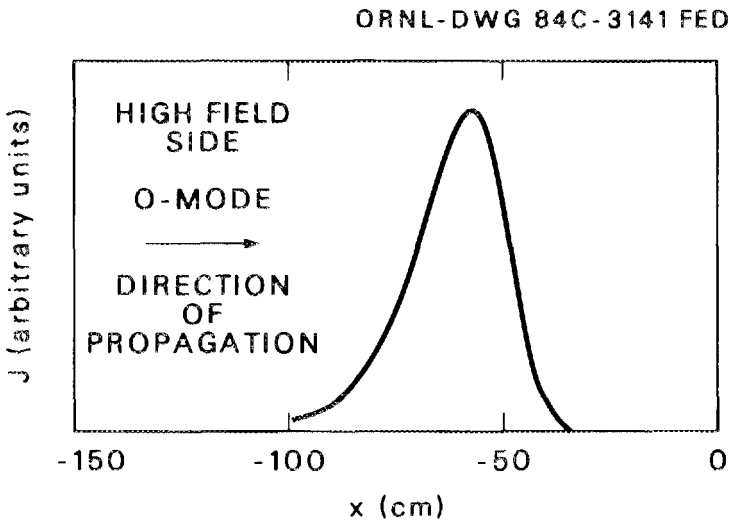

Fig. 4.13. Current profile for O-mode incident from the high-field side for a plasma with $T = 5$ keV, $R_o = 5$ m, $f = 150$ GHz, $\omega_{pe}^2/\omega^2 = 0.75$, and $\eta_{\parallel} = 0.1$. Current starts to be driven at 1 m from resonance and falls to zero at about 30 cm before the resonance is reached, because the wave has been completely absorbed by then (not because current cannot be driven nearer the resonance). (Based on a similar figure from ref. [53]).

(Sect. 4.5). It is not, however, clear whether this correction will improve or reduce the reactor potential of ECRH current drive. Nonlinear calculations including all significant effects have yet to be carried out.

5. CURRENT DRIVE BY ION CYCLOTRON WAVES – MINORITY SPECIES HEATING [54–57,60,70,84]

Another scheme to drive the toroidal current is the use of rf waves in the ion cyclotron range of frequencies (ICRF). The ICRF scheme differs fundamentally from LH and ECRH schemes (discussed in Sects. 3 and 4, respectively) in that waves interact with ions rather than with electrons. As in the case of ECRH, these waves do not have net toroidal momentum.

The possibility of using ICRF waves to drive currents in a plasma was first proposed by Fisch [54] as an extension of the Fisch–Boozer mechanism [41] discussed in Sect. 4.1. In this scheme, the interaction of a traveling wave with minority ions of a particular parallel velocity [such that they are Doppler-shifted into resonance with the wave $(\omega - \ell\Omega_i)/k_{\parallel}$, where Ω_i is the ion cyclotron frequency] leads to an increase in their perpendicular (and hence total) velocity. The resulting reduction in collisionality with the bulk plasma ions sets up a relative drift between the two ion species [i.e., between majority (bulk) and minority ions]. Collisions between the bulk and minority ions and the plasma electrons generate an electron drift. As a result, a net current is produced. Thus, ICRF current drive may be considered a combination of the Fisch–Boozer mechanism (discussed in Sect. 4) and Ohkawa's method of driving current by neutral beams (discussed in Sect. 2). It is similar to neutral beam current drive in that it requires a relative drift between the bulk ions and the minority ions. This relative drift is achieved by the Fisch–Boozer mechanism, that is, by asymmetrically heating minority ions (see Fig. 4.1).

The main disadvantage of this scheme is that a traveling ICRF wave is required if a net drift between the ion species is to be generated. In principle, this may be achieved by the use of an array of phase-shifted antennae, although production of such waves has not yet been attempted experimentally. As such, no experimental measurements of current drive by ICRF waves have been recorded to date. However, the theory has been pursued vigorously.

It is also possible to use the ICRF wave not only to stand alone for current drive but also to enhance the current driven by beams. In this hybrid scheme, the neutral beam injection mainly supplies toroidal momentum and is sustained by ICRF wave heating [84].

If power is viable, one of the advantages of the ICRF minority heating scheme might be the fact that there are several parameters

expression for the net current density, including the electron trapping contribution, is then given by

$$J \simeq J_h \left[1 - \frac{Z_h}{Z_{eff}} + 1.46\, \epsilon^{1/2} \frac{Z_h}{Z_{eff}} A(Z_{eff}) \right] , \qquad (5\text{-}19)$$

where $A(Z_{eff})$ is a function of Z_{eff}, tabulated in Table 2.1. For $Z_{eff} = 1$, $A(1) \simeq 1.68$. The electrons in the trapped region participate in dragging the ions but do not contribute to current. The fraction of them is proportional to $\epsilon^{1/2}$ ($\epsilon = r/R_o$, the inverse aspect ratio). Depending on the choice of minority species, the trapped electron effect, which is the last term in Eq. (5-19), can qualitatively change the generated current.

The amount of minority current J_h generated can be appreciably altered by the consideration of the trapped ions. Depending on the minority-majority species mix (D-H, D-He^3, etc.), the trapped ions can decrease the minority current appreciably [55]. Usually, the effect of trapped electrons on total current J is much more pronounced than the effect of trapped ions on minority current J_h [55].

Before calculating an efficiency factor, a few observations can be made from Eq. (5-18) [or (5-19)]. For the ICRF scheme of current generation to be useful, a number of criteria must be satisfied.

We first examine the criteria to be satisfied by the charge states of the minority and majority species. If toroidal effects are neglected, from Eq. (5-18) we note the condition

$$Z_h(1 - Z_h/Z_{eff}) \neq 0 \qquad (5\text{-}20)$$

for current generation. Satisfying this condition implies that $Z_h \neq 0$ $Z_h \neq Z_{eff}(\simeq Z_i)$.

For ICRF waves to be employed for current generation via minority species heating a second condition must be imposed:

$$\Omega_h \neq \Omega_i \qquad (5\text{-}21)$$

or

(type of minority species, minority concentration, and the $k_{\parallel}$ spectrum) that can be adjusted and controlled for optimized experimental conditions (and optimum efficiency).

In this section we give a brief description of the ICRF current drive mechanism by minority species heating and identify the wave regime and plasma parameters for which this scheme operates optimally in reactor applications. We shall also discuss the wave penetration and power deposition characteristics and modifications to the current generated by trapped particles and majority-minority species mix.

5.1. Basic Mechanism of ICRF Current Generation by Minority Species Heating [54]

The operation of the ICRF scheme may be thought of as a two-step process. The first step is the inducement of a relative (toroidal) drift velocity between the bulk (majority) ions and the minority ions. The second step is the response of the electrons to the ion distribution. The electrons can drift even when the total ion current vanishes.

The relative drift can be accomplished by selective heating of minority ions in one direction of parallel velocity space (see Fig. 4.1). Consider, for example, a single-test minority-species ion that moves to the right, which is the direction parallel to the magnetic field. The collision frequency between the test (minority) ion and the background majority ions, which exert a drag force, is sensitive to the test (minority) in energy. By preferential heating of this test ion from energy W_1 (and collision frequency ν_1) to a higher energy W_2 (and lower collision frequency ν_2), the drag force on the test ions can be reduced, and as a result the relative drift can be produced. The energy increase need not occur as a result of increase in any specific velocity component. The increase in energy can be accomplished through the damping of a traveling plasma wave that is in resonance with these minority ions. Such a wave is the ion cyclotron wave at a frequency near the minority-ion cyclotron frequency. These waves are fast waves or magnetosonic waves and, in principle, would be launched unidirectionally in the toroidal direction in a tokamak.

We first calculate the amount of power necessary to establish a given minority species ion drift.

5.1.1 Power Dissipation

Consider the displacement in velocity space of a small number, δf, of minority ions from region 1 to region 2 due to rf heating, as illustrated in Fig. 4.1. Let us assume that momentum in the direction of interest is lost from the minority ions at a rate ν_1 and ν_2 in locations 1 and 2, respectively. These rates include collisions with the background majority ions and with electrons. For small minority ion concentrations, self-collisions may be neglected.

Here we follow the analysis of Sect. 4.1. Basically, the amount of energy required to displace the minority ions from location 1 to location 2 is given by Eq. (4-4), that is,

$$\Delta W = (W_2 - W_1)\delta f \ , \tag{5-1a}$$

$$W_{1,2} = m_h v_{1,2}^2/2 \ , \tag{5-1b}$$

where $v_{1,2}$ is the velocity at location 1,2 and m_h is the mass of minority-species ions.

The change in parallel momentum in the minority species induced by this displacement (i.e., by this preferential heating) is given approximately by

$$\Delta p_{\parallel} \simeq m_h \delta f \left[v_{2,\parallel} \exp(-\nu_2 t) - v_{1,\parallel} \exp(-\nu_1 t) \right] \ , \tag{5-2}$$

where energy scattering is neglected.

Note that at $t = 0$, the instant in which the displacement occurs, there is no change in parallel momentum unless $v_{2,\parallel} \neq v_{1,\parallel}$. That is, unless there is an impulse given to the minority ions in the parallel direction, there initially can be no flow in that direction. At $t \to \infty$, however, even if $v_{1,\parallel} \neq v_{2,\parallel}$, all directed momentum has relaxed through collisions with other species so that there can be no relative drift of the minority ion species with respect to the majority ions.

Consider the case $v_{1,\parallel} = v_{2,\parallel}$. In view of the above, $\Delta p_{\parallel}$ vanishes at both $t = 0$ and $t \to \infty$. At finite times, however, there will be a

finite $\Delta p_{\parallel}$ if $\nu_1 \neq \nu_2$. Implied here is an asymmetric drag on the minority ion species. By continuously supplying energy, the resulting drift can be continuously maintained.

The time average of the parallel momentum over an interval Δt that is long compared to the momentum destruction times $1/\nu_1$ and $1/\nu_2$ is

$$p_h \equiv \frac{1}{\Delta t} \int_0^{\Delta t} dt\, \Delta p_{\parallel} \simeq \frac{m_h \delta f}{\Delta t} \left(\frac{v_{2,\parallel}}{\nu_2} - \frac{v_{1,\parallel}}{\nu_1} \right) . \tag{5-3}$$

The dissipated power over this time interval is

$$P_{rf} \simeq \Delta W/\Delta t = (W_2 - W_1)\delta f/\Delta t \ . \tag{5-4}$$

Combining Eqs. (5-3) and (5-4) we find the ratio of minority species momentum to power dissipated:

$$\frac{p_h}{P_{rf}} = m_h \frac{(v_{2,\parallel}/\nu_2 - v_{1,\parallel}/\nu_1)}{(W_2 - W_1)} \ . \tag{5-5}$$

In the limit $\mathbf{v}_1 \to \mathbf{v}_2$

$$\frac{p_h}{P_{rf}} = m_h \frac{\mathbf{s} \cdot \nabla_v (v_{\parallel}/\nu)}{\mathbf{s} \cdot \nabla_v W} , \tag{5-6}$$

where $\mathbf{s}$ is the unit vector in the direction of velocity displacement, ∇_v is the velocity space del operator, and $W = m_h v^2/2$.

5.1.2 Current Density

The current arises from the motion of electrons reacting to the relative drift between the two ion species. We see from Eq. (5-6) that there is a drift of the minority species if

$$\mathbf{s} \cdot \nabla_v (v_{\parallel}/\nu) \neq 0 \ ,$$

which occurs in two ways; that is, either

$$\mathbf{s} \cdot \nabla_v v_{\parallel} \neq 0 \tag{5-7a}$$

or

$$\mathbf{s} \cdot \nabla_v \nu \neq 0 \ . \tag{5-7b}$$

When Eq. (5-7a) holds, net momentum is imparted from an external source directly to the minority species as the ions are pushed to higher $v_{\parallel}$. To keep the plasma from rotating, it is necessary that an equal amount of momentum, but in the opposite direction, be imparted to the majority species, also from an external source. If the minority species is fast enough to collide mainly with the electrons, an electric current is driven and can be maintained efficiently. The process just described is similar in concept and efficiency to driving currents by neutral beams (see Sect. 2).

When Eq. (5-7b) holds, but not Eq. (5-7a), a minority ion species drift develops even though no net momentum is injected. This is similar to the Fisch-Boozer mechanism, which is considered for electrons in Sect. 4. There is, however, one constraint here in that the minority ions should not collide either too frequently or too infrequently with the electrons as compared to the frequency of collisions with the majority ions.

To calculate the amount of current generated, we assume that the effective collision frequency is

$$\nu = \nu_e + \nu_i \ , \tag{5-8}$$

where ν_e and ν_i are the rates of momentum loss (from minority species ions) to electrons and to majority ions, respectively. The regime of interest is

$$v_i \ll v \ll v_e \ , \tag{5-9}$$

where $v_i = (kT_i/m_i)^{1/2}$, $v_e = (kT_e/m_e)^{1/2}$, and v is the velocity of the minority ions. Here, the first inequality ($v_i \ll v$) ensures that Eq. (5-7b) is satisfied. The second inequality ($v \ll v_e$) arises in practical situations simply because $m_e \ll m_i$. In this limit [i.e., Eq. (5-9)], neglecting energy scattering, momentum loss rates are those of slowing-down rates; thus, we have

$$\nu = \nu_i + \nu_e ,$$

$$= \frac{n_e Z_h^2 e^4 \ \ell n \ \Lambda}{4\pi\epsilon_o^2 m_h^2} \left[\frac{Z_i}{v^3}\left(1 + \frac{m_h}{m_i}\right) + \frac{1}{3}\left(\frac{2}{\pi}\right)^{1/2} \frac{1}{v_e^3}\left(1 + \frac{m_h}{m_e}\right)\right] \qquad (5\text{-}10a)$$

$$= \frac{\nu_o}{2} Z_h^2 \left(\frac{m_e}{m_h}\right)^2 \left[Z_i \left(\frac{v_e}{v}\right)^3\left(1 + \frac{m_h}{m_i}\right) + \frac{1}{3}\left(\frac{2}{\pi}\right)^{1/2}\left(1 + \frac{m_h}{m_e}\right)\right] , \qquad (5\text{-}10b)$$

where $\nu_o = n_e e^4 \ \ell n \ \Lambda/2\pi\epsilon_o^2 m_e^2 v_e^3$. The first term in square brackets is the ion contribution (slowing down of the test minority ions on background majority ions in the limit $v_i \ll v$), and the second term is due to the electrons. Since the ions are much slower than the electrons, ν_e is insensitive to the test ion (minority ion) velocity, as we see from Eq. (5-10). Basically, we have

$$\nu_e = C_e , \qquad (5\text{-}11a)$$

$$\nu_i = C_i (v_e/v)^3 = C_i (T_e/W)^{3/2} (m_h/2m_e)^{3/2} , \qquad (5\text{-}11b)$$

where $W = m_h v^2/2$ is the minority species energy and C_e and C_i are constants, which are given by Eq. (5-10):

$$C_e = \frac{\nu_o}{2}\frac{Z_h^2}{3}\left(\frac{2}{\pi}\right)^{1/2}\left(\frac{m_e}{m_h}\right)^2\left(1 + \frac{m_h}{m_e}\right), \tag{5-11c}$$

$$C_i = \frac{\nu_o}{2} Z_h^2 Z_i \left(\frac{m_e}{m_h}\right)^2\left(1 + \frac{m_h}{m_i}\right). \tag{5-11d}$$

[Note that once again the subscripts e, i, and h correspond to electrons, majority ions, and minority ions, respectively.] In Eqs. (5-10) and (5-11), it is assumed that $n_e \simeq n_i Z_i \gg n_h Z_h$.

Using Eqs. (5-10) and (5-11) in Eq. (5-6), we obtain

$$\frac{p_h}{P_{rf}} = \frac{m_h}{\mathbf{s}\cdot\nabla_v W}\left[\mathbf{s}\cdot\nabla_v(v_\parallel/\nu)\right]$$

$$= \frac{m_h}{\mathbf{s}\cdot\nabla_v W}\left[\frac{1}{\nu}\mathbf{s}\cdot\nabla_v v_\parallel + v_\parallel \mathbf{s}\cdot\nabla_v\left(\frac{1}{\nu}\right)\right]$$

$$= \frac{m_h}{\mathbf{s}\cdot\nabla_v W}\left[\frac{1}{\nu}\mathbf{s}\cdot\nabla_v v_\parallel + \frac{3v_\parallel\nu_i}{2\nu^2}\frac{\mathbf{s}\cdot\nabla_v W}{W}\right]. \tag{5-12}$$

For a purely perpendicular heating ($\mathbf{s} = \mathbf{v}_\perp/v_\perp$), the first term in the square bracket of Eq. (5-12) is zero [i.e., $\mathbf{s}\cdot\nabla_v v_\parallel = 0$, which means Eq. (5-7a) does not hold, but Eq. (5-7b) does hold], and we have

$$\frac{p_h}{P_{rf}} = \frac{3}{2} m_h v_\parallel \left(\frac{\nu_i}{\nu}\right)\left(\frac{1}{\nu W}\right). \tag{5-13}$$

It is obvious from Eq. (5-13) that p_h vanishes when $\nu_i \to 0$ and $\nu_i \to \infty$. The largest and, hence, more favorable p_h/P_{rf} will be attained when $\nu_i \sim \nu_e \sim \nu/2$.

We now calculate the amount of current generated per power dissipated. The calculations are similar to those given in Sect. 2.1.2. Assume that the minority ion species drifts at a speed $v_{h\parallel}$ parallel to the magnetic field whereas the majority ion species

drifts at a speed $\bar{v}_i$. The electron parallel drift speed $\bar{v}_e$ can be obtained from the force balance equation [Eq. (2-8)]; that is, in the steady state $\bar{v}_e$ must obey

$$n_e m_e \frac{d\bar{v}_e}{dt} = 0 = n_h m_h \frac{v_{h\parallel} - \bar{v}_e}{\tau_{he}} + n_i m_i \frac{\bar{v}_i - \bar{v}_e}{\tau_{ie}}$$

$$= n_h m_h \nu_{he}(v_{h\parallel} - \bar{v}_e) + n_i m_i \nu_{ie} (\bar{v}_i - \bar{v}_e) \qquad (5\text{-}14a)$$

$$\simeq n_h Z_h^2 (v_{h\parallel} - \bar{v}_e) + n_i Z_i^2 (\bar{v}_i - \bar{v}_e) \ , \qquad (5\text{-}14b)$$

where in the last step we have used the ordering $\bar{v}_i \ll v \ll \bar{v}_e$ [Eq. (5-9)]. The first term in Eq. (5-14) is associated with the momentum gained by the electrons from the minority species ions and the second term represents the momentum lost by the electrons to the background majority ions. For the ordering of velocities,

$$\nu_{he}/\nu_{ie} \simeq (m_i/m_h)(Z_h^2/Z_i^2) \ ,$$

that is, the electrons collide with the minority ions $(Z_h^2/m_h)/(Z_i^2/m_i)$ times more often than with the majority ions.

In the case of no net parallel momentum injected into the minority species, the plasma will have no net parallel momentum so that the drifts must satisfy

$$n_h m_h v_{h\parallel} + n_i m_i \bar{v}_i + n_e m_e \bar{v}_e = 0 \ . \qquad (5\text{-}15)$$

Note that in the case where there is an injected net parallel momentum [Eq. (5-15)] conservation of total momentum can be considered to apply in the center-of-mass frame instead of the rest frame. This transformation does not affect the current as long as the charge neutrality is obeyed, that is,

$$n_e = n_i Z_i + n_h Z_h \ . \tag{5-16}$$

The current density is given by

$$J = e(Z_h n_h v_{h\parallel} + Z_i n_i \bar{v}_i - n_e \bar{v}_e) \ . \tag{5-17}$$

Using Eqs. (5-14)-(5-16) in Eq. (5-17) and taking the limit $m_e/m_i \to 0$, we obtain

$$J = e n_h v_{h\parallel} Z_h \left[1 - \frac{Z_h}{Z_{eff}} - \frac{m_h}{m_i} \frac{Z_i}{Z_h} \left(1 - \frac{Z_i}{Z_{eff}} \right) \right] \tag{5-18a}$$

$$\simeq e n_h v_{h\parallel} Z_h (1 - Z_h/Z_{eff}) \simeq e n_h v_{h\parallel} Z_h (1 - Z_h/Z_i)$$

$$= J_h (1 - Z_h/Z_{eff}) \ , \tag{5-18b}$$

where $Z_{eff} = \sum_j n_j Z_j^2/n_e = (n_i Z_i^2 + n_h Z_h^2)/n_e$ and $J_h = e n_h v_{h\parallel} Z_h$ is the minority species (ion) current. In writing Eq. (5-18b) we assume a practical regime, where

$$n_e \simeq n_i Z_i \gg n_h Z_h$$

and $n_i Z_i^2 \gg n_h Z_h^2$, which leads to $Z_{eff} \simeq Z_i$. In Eq. (5-18), the first term is clearly due to minority-driven current. The rest of Eq. (5-18) is the sum of the majority ion and electron currents. [Note the similarity of Eqs. (2-11) and (5-18).] In Eq. (5-18) trapped electrons (i.e., toroidal effects) are not included.

As mentioned previously, there are certain similarities between the neutral beam method of driving current and the ICRF minority heating scheme; both rely on the generation of a minority current. Thus, the techniques used to calculate electron trapping effects on current can be directly applied [see Eqs. (2-13)-(2-16)]. The

$$Z_h/m_h \neq Z_i/m_i \ .$$

This is the requirement that the ion species cyclotron frequencies be disparate. This is necessary for the ICRF wave to distinguish between the two ion species so that energy can be transferred selectively to the minority species. In most cases Eq. (5-21) should be satisfied for the first few harmonics (i.e., $\Omega_h \neq \ell\Omega_i$ $\ell = 1, 2$) to avoid heating of the majority ions, especially at the second harmonic ($\ell = 2$), where wave absorption can be appreciable.

When toroidal effects are included a significant current can be generated even when $Z_h = Z_{eff}$; thus, a condition given by Eq. (5-20) is relaxed.

5.1.3 Efficiency Factor

The amount of current generated by power dissipated, J/P, can now be obtained by making use of Eqs. (5-13) and (5-18) [or (5-19) if toroidal effects need to be considered]:

$$\frac{J}{P_{rf}} \simeq \frac{J}{P_h}\frac{P_h}{P_{rf}} = \frac{en_h v_{h\parallel} Z_h(1 - Z_h/Z_{eff})}{n_h m_h v_{h\parallel}} \cdot \frac{3}{2} m_h v_\parallel \frac{\nu_i}{\nu^2 W}$$

$$= \frac{3}{2} e v_\parallel Z_h \left(1 - \frac{Z_h}{Z_{eff}}\right)\frac{\nu_i}{\nu^2 W} \ . \qquad (5\text{-}22)$$

We note that Eq. (5-22) applies only when the parallel momentum injected into the minority species from the external source is negligible. That is, Eq. (5-22) is valid only for perpendicular heating. If there exists a net parallel momentum input to the minority species, we must retain both terms in Eq. (5-12). [Note that the first term in Eq. (5-12) was set equal to zero for perpendicular heating.] Inclusion of toroidal effects modifies the term in the parentheses in Eq. (5-22), similar to Eq. (5-19).

In terms of normalized quantities we may rewrite Eq. (5-22) as

$$\hat{J}/\hat{P} = (-\, en_e v_e/\nu_o m_e n_e v_e^2)^{-1} \cdot J/P$$

$$= \frac{3}{2}\frac{m_e(v_e v_{\parallel})}{W} Z_h \left(\frac{Z_h}{Z_{eff}} - 1\right)\left(\frac{\nu_o \nu_i}{\nu^2}\right)$$

$$= 3\left(\frac{m_e}{m_h}\right)\left(\frac{v_e v_{\parallel}}{v^2}\right) Z_h\left(\frac{Z_h}{Z_{eff}} - 1\right)\left(\frac{\nu_o}{\nu_i}\right)\frac{1}{(1 + \nu_e/n_i)^2}\,, \qquad (5\text{-}23)$$

where in the last step we used $W = m_h v^2/2$ and $\nu = \nu_e + \nu_i$, both of which were defined previously.

We now calculate the maximum attainable $\hat{J}/\hat{P}$:

$$\left(\frac{\hat{J}}{\hat{P}}\right)_{max} = 3\left(\frac{m_e}{m_h}\right) Z_h \left(\frac{Z_h}{Z_{eff}} - 1\right)[F(v)]_{max}\,, \qquad (5\text{-}24)$$

where we define

$$F(v) \equiv \left(\frac{v_e v_{\parallel}}{v^2}\right)\left(\frac{\nu_o}{\nu_i}\right)\frac{1}{(1 + \nu_e/\nu_i)^2}\,. \qquad (5\text{-}25a)$$

For thermal particles assuming $T_e \simeq T_i \simeq T$, we define thermal velocity far the minority species as $v_{th} = (kT/m_h)^{1/2}$. Normalizing velocities to v_{th},

$$F(v) \equiv \left(\frac{v_{th}}{v_e}\right)^2\left(\frac{\nu_o}{C_i}\right)\left(\frac{U_{\parallel}}{U^2}\right)\frac{U^3}{\left[1 + \frac{C_e}{C_i}\left(\frac{v_{th}}{v_e}\right)^3 U^3\right]^2} \qquad (5\text{-}25b)$$

$$= \left(\frac{m_e}{m_h}\right)\left(\frac{\nu_o}{C_i}\right)\frac{U_{\parallel}U}{\left[1 + \frac{C_e}{C_i}\left(\frac{m_e}{m_h}\right)^{3/2} U^3\right]^2} \qquad (5\text{-}25c)$$

$$\simeq \left(\frac{m_e}{m_h}\right)\left(\frac{\nu_o}{C_i}\right)\frac{U^2}{(1 + KU^3)^2} \tag{5-25d}$$

$$= \left(\frac{m_e}{m_h}\right)\left(\frac{\nu_o}{C_i}\right) F(U) \ , \tag{5-25e}$$

where C_e and C_i are constants defined in Eq. (5-11), $U_{\parallel} = v_{\parallel}/v_{th}$, $U = v/v_{th}$,

$$K = \frac{C_e}{C_i}\left(\frac{m_e}{m_h}\right)^{3/2} = \frac{1}{3Z_i}\left(\frac{2}{\pi}\right)^{1/2}\frac{(m_e/m_h)^{1/2}}{(1 + m_h/m_i)} \ , \tag{5-26a}$$

and

$$F(U) \equiv U^2/(1 + KU^3)^2 \ . \tag{5-26b}$$

In writing Eq. (5-25d) we assume $U_{\parallel} \approx U$, which is a reasonable approximation for resonant ions ($v_{\parallel} >> v_{th}$).

The quantity F(U) [Eq. (5-26b)] is a maximum when

$$U = U_o = (1/2K)^{1/3} \ , \tag{5-27a}$$

$$[F(U)]_{max} = F(U_o) = \frac{4}{9}\left(\frac{1}{2K}\right)^{2/3}$$

$$= \frac{2}{3}\left(\frac{\pi}{3}\right)^{1/3} Z_i^{2/3}(1 + m_h/m_i)^{2/3}(m_h/m_e)^{1/3} \ . \tag{5-27b}$$

From Eq. (5-11d) we have

$$\nu_o/C_i = (2/Z_h^2 Z_i)(m_h/m_e)^2(1 + m_h/m_i)^{-1} \ . \tag{5-28}$$

Combining Eqs. (5-25) through (5-28) in Eq. (5-24), we obtain the following simple form for the maximum $\hat{J}/\hat{P}$:

$$\left(\frac{\hat{J}}{\hat{P}}\right)_{max} = \frac{4}{Z_i^{1/3}} \left(\frac{\pi}{3}\right)^{1/3} \left(\frac{1}{Z_{eff}} - \frac{1}{Z_h}\right) \frac{(m_h/m_e)^{1/3}}{(1 + m_h/m_i)^{1/3}} \tag{5-29}$$

$$= 4Z_i^{-1/3} (\pi/3)^{1/3} \left(Z_{eff}^{-1} - Z_h^{-1}\right) (M/m_e)^{1/3} \ , \tag{5-30}$$

where M is the reduced ion mass,

$$M \equiv \frac{m_i m_h}{m_i + m_h} \ .$$

Under most optimum conditions, for a dueterium plasma with, for example, a He^3 minority species, $\hat{J}/\hat{P} \simeq 25$. In this case $U_o \simeq 7$ (i.e., $v_{\parallel} \simeq 7\ v_{th}$). In general $\hat{J}/\hat{P}$ is not a very peaked function of U; thus, the minority species ions over a range of $3 < U < 8$ $(3 < v_{\parallel}/v_{th} < 8)$ would allow reasonable current drive efficiencies.

As indicated before, the effect of trapped electrons can qualitatively change the generated current and the current drive efficiency. To consider this effect, Eq. (5-23) should be modified by using Eq. (5-19) [instead of Eq. (5-18)].

5.1.4 Simple Reactor Application

Here we assume that the restrictions on the minority charge state and disparate cyclotron frequency requirements [i.e., Eqs. (5-20) and (5-21)] are met and that the ICRF wave is capable of depositing its energy fully to the minority species. To be practical for reactor application, dissipated power should be minimal. Thus, we further assume that all the required current can be generated at near the maximum efficiency [Eq. (5-29)].

Consider a steady-state tokamak reactor with the poloidal magnetic field sustained by a toroidal current generated by means of minority species heating. If maximum efficiency $(\hat{J}/\hat{P})_{max} \simeq 25$ is attained in a reactor and operation at $\beta_p = R_o/a$ is achievable, then the recirculating power fraction [Eq. (1-25)] is

$$\epsilon = \frac{P_{rf}(ICRH)}{P_{fus}} = 0.72(aR_o n_{20} T_{10})^{-1/2} \left(10^{-22}/\langle\sigma v\rangle_{DT}\right) \ .$$

For a reactor with parameters $n \sim 10^{20}$ m^{-3}, $T \sim 15$ keV, $a \sim 1.5$ m, and $R_o \sim 6$ m, we find $\epsilon \sim 7.5\%$ (without any efficiency considerations). Note that $\epsilon \sim 4\%$ at $T = 20$ keV and $\epsilon \sim 24\%$ at 10 keV. Whereas 4% recirculating fusion power (which translates into roughly 20% of electrical power, assuming a thermal conversion efficiency of 0.35 and electric-to-rf conversion efficiency of ~ 0.6) could be acceptable, $\epsilon \sim 24\%$ is definitely not practical. For these reactor parameters, $I/P \sim 0.1$ MA/MW (i.e., about 10 MW of power is necessary to maintain each 1 MA of current). It is important to note that these are highly idealized (optimistic) numbers; they are given here only to provide a rough feeling.

It is important also to see whether there are enough resonant minority ions to generate the current required. To answer this quantitatively, we use Eq. (1-21b), that is, the normalized current required to operate a tokamak at $\beta_p = R_o/a$:

$$\hat{J} = 2.1 \times 10^{-3} (n_{20} R_o a)^{-1/2} \simeq 7 \times 10^{-4} \ .$$

To obtain this current we need a minority species drift large enough such that

$$\frac{n_h v_{h\parallel}}{n_e v_e} > \frac{7 \times 10^{-4}}{Z_h^2/Z_{eff}}$$

or, in terms of total current,

$$\frac{n_h v_{h\parallel}}{n_e v_e} = \frac{7 \times 10^{-4}}{Z_h^2 (Z_{eff}^{-1} - Z_h^{-1})} \ ,$$

where Eq. (5-18) is used. As a crude approximation, if we assume that the minority current is of the same order of magnitude as the current of resonant ions [i.e.,

$$n_h v_{h\parallel} \approx n_r U_\parallel v_{th} \ ,$$

where n_r is the density of resonant minority ions, $U_\parallel = v_\parallel / v_{th}$ is the normalized parallel velocity of resonant ions, and $v_{th} = (T/m_h)^{1/2}$ is

the thermal velocity of minority ions], the requirement can be written as

$$\frac{n_r}{n_e} \simeq \frac{7 \times 10^{-4}}{Z_h^2(Z_{eff}^{-1} - Z_h^{-1})} \left(\frac{m_h}{m_e}\right)^{1/2} \frac{1}{U_\parallel} .$$

For example, for He^3 minority species ($Z_h \sim 2$, $m_h \sim 3\ m_{proton}$) with $Z_{eff} \sim 1$,

$$\frac{n_r}{n_e} \simeq 2.6 \times 10^{-2}/U_\parallel .$$

For representative values of $U_\parallel \sim 3\text{–}5$, $n_r/n_e \sim 5\text{–}8 \times 10^{-3}$.

Taking $U_1 < U_\parallel < U_2$ to be the resonance region and since $U_\parallel \gg 1$, we have $U_\parallel \sim U(= v/v_{th})$; thus,

$$n_r \simeq n_h \int_{U_1}^{U_2} f_o(U)\ d^3U = n_h \int_{U_1}^{U_2} 4\pi U^2 f_o(U)\ dU .$$

Assuming that the distribution function flattens in the resonant region of velocity space [i.e., $f_o(U) \approx f_o(U_1)$ for $U > U_1$], we have roughly

$$\frac{n_r}{n_e} \simeq \frac{n_h}{n_e} f_o(U_1) \int_{U_1}^{U_2} 4\pi U^2\ dU = \frac{n_h}{n_e} \left(\frac{2}{\pi}\right)^{1/2} e^{-U_1^2/2} \left(\frac{U_2^3 - U_1^3}{3}\right),$$

where $f_o(U_1) = (2\pi)^{-3/2}\exp(-U_1^2/2)$. The dependence of n_r on U_1 is so strong that any slight variation of U_1 can change the answer drastically and on the positive side, thus, any slight adjustment to U_1 can give the required minority current. For example, in the range of $3 < U < 5$, $n_r/n_e \simeq 0.3(n_h/n_e)$ and only a few percent of minority concentration ($n_h/n_e \gtrsim 3\%$) can satisfy the requirement. However, for $4 < U < 7$ the necessary minority concentration increases an order of magnitude ($n_h/n_e \sim 30\%$) to produce the required minority current, which is not a practical case for a reactor. It is thus important to determine (and select) resonance conditions and wave $k_\parallel$ spectrum properly. [Note that the resonant velocity is $v_\parallel = (\omega - \Omega_h)/k_\parallel$ and $U_1 = (v_\parallel/v_{th})_{min}$ is the minimum normalized velocity of the resonant ions.]

5.2. Wave Propagation and Absorption

Wave propagation in the ion cyclotron range of frequencies can be accurately represented by the cold plasma approximation. Plasma kinetic effects, however, enter into the mode conversion and collisionless absorption.

In a single-ion-species plasma the dispersion relation for ICRF waves exhibits two modes: the ion cyclotron (slow) wave and the magnetosonic (fast) wave. The presence of two or more ion species in a plasma introduces a new mode, called the ion-ion hybrid wave. This allows strong interaction of the fast wave with the ions near the location of the ion-ion hybrid resonance, which occurs when

$$\Omega_{ii}^2 = \Omega_{i1}\Omega_{i2}\frac{m_1 n_1 + m_2 n_2}{m_2 n_1 + m_1 n_2} ,$$

where m_j and n_j are the mass and density of ion species $j(= 1, 2)$. This resonance lies intermediate between the cyclotron frequencies of the two ion species and approaches the cyclotron frequency of the most dilute (minority) species.

5.2.1 Dispersion Relation

Considering the ion cyclotron range of frequencies, $\omega^2 \sim \Omega_i^2 \ll \Omega_e^2$, ω_{pe}^2, we approximate the components of the dielectric tensor [Eq. (3-6)] for a multiple ion species plasma as follows:

$$\epsilon_1 \simeq 1 - \sum_j \frac{\omega_{pj}^2}{\omega^2 - \Omega_j^2} \simeq \sum_j \frac{\omega_{pj}^2}{\Omega_j^2}\frac{\Omega_j^2}{\Omega_j^2 - \omega^2} ,$$

$$\epsilon_2 \simeq \sum_j \frac{\omega_{pj}^2}{\Omega_j^2}\frac{\omega\Omega_j}{\omega^2 - \Omega_j^2} , \qquad (5\text{-}31)$$

$$\epsilon_3 \simeq 1 - \frac{\omega_{pe}^2}{\omega^2} \simeq - \omega_{pe}^2/\omega^2 .$$

Here j refers to the ion species (for example, majority and minority ions). Note that $|\epsilon_3| \gg |\epsilon_1|, |\epsilon_2|$, so that $E_z = E_\parallel \simeq 0$. That is, the high conductivity of the plasma shorts out the parallel electric field. With $E_\parallel \simeq 0$, the dispersion relation [obtained from Eq. (3-7)] is

$$(\epsilon_1 - \eta_\parallel^2)(\epsilon_1 - \eta_\perp^2 - \eta_\parallel^2) - \epsilon_2^2 = 0 \ , \tag{5-32a}$$

which can be rearranged as

$$\eta_\perp^2(\epsilon_1 - \eta_\parallel^2) - (\eta_\parallel^2 - (\epsilon_1 - \epsilon_2)][\eta_\parallel^2 - (\epsilon_1 + \epsilon_2)] = 0$$

to yield

$$k_\perp^2(A - k_\parallel^2) - (B - k_\parallel^2)(C - k_\parallel^2) = 0 \ , \tag{5-32b}$$

where $A = (\omega^2/c^2)\epsilon_1$, $B = (\omega^2/c^2)(\epsilon_1 - \epsilon_2)$, and $C = (\omega^2/c^2)(\epsilon_1 + \epsilon_2)$. Note that $A = (B + C)/2$.

In a tokamak, wave propagation proceeds at almost constant $k_\parallel$ ($\simeq n/R_o \simeq$ constant, where n is the toroidal mode number). In Eq. (5-32b) the surface where

$$A - k_\parallel^2 = 0$$

defines the ion-ion hybrid resonance ($k_\perp^2 \to \infty$). This also represents a mode conversion surface. The vanishing of $B - k_\parallel^2 = 0$ and $C - k_\parallel^2 = 0$ leads to cutoffs ($k_\perp \to 0$). The fast-wave cutoff $C - k_\parallel^2 = 0$ is not affected by the resonances. However, cutoff for the ion cyclotron (slow) wave $B - k_\parallel^2 = 0$ occurs near the resonance. For a tokamak cross section, representative dispersion surfaces for the case of a light minority in a heavy background majority species are shown in Fig. 5.1.

In the presence of minority species, the polarization of the wave electric field for magnetosonic fast waves is significantly altered with $|E^+| \neq 0$ (where $E^+ = E_x + iE_y$ is the left-hand component of the wave that rotates in the same sense as ions).

5.2.2 Absorption

A characteristic feature of fast waves in the ion cyclotron range of frequencies of a multi-ion-species plasma is the localization of the wave damping mechanism around the hybrid resonance layer (shaded area in Fig. 5.1). Most of the wave power is absorbed around the thin vertical layer, where $A - k_\parallel^2 = 0$ (resonance) and $B - k_\parallel^2 = 0$ (cutoff) occur (see Fig. 5.1). The thickness of hybrid layer is $\Delta x = x_A - x_B$.

When the concentration of the minority species is low, rf power is absorbed mainly by the minority ions, producing an energetic minority distribution. When the minority concentration is above a certain threshold (determined by T, $\eta_\parallel$, etc.), the fast wave can mode-convert into an electrostatic ion Bernstein wave, which can then tend to heat the electrons through electron Landau damping.

In order to calculate the left-hand component of the wave electric field properly, we need to consider the complete warm plasma dispersion relation. Figure 5.2 is a plot of the left-hand component $|E^+|$ of the fast wave, showing the strong peaking of $|E^+|$ around a thin hybrid resonance layer. Results shown are for a D (deuterium) plasma with H^+ minority with the following plasma parameters: T = 4 keV, n_D(background) = 10^{20} m^{-3}, n_h(minority) = 5×10^{18} m^{-3} ($n_h/n_D \simeq 5\%$), B_o = 2 T, and R_o = 2 m.

The distance of the hybrid layer from the cyclotron resonance of the minority ions is proportional to the minority concentration and the major radius of the torus. Because the cyclotron resonance heating is

ORNL-DWG 84-3142 FED

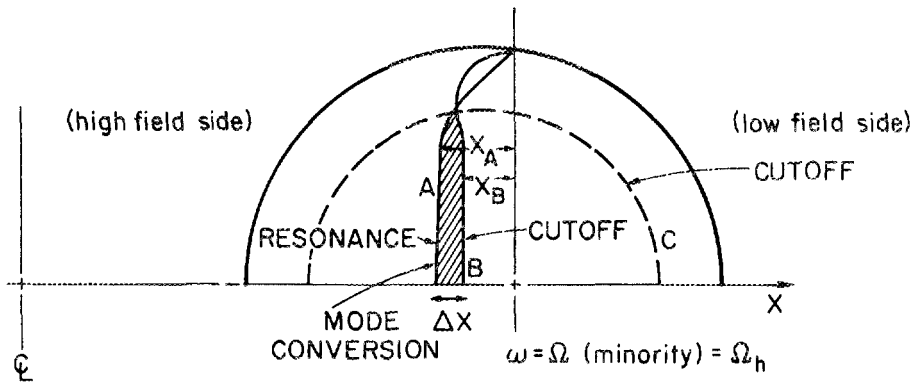

Fig. 5.1. Mode conversion surfaces and cutoffs for a light minority species in a heavy background majority species plasma. Curve A is the mode conversion resonance ($A - k_{\parallel}^2 = 0$) whereas curve B is the associated cutoff ($B - k_{\parallel}^2 = 0$). Curve C is the fast wave cutoff $C - k_{\parallel}^2 = 0$. $\omega = \Omega_h$ is the minority species ion cyclotron resonance layer. Wave power is absorbed around shaded area, hybrid layer $\Delta x = x_A - x_B$.

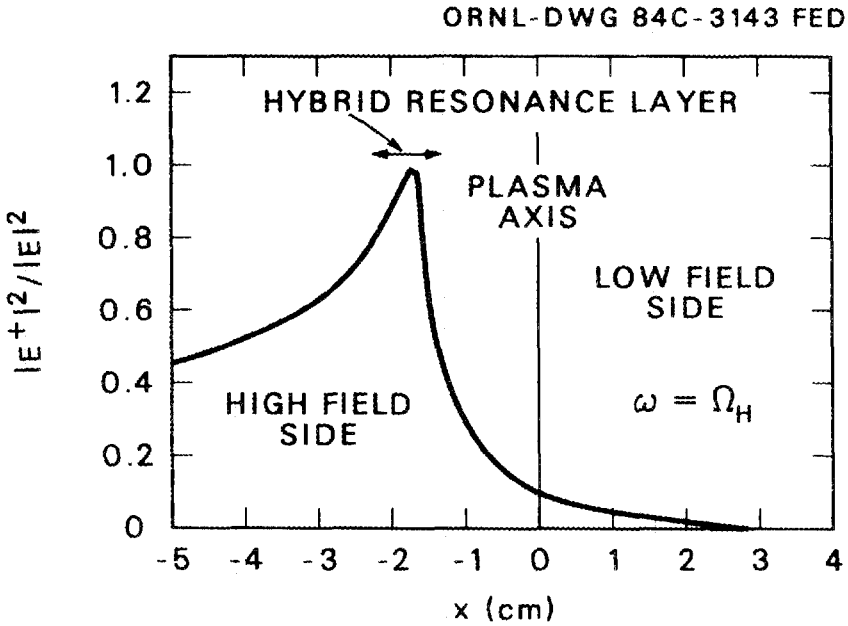

Fig. 5.2. Fraction of left-hand component of total power as a function of radius for D-H plasma (D-majority, H-minority). Plasma axis is at $x = 0$ ($x > 0$ is the low-field side). Plasma parameters are given in text. Note that $|E^+|$ peaks around hybrid resonance layer and in the high field side ($x < 0$). Bernstein waves are also strongly absorbed (ref. [55]).

governed by the resonance condition $v_{\parallel} = (\omega - \Omega_h)/k_{\parallel}$ (where $\Omega_h = eZ_hB_o/m_h$ is the minority species cyclotron frequency), varying the $k_{\parallel}$ spectrum and minority concentration will vary the velocity space region of resonantly heated ions. To drive a current, asymmetrical heating of superthermal minority ions is required. This can be realized by creating an energetic tail of minority ions.

We note that both the localization of $|E^+|$ and the asymmetry of $k_{\parallel}$ spectrum are necessary to achieve asymmetric heating of minority ions.

5.2.3 $k_{\parallel}$ Spectrum [55]

A traveling ICRF wave is required if a net drift between the ion species is to be generated. The calculation in ref. [55] indicates that this can be achieved by the use of an array of phase-shifted antennae. Assuming that (1) the wave propagation proceeds at almost constant $k_{\parallel}$, (2) the weak shear does not change the spectrum launched from the edge of the plasma, and (3) the poloidal variation of the wave field is weak (long antennae), a slab model for antenna coupling can be used to determine the plasma parameters that are necessary to produce an asymmetric $k_{\parallel}$ spectrum required for asymmetric heating. [Note that approximation of almost constant $k_{\parallel}$ does not remain uniformly valid, especially in regions where mode conversion plays a role and the perpendicular wave number ($k_{\perp}$) becomes very large.] In this mode, the antennae are treated as current filaments infinite in the y (i.e., poloidal) direction. The density gradient is taken to be in the x direction, and toroidal magnetic field is in the z-direction, $\mathbf{B} = B_o\hat{\mathbf{e}}_z$ (Fig. 5.3).

For the fast wave the wave equation [Eq. (3-5)] is solved, and the $k_{\parallel}$ spectrum for four antennae phased at $\phi = \pi/2$ is shown in Fig. 5.4 for two different thicknesses of the low-density edge plasma region in front of the antennae. The asymmetry of the $k_{\parallel}$ spectrum depends sensitively on the thickness of the low-density region with a thicker low-density region producing a more asymmetric spectrum. (This is because at sufficiently high $k_{\parallel}$, the low-density region becomes evanescent, thus suppressing the peaks of the spectrum at higher $k_{\parallel}$.) These results indicate that it is easier to launch a traveling fast wave in larger tokamaks.

ORNL-DWG 84C-3144 FED

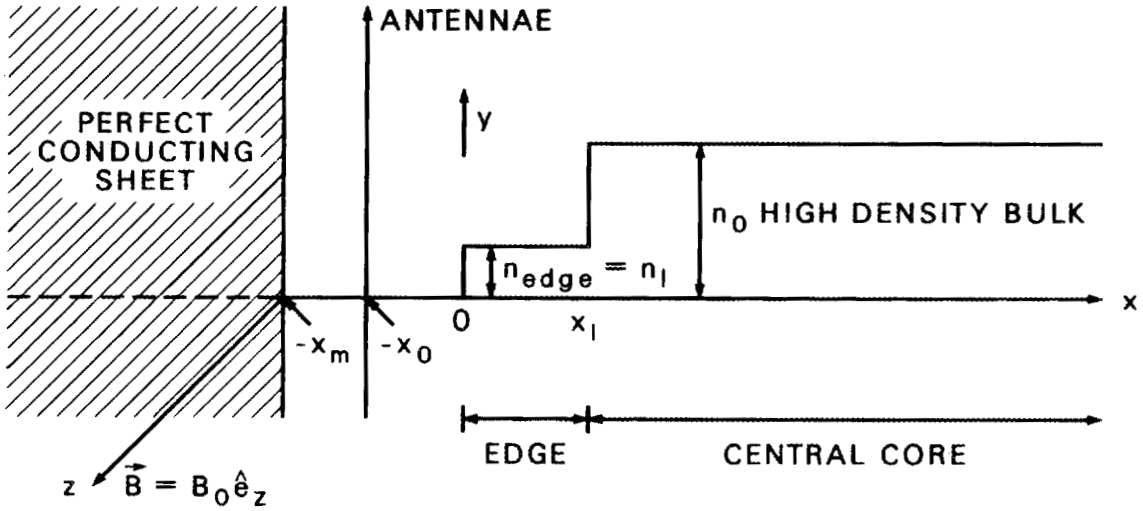

Fig. 5.3. Configuration of antennae-plasma coupling model (edge plasma $0 < x < x_1$, bulk plasma $x > x_1$) for fast wave coupling.

5.2.4 Resonance Condition

As mentioned earlier, cyclotron resonance heating occurs when the resonance condition is satisfied:

$$\omega - \ell\Omega_h - k_{\parallel}v_{\parallel} = 0 \ .$$

The thickness of the hybrid layer $\Delta x = x_A - x_B$ (Fig. 5.1), where most of the wave power is absorbed, depends on $k_{\parallel}$. Within the main peak of a spectrum (such as that given by Fig. 5.4), we can approximate the wave spectrum as flattopped within some upper (k_1) and lower (k_2) limit of the main peak ($k_2 < k_{\parallel} < k_1$). With this assumption, Δx can be regarded as constant. The minimum (v_1) and maximum (v_2) parallel velocities of the resonant ions can then be approximated (for $\ell = 1$) as

$$v_1 \simeq \frac{\omega - \Omega_h(x_B)}{k_1} \ , \qquad v_2 \simeq \frac{\omega - \Omega_h(x_A)}{k_2} \ ; \tag{5-33}$$

that is, the velocity space resonance region is $v_1 < v_{\parallel} < v_2$.

5.3. Results From the Quasi-Linear Fokker-Planck Theory [55]

The quasi-linear Fokker-Planck equation of the form given by Eq. (3-28) is solved numerically for minority ions in the presence of a weak rf field in ref. [55]. For fundamental cyclotron heating, the quasi-linear operator for the minority ions is

$$\left(\frac{\partial f_h}{\partial t}\right)_w = \frac{1}{v_\perp}\frac{\partial}{\partial v_\perp}\left[\frac{\pi e^2 Z_h^2}{4m_h^2 k_{\parallel}}\,|E^+|^2 v_\perp \delta\left(\frac{\omega - \Omega_h}{k_{\parallel} - v_{\parallel}}\right)\frac{\partial f_h}{\partial v_\perp}\right] \ . \tag{5-34}$$

A spread in the $k_{\parallel}$ spectrum can simply be introduced in Eq. (5-34) as an integral (or summation) over the $k_{\parallel}$ spectrum. Within the hybrid resonance layer, $|E^+|$ is localized (Fig. 5.2) and thus can be taken as a constant in velocity space.

Knowing the distribution function f_h, the minority current J_h and the power absorbed by the minority P_{rf} can be calculated. To

ORNL-DWG 84C-3145 FED

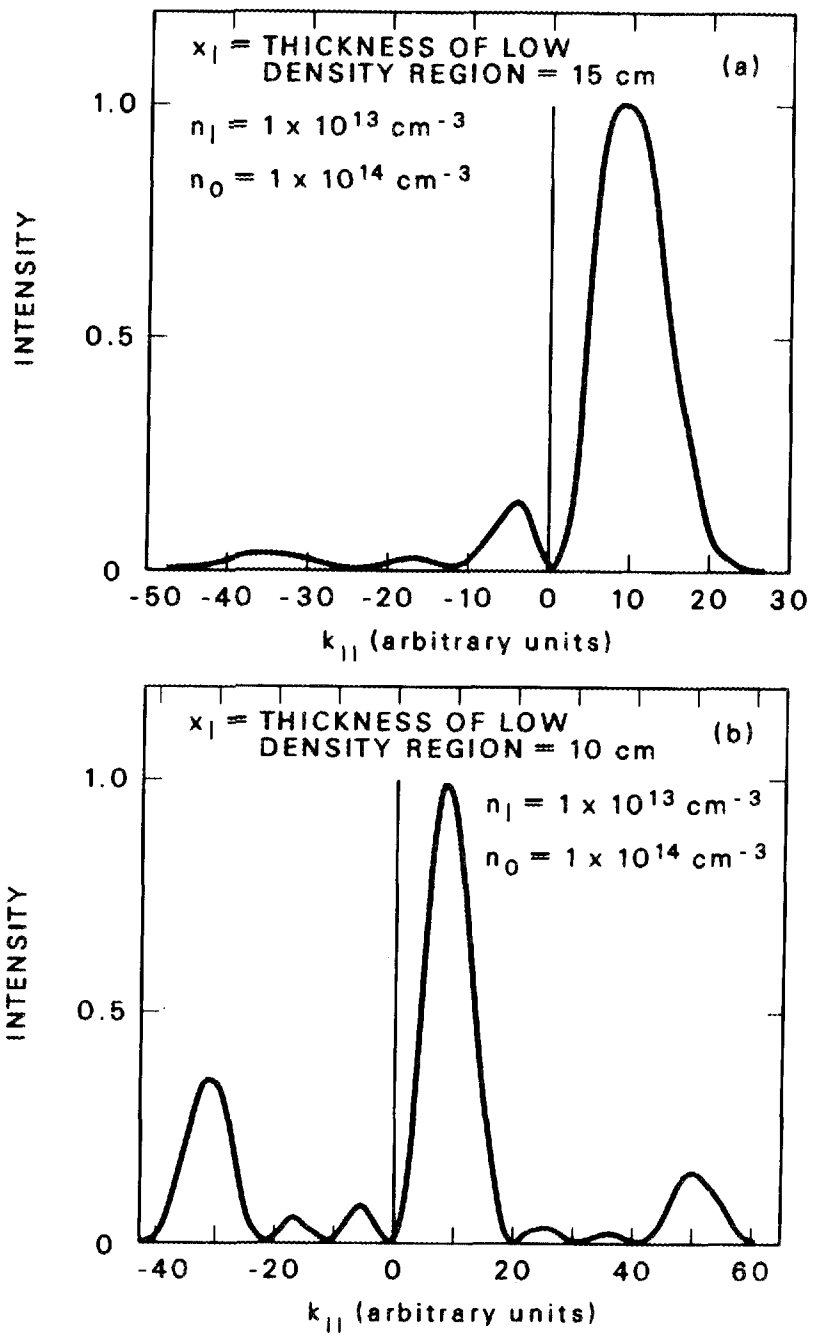

Fig. 5.4. $k_{\parallel}$-spectrum of rf power excited by four antennae 90° out of phase: (a) thickness of low-density region = 15 cm; (b) thickness of low density region = 10 cm (ref. [55]).

calculate the total current response of bulk plasma majority ions and electrons need to be estimated. Calculation of the response of the majority ions requires knowledge of the external momentum source. Assuming that the parallel momentum of ICRF is zero (or negligible), the following are possible: (1) there is a momentum source on the majority ions (e.g., neutral beam) such that the total ion momentum remains zero (i.e., $m_i n_i \bar{v}_i = -m_h n_h v_{h\parallel}$), and (2) the majority ion velocity remains zero (i.e., $v_i = 0$). In the first case the majority ion current is obtained from conservation of total momentum [Eq. (5-15)], and in the second case there is no majority ion current.

The electron current is calculated from an electron Fokker-Planck equation in which the electron drag on the energetic minority ions results in a relative electron drift and thus an electron (return) current. The total current for a single majority ion is

$$J = J_h + J_i + J_e$$

$$= J_h \left[1 - \frac{Z_h}{Z_i} + 1.46\epsilon^{1/2} \left(\frac{Z_h}{Z_i} - \lambda \frac{Z_i}{Z_h} \frac{m_h}{m_i} \right) A(Z_i) \right] ; \qquad (5\text{-}35)$$

for more than one majority ion species, one can replace Z_i with Z_{eff}. Note that this is the same equation given by Eq. (5-19) with $\lambda = 1$ corresponding to case 1 (i.e., total ion momentum being zero) and $\lambda = 0$ corresponding to case 2 (i.e., $\bar{v}_i = 0$); that is, $\bar{v}_i = -\lambda m_h n_h v_{h\parallel}/m_i n_i$.

As discussed in Sect. 5.1.2, Eq. (5-35) shows that the current profile generated and its direction depend strongly on the composition of the minority-majority species (Z_h/Z_i). The efficiency of the total current generated is given by

$$\frac{I}{P_{tot}} = \frac{1}{2\pi} \frac{J}{R_o P_{rf}} ,$$

which is shown in Fig. 5.5 for D-He^3. For this case, the current generated is peaked near the plasma axis ($\epsilon = r/R_o = 0$). The current driven in a D-H plasma (H is the minority species) is shown in Fig. 5.6, where the profile can be seen to be quite flat except near

ORNL-DWG 84C-3146 FED

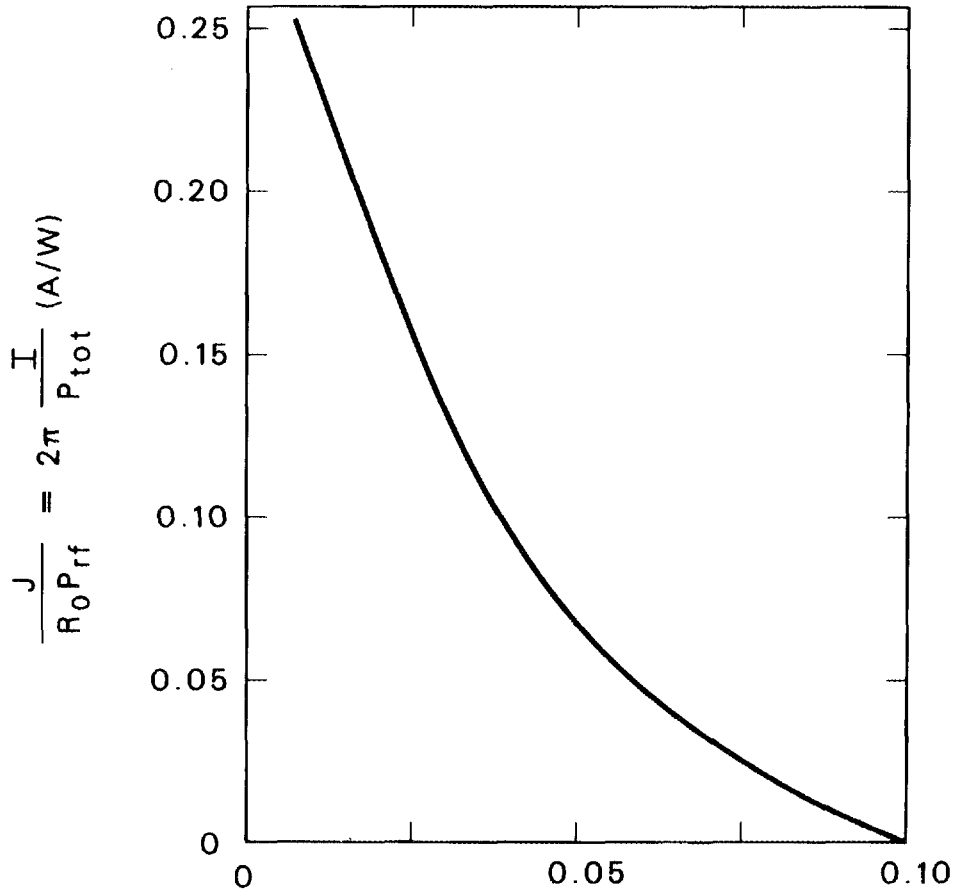

Fig. 5.5. Efficiency of total current generation vs inverse aspect ratio for a D–He^3 plasma. Plasma parameters are T_D = 4 keV, $n_D = 10^{20}$ m^{-3}, $n_{He^3} = 5 \times 10^{18}$ m^{-3}, R_o = 2 m, $\omega/2\pi$ = 20 MHz, $v_1 = 2\ v_D$, and λ = 1 (ref. [55]).

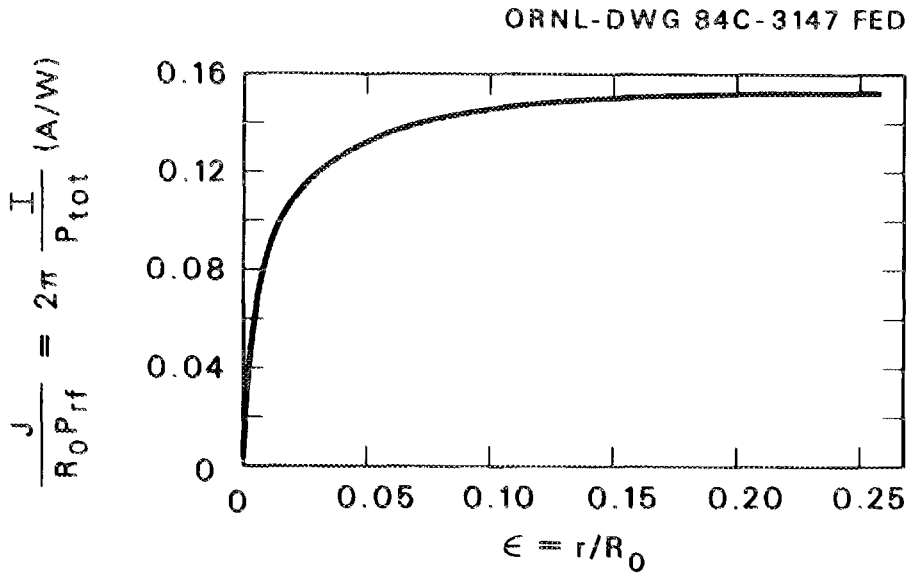

Fig. 5.6. Efficiency of total current generation vs inverse aspect ratio for D–H plasma. Plasma parameters are the same as those in Fig. 5.5 except: $n_H = 5 \times 10^{18}$ m^{-3}, $\omega/2\pi = 30$ MHz, and $\lambda = 0$ (ref. [55]).

the axis. This is because in the D-He^3 case $1 - Z_h/Z_i$ and the last term in Eq. (5-35) are opposite in sign and can cancel each other for increasing ϵ, whereas for the D-H case only the last term (trapped electrons) contribute.

5.4. Comments

The basic mechanism of current generation by ICRF minority species heating relies on the Fisch-Boozer mechanism by asymmetrically heating the minority ion species to create a relative drift (between minority ions and background majority ions and electrons) and on the mechanism of neutral beam current drive that requires this relative drift between the species. When considered separately, both of these techniques are well established. However, a combination of both has not yet been demonstrated experimentally.

In general, calculations based on single-particle treatment and quasi-linear Fokker-Planck analysis are in reasonable agreement. Fokker-Planck calculations are for the weak rf limit, which assumes isotropic distribution (not valid for an enhanced tail from a strong asymmetric rf). No study is yet available for a strong rf case.

There are some practical limits, some of which were discussed previously. For example, calculations assume that the wave power is absorbed exclusively by the resonant minority species within the narrow hybrid resonance layer (Fig. 5.2). Also, only ions in the most favorable region of velocity space are assumed to be resonant [Eqs. (5-24)-(5-29)]. In order to avoid power absorption by majority species ions, the wave phase velocity must satisfy certain constraints. To obtain high efficiencies, the velocity of resonant (minority) ions should lie in the range of, for example, $v_{\parallel} \sim (3\text{-}5)v_{th}$; that is,

$$\frac{\omega - \Omega_h}{k_{\parallel}} \sim (3\text{-}5)\ v_{th} \ .$$

On the other hand, for the resonance condition to avoid heating a substantial number of majority ions, one requires

$$\frac{\omega - \Omega_i}{k_{\parallel}} > 5v_i \ .$$

For minority (not majority) heating to occur at the first harmonic ($\ell = 1$), we combine these two requirements to obtain a condition on the parallel wave phase velocity ($\omega/k_{\parallel}$); that is, for $v_{\parallel} \sim 3\, v_{th}$ and $\Omega_h > \Omega_i$,

$$\frac{\omega}{k_{\parallel}} > \frac{\left[5(m_h/m_i)^{1/2} - 3(\Omega_i/\Omega_h)\right]}{(1 - \Omega_i/\Omega_h)} v_{th} \; .$$

A similar condition may be obtained when $\Omega_h < \Omega_i$. For example, for D–He^3 plasma ($m_i = 2$, $m_h = 3$, $Z_h = 2$), $\omega/k_{\parallel} > 16v_{th}$ for $v_{\parallel} \sim 3v_{th}$ and $\omega/k_{\parallel} > 13v_{th}$ for $v_{\parallel} \sim 5v_{th}$.

Competing with the cyclotron damping of the wave by minority ions is the Landau damping of the wave by electrons (Sect. 5.2.2). This may become the case when the required minority concentration is high enough, in which case the fast wave can mode-convert into a Bernstein wave. As can be seen from Fig. 5.2, even though the cyclotron damping dominates near resonance (hybrid layer), electron damping dominates off resonance.

There are also constraints on the majority–minority species mix [see discussion following Eq. (5–21)]. For example, for the D–H case considered in Fig. 5.6, the fundamental harmonic of H coincides with the second harmonic of D. At high temperatures, the second harmonic absorption of D can be appreciable.

Probably the best candidate for a D–T reactor is the He^3 minority ions. However, the He^3 fundamental resonance coincides with the second harmonic of tritium, and some inefficiency in current drive will result due to direct tritium heating (similar to the D–H case).

One undesirable feature of ICRF minority current drive will come from the fact that at fixed beta (toroidal beta) any injection of minority ions will dilute the D–T fuel density. This will result in an undesirable reduction in reactor power output. The presence of several ion species (three, four, or five) will result in substantial parasitic heating losses, and in a reactor this may severely limit the efficiency of current drive via minority heating.

Although the ICRF minority heating scheme might not be highly desirable as a reactor candidate for current drive, ICRF waves could be used to enhance the beam driven current efficiency or to accelerate

alpha particles (asymmetrically) to generate a current. These options will be discussed with the other hybrid schemes.

6. BRIEF DISCUSSION OF OTHER CURRENT DRIVE SCHEMES

In previous sections we discussed the possibility of maintaining a steady-state current based on more developed schemes such as neutral beam injection, lower hybrid waves, electron cyclotron waves, and ion cyclotron waves. In this section we briefly comment on some of the other schemes listed in Table 0.1.

6.1. ICRF Enhancement of Beam-Driven Currents [57,70,84]

A current drive scheme based on the use of ICRF waves to enhance the efficiency of the beam-driven current was proposed by Okano et al. [57,84]. This scheme uses ICRF to increase the perpendicular energy of fast beam ions in order to reduce their collisions with background thermal ions, thereby increasing their thermalization time. The mechanism is illustrated in Fig. 6.1, where the slowing down trajectory of the beam ions is shown schematically in velocity space. Without ICRF, the beam ions slow down due to Coulomb collisions along a trajectory, (1) shown in Fig. 6.1. With ICRF, on the other hand, the slowing-down trajectory is deformed due to perpendicular acceleration of fast beam ions by the ICRF wave, as illustrated by a trajectory, (2) in Fig. 6.1. This deformation causes the extension of the beam-ion lifetime; thus, in equilibrium, the density of and the current carried by the fast ions are enhanced [see Eq. (2.2)]. A 2-D Fokker-Planck treatment of the interaction between an ICRF wave and fast ions arising from neutral beam injection is discussed in detail in ref. [70]. The results indicate that the current carried by the injected fast ions is increased by the wave interaction in most circumstances. The optimum current drive efficiency, with the application of ICRF, is found to be about twice the optimum efficiency of generation of the straightforward beam-driven current discussed in Sect. 2. For pure beam-driven currents, the peak efficiency occurs for an injected beam energy around $E_0 \sim (30\text{-}50)A_f T_e$ (see Fig. 2.2). The results of ref. [70] indicate that applying ICRF can reduce the optimum beam energy by up to a factor of 4. For example, with $T_e \sim 15$ keV the optimum injection energy for a deuterium beam ($A_f = 2$) is around 1 to 1.5 MeV for the straightforward beam-driven current scheme, whereas it is around 250 to 400 keV for the wave-enhanced beam-driven scheme. This is certainly important to the overall efficiency of the driver. In practice, the overall efficiency of the rf scheme might be expected to be even more improved because the

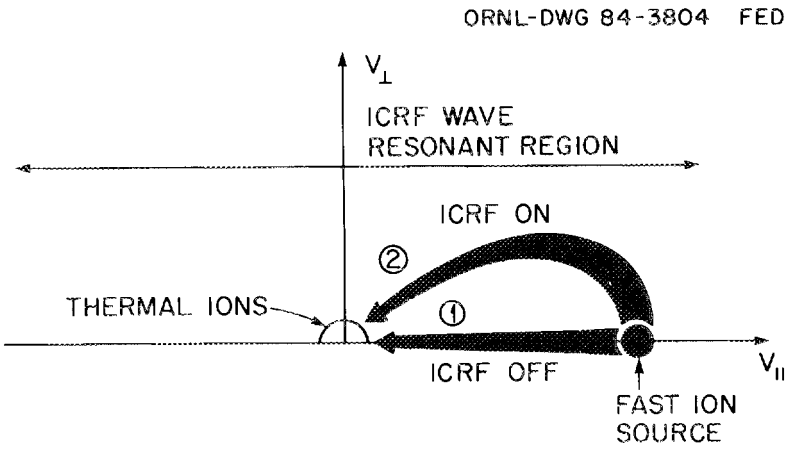

Fig. 6.1. Slowing-down trajectory of fast beam ions with and without ICRF (ref. [57]).

efficiency of generating the rf should almost certainly exceed that of high-energy neutral beams. Against this advantage, the complications inherent in the simultaneous use of two different heating systems should be offset.

6.2. Current Drive by α Particles-rf Wave Interaction [57,59-61]

It is possible to use the high-energy α particles produced by fusion reactors to sustain a steady-state current in a tokamak plasma. The idea is to use rf power to prohibit the α particles from slowing down isotropically and to push the α particles in a preferential direction and thus form an α-particle beam. This α-particle beam will then transfer the momentum to electrons and sustain a current. In a reactor, α particles are born isotropically in velocity space and slow down via Coulomb collisions with the background plasma particles. The α-particle distribution function, in ideal circumstances, remains isotropic during the slowing down, and there is no net current. However, to generate a current, the α-particle distribution has to be made asymmetric by means of rf power, particle loss, etc.

6.2.1 Asymmetric Heating of α Particles with ICRF [57,60]

A mechanism similar to that discussed in Sect. 6.1 can also be used with fusion products (α particles). The scheme proposed by Okano et al. [57,60] uses ICRF waves to clamp the energy of α particles produced in the resonant region in velocity space. The ICRF waves have no toroidal momentum (see Sect. 5) and accelerate α particles only in the perpendicular direction (i.e., increase $v_\perp$) with respect to the toroidal field. However, this acceleration is effective in clamping the particle momentum in the parallel direction. If the ICRF wave traveling unidirectionally along the toroidal field is launched to the tokamak plasma, the resonant region in velocity space becomes asymmetric, and it produces an asymmetric velocity distribution of α particles (Fig. 6.2). As a result, the average drift of α particles is established and the net toroidal current is induced. This mechanism is essentially identical to the basic mechanism of ICRF current generation by minority species heating (Sect. 5). The present scheme using α-particles is specific to reactor plasma conditions. As such, it does not favor low-density, low-temperature startup operations because of the insufficient amount of resonant α particles.

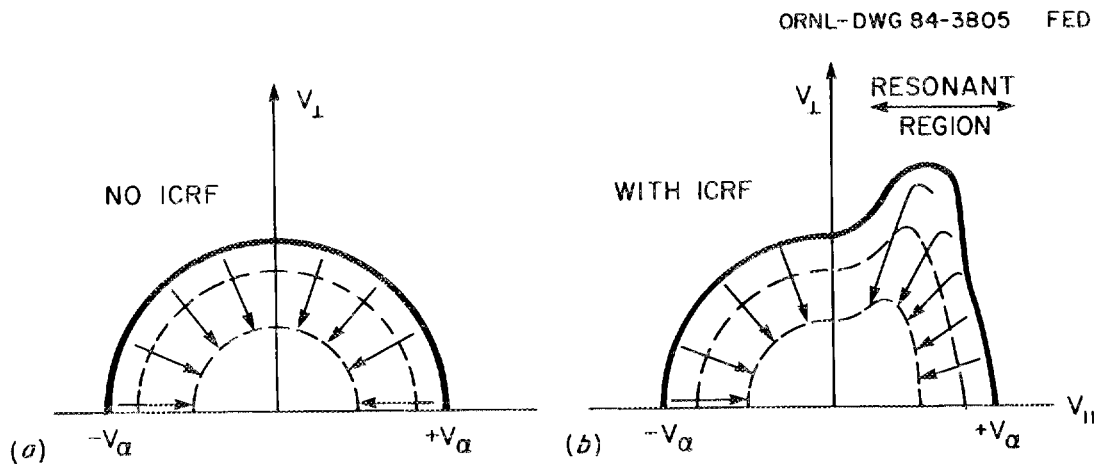

Fig. 6.2. (a) Isotropic source of α particles at birth and their slowing-down trajectory (no ICRF) and (b) asymmetric velocity distribution of α particles due to ICRF waves.

In steady state, the total current J induced by the drift of α particles is described fairly well with Eq. (5-18)

$$J \simeq en_\alpha Z_\alpha \bar{v}_\alpha (1 - Z_\alpha/Z_{eff})$$

$$= J_\alpha (1 - Z_\alpha/Z_{eff}) \ , \qquad (6\text{-}1)$$

where $\bar{v}_\alpha$ is the α-particle drift speed and $J_\alpha = en_\alpha Z_\alpha \bar{v}_\alpha$ is the α-particle current. In this expression, neoclassical electron orbit effects are not taken into account. As in the case of minority current (Sect. 5) or beam current (Sect. 2), there is a net current in the plasma if $Z_\alpha \neq Z_{eff}$.

The current drive efficiency $(\hat{J}/\hat{P})$ is no better than the case of minority heating. When one applies this scheme to fusion reactors, the first difficulty arises from the equality of the ion cyclotron resonance frequency between α particles and deuterons $(\Omega_D = \Omega_\alpha)$, because both have the same charge-to-mass ratio. To avoid majority cyclotron damping, the resonant condition $[v_\parallel = (\omega - \Omega)/k_\parallel]$ and rf frequency ω must be chosen carefully. Usually α particles have very high energy (up to 3.5 MeV in a D-T plasma) compared to background majority deuterons ($T_i \sim$ 10-20 keV). If the minimum resonant velocity $v_{\parallel,min} = (\omega - \Omega_{D,max})/k_\parallel$ is selected such that $v_{\parallel,min} \gg v_D$, there will be no (or very few) deuterons to resonate in the resonant region, but most α particles can resonant. Here, $\Omega_{D,max}$ is the maximum deuteron cyclotron frequency within the plasma. Thus, a favorable resonant condition can be obtained by choosing a wave frequency such that $\omega - k_\parallel v_D \gg \Omega_{D,max}$.

6.2.2 Asymmetric Heating of α Particles with Traveling Magnetosonic (Fast) Waves [59,61]

In principle a state of induced anisotropy (namely, asymmetric α particle distribution) can be created by interaction of α particles with the fast traveling (magnetosonic) waves. In general, the fast wave is an electromagnetic mode in which the wave electric field is primarily perpendicular to the dc (static) magnetic field; because of this property, it can propagate in a plasma over a wide frequency range

from below the ion cyclotron frequency Ω_i all the way up to the electron cyclotron frequency Ω_e. When $\omega < \Omega_i$, it is called the compressional Alfvén wave. When $\Omega_i < \omega < \omega_{LH}$, it has the names magnetosonic wave, high-frequency Alfvén wave, etc. When $\omega > \omega_{LH}$, it is generally named the Whistler wave. The magnetosonic wave ($\omega > \Omega_i$) seems particularly interesting for producing an asymmetric α-particle distribution. The phase velocity of such waves is of the order of Alfvén speed v_A

$$v_A^2 = B_o^2/\mu_o n m_i = c^2\Omega_i^2/\omega_{pi}^2 ,$$

which, in a reactor-like plasma, is roughly the same as the speed of α-particles ($v_P = \omega/k_{\parallel} \sim v_A \sim v_\alpha$).

For the purpose of current drive the interest is in converting wave momentum to that of α particles. Thus, it is convenient to have the wave parallel phase speed be of the order of α-particle speed ($v_{P\parallel} \sim v_\alpha$) to maximize the collisionless wave damping, and, at the same time, to have a frequency ω not too close to the ion cyclotron frequency to avoid cyclotron damping on the background ions. The choice of $\omega \sim 5\Omega_i$ appears most suitable, in that Landau damping and transit time magnetic pumping (TTMP) can now selectively interact with α particles generate an asymmetric distribution, thereby a circulating α particle (minority) beam.

The force exerted on α particles in the direction of static magnetic field B_o is

$$m_\alpha \frac{dv_{\alpha\parallel}}{dt} = qE_{\parallel} - \mu_\alpha \partial\tilde{B}_{\parallel}/\partial z$$

$$= 2eE_{\parallel} - \mu_\alpha \partial\tilde{B}_{\parallel}/\partial z , \qquad (6\text{-}2)$$

where $\mu_\alpha \equiv m_\alpha v_{\alpha\perp}^2/2B_o$ is the magnetic moment; $E_{\parallel}$ and $\tilde{B}_{\parallel}$ are the parallel wave electric and magnetic fields, respectively; and the z direction is taken to be parallel to B_o. For Landau damping, the interaction of $E_{\parallel}$ with α particles whose parallel velocities are equal to the wave phase

velocity leads to transfer to momentum and energy. The quasi-linear diffusion coefficient due to Landau damping is given by Eq. (3-39)

$$D_L(v_\parallel) = \begin{cases} \dfrac{4\pi e^2 \langle E_\parallel \rangle^2}{m_\alpha^2 v_\parallel \Delta k_\parallel} & v_1 < v_\parallel < v_2 \\ 0 & \text{otherwise} \end{cases} \tag{6-3}$$

for a narrow spectrum of wave within the resonance region $v_1 < v_{\alpha\parallel} = v_p < v_2$. For transit time damping, it is the $\mu_\alpha \nabla \tilde{B}_\parallel$ term that transfers momentum to the particles. By strict analogy to the Landau damping case, substituting the magnetic acceleration term for the electric acceleration term, we can form a quasi-linear diffusion coefficient of the form of Eq. (6-3) as

$$D_{TTMP}(v_\parallel) = \begin{cases} \dfrac{\pi \mu_\alpha^2 k_\parallel^2 \langle \tilde{B}_\parallel \rangle^2}{m_\alpha^2 v_\parallel \Delta k_\parallel} & v_1 < v_\parallel < v_2 \\ 0 & \text{otherwise} \end{cases} \tag{6-4}$$

The main difference between D_L and D_{TTMP} is that D_{TTMP} exhibits strong dependence on $v_\perp$ ($D_{TTMP} \sim \mu_\alpha^2 \sim v_{\alpha\perp}^4$). The parallel wave electric field is related to the wave magnetic field by the relation

$$E_\parallel \simeq -\frac{v_e^2}{\Omega_e} \frac{\partial \tilde{B}_\parallel}{\partial z} . \tag{6-5}$$

Using Eq. (6-5) in Eq. (6-2), we have

$$m_\alpha \frac{dv_{\alpha\parallel}}{dt} = -\frac{e}{2\Omega_e} \left(4v_e^2 + \frac{m_\alpha}{m_e} v_{\alpha\perp}^2 \right) \frac{\partial \tilde{B}_\parallel}{\partial z} . \tag{6-6}$$

Note that Landau damping and magnetic pumping forces are in phase and additive, with the primary contribution coming from the TTMP.

In the frequency range considered ($\omega > 5\Omega_i$), one expects the magnetosonic waves to interact also with electrons through Landau damping and TTMP [64]. It is interesting to note that Landau damping and TTMP forces are always out of phase for electrons and there is an exact cancellation of these forces when $v_\perp^2 = 2v_e^2$ [64].

The efficiency of this current drive scheme is calculated in refs. [59,61]. The results show that the efficiency of α-driven current can be a factor of 3 to 4 larger than that obtained from direct magnetosonic wave interaction with electrons [64]. Also, with $Z_{eff} < Z_\alpha$, the total current due to α particles $[J = J_\alpha(1 - Z_{eff}/Z_\alpha)]$ is in the same direction as the electron current generated due to the direct interaction of the waves with the electrons; thus, the currents are additive. The results obtained in refs. [59,61] have not taken into account the neoclassical electron orbit effects (i.e., the effect of magnetically trapped electrons). If these effects exist, the scheme could be susceptible to a large reduction in efficiency. On the other hand, there may be effects such as the bootstrap current, which could be helpful.

6.3. Current Drive by Synchrotron Radiation [58,85]

This is one of the unconventional means of current drive, in that it requires no external current-driving scheme (beams and/or rf sources), but it requires very high temperature reactor plasma conditions. The idea is that at high temperatures a reactor plasma generates a significant amount of rf power as synchrotron radiation. This is particularly true for D-D and D-He^3 reactors, where most or all of the energy is in the charged particles, and an appreciable fraction of the charged particle power comes out in the form of synchrotron radiation. For example, in a 1000-MW reactor, radiation powers in the tens-to-hundreds if megawatts range may be involved. These powers are comparable to those being considered for other current drive schemes. At high electron temperatures ($T_e \sim 30$-50 keV), most of the emission is in the higher harmonics of the cyclotron frequency, implying that the radiation is not only strongly emitted by the plasma but is also strongly absorbed. At these high radiation frequencies, the radiation is strongly reflected by the walls or the walls can be made highly reflecting to it. This means that the radiation forms an ideal medium

for interaction of the plasma with the walls. Because the walls and the plasma are not in thermal equilibrium, the exchange in momentum between the plasma electrons and the wall provides the possibility of driving a current.

Figure 6.3 illustrates one method for driving such a current where an anisotropic wall configuration is used to cause the synchrotron radiation to rotate preferentially around the device in one direction. The method uses fins on the tokamak wall that are absorbing (A) on one side and reflecting (R) on the other. The reflected radiation passes through the plasma and a fraction is absorbed. As radiation repeatedly reflects from the walls, its direction of propagation rotates until it is propagating in one direction. As it does so, it repeatedly passes through the plasma and pushes the electrons. This gives the current. The magnitude of the current is proportional to T_e^4 and apparently becomes sufficient for a reactor at $T_e \sim 50$ keV. A simple theoretical treatment based on a momentum-balance calculation is given in refs. [58,85]. The expression for driven current is given as follows (in mks units with T_e in kiloelectron volts):

$$I \simeq 3 \times 10^{14}\ \alpha\ a^{3/2} \left(\frac{T_e}{m_e c^2}\right)^{5/2} \frac{T_e^{3/2} B^{5/2} (1 - R_w)^{1/2}}{Z_{eff} n_e^{1/2}}\ , \qquad (6\text{-}7)$$

where R_w is the wall reflectivity and $\alpha \simeq 5$–10 is a numerical factor that takes into account the fact that the more energetic electrons radiate and absorb the synchrotron radiation most strongly and collide with ions less frequently so that they carry more current. In other words, the electrons carrying most of the current have an energy greater than the average electron energy $3T_e/2$ and have a lower effective resistivity.

We see that the current is a very strong function of T_e ($\sim T_e^4$); thus synchrotron current drive works best at high temperatures. It also works best at high magnetic fields. These are the conditions that would be found in D-D and D-H_e^3 advanced fuel tokamak reactors, so this method of current drive should work best there.

As an example, consider a D-D or D-H_e^3 plasma at $T_e \simeq 50$ keV, $n_e \simeq 1 \times 10^{20}\ m^{-3}$, $a \simeq 1.5$ m, $B = 10$ T, and a wall reflectivity $R_w = 0.9$. This plasma has a beta of 4% (if $T_e \simeq T_i$) and Eq. (6-7) predicts a current of

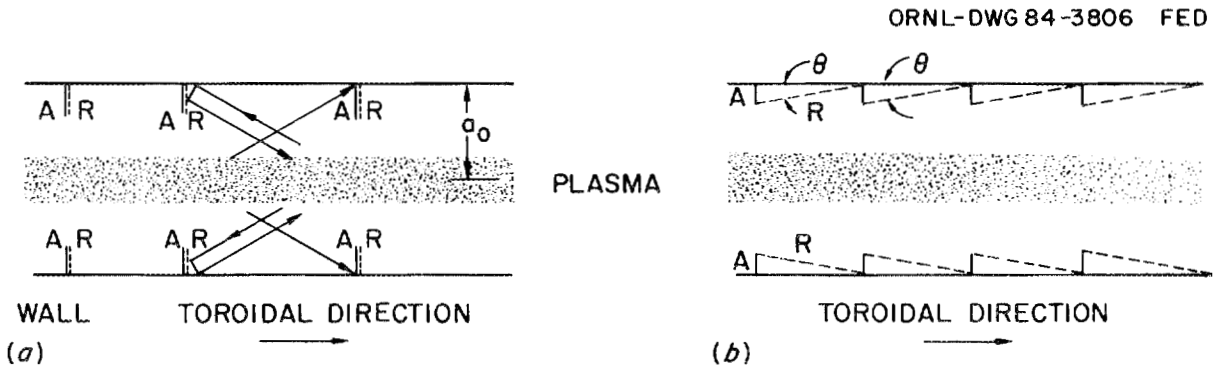

Fig. 6.3. (a) A simple configuration (fins) for achieving current drive by synchrotron radiation. Absorping (A) and reflecting (R) surfaces are shown with solid and dotted lines, respectively. (b) A more efficient fish-scale wall configuration (ref. [85]).

$$I \simeq 6 \times 10^6 \ \alpha/Z_{eff}$$

for $Z_{eff} \simeq 2$ and $\alpha \simeq 5$, $I \simeq 15$ MA.

The problem of controlling the current is important. This could probably be achieved by ports in the wall that could be opened or closed to control the level of synchrotron radiation in the device. The problem of maintenance of the appropriate reflectivity of the first wall may also be important in light of wall erosion due to sputtering and plasma disruption.

6.4. Current Drive with Low-Frequency Waves

Here we are primarily interested in current generation with low-frequency fast waves. These are (1) magnetosonic waves ($\omega > \Omega_i$), the fast wave branch of ion cyclotron waves, and (2) compressional Alfvén wave ($\omega \ll \Omega_i$), the fast wave branch of Alfvén waves. As illustrated in Fig. 1.2, there are two wave regimes that are attractive for obtaining a large current drive efficiency factor ($\hat{J}/\hat{P}$): low- and high-parallel-phase-velocity waves, i.e., $\omega/k_{\parallel} \ll v_e$ and $\omega/k_{\parallel} \gg v_e$, respectively. Current drive with the LH wave is an example of high-phase-velocity waves (Sect. 3). Because of the lower frequencies, magnetosonic waves and compressional Alfvén waves (CAW) are generally low-phase-speed waves. It is, however, possible to generate a high-phase-velocity magnetosonic wave as well.

As compared to high-phase-velocity waves, low-phase-velocity waves have a high momentum content per unit energy, which makes them attractive for a current drive. This is because the momentum in a wave is proportional to its wave number k, whereas the energy carried by the wave is proportional to its frequency ω, so that waves with low $\omega/k_{\parallel}$ have a high parallel momentum content. When the energy of such waves is absorbed by electrons, the momentum absorbed is proportionately higher. The current is carried by slower (thermal) electrons, which are relatively collisional as compared to superthermal (tail) electrons that carry the current where high $\omega/k_{\parallel}$ waves (such as LH waves) are employed.

The frequency regime of interest spans from a few megahertz (Alfvén waves) to a few hundred megahertz (magnetosonic waves). At these frequencies large amounts of cw power are readily available at high efficencies and in high-power units. On the other hand, at the

lowest frequencies, the required coupling structures become large, and the necessity to use coils, loops, or other internal antennas to excite lower frequency waves may pose technological problems in a fusion environment.

6.4.1 Dispersion Relation

The dispersion relation (valid for $\omega \ll \Omega_e$) that characterizes these waves is given by Eq. (5-32):

$$k_\perp^2(A - k_\parallel^2) - (B - k_\parallel^2)(C - k_\parallel^2) = 0 \ , \tag{6-8}$$

where

$$\begin{aligned} A &\equiv \frac{\omega^2}{c^2}\epsilon_1 = \frac{\omega^2}{v_A^2}\frac{\Omega_i^2}{\Omega_i^2 - \omega^2} \ , \\ B &\equiv \frac{\omega^2}{c^2}(\epsilon_1 - \epsilon_2) = \frac{\omega^2}{v_A^2}\frac{\Omega_i}{\Omega_i - \omega} \ , \\ C &\equiv \frac{\omega^2}{c^2}(\epsilon_1 + \epsilon_2) = \frac{\omega^2}{v_A^2}\frac{\Omega_i}{\Omega_i + \omega} \ . \end{aligned} \tag{6-9}$$

Here ϵ_1 and ϵ_2 are the components of dielectric tensor, given by Eq. (5-31), and v_A is the Alfvén speed

$$v_A^2 = c^2\Omega_i^2/\omega_{pi}^2 = B_o^2/\mu_o n m_i \ . \tag{6-10}$$

Equation (6-8) can be rearranged to read [86]

$$\omega^2 = (k_\parallel^2 + k_\perp^2)v_A^2\left[\frac{\bar{A} - N_\parallel^2}{\bar{A}(1 - N_\parallel^2)}\right] \ , \tag{6-11a}$$

or, equivalently,

$$N_\perp^2 + N_\parallel^2 = \left[\frac{\bar{A}(1 - N_\parallel^2)}{\bar{A} - N_\parallel^2}\right], \tag{6-11b}$$

where we define

$$\bar{A} \equiv \frac{v_A^2}{\omega^2} A \equiv \frac{\Omega_i^2}{\Omega_i^2 - \omega^2}, \tag{6-12a}$$

$$N_\parallel^2 \equiv \frac{k_\parallel^2 v_A^2}{\omega^2} = \left(\frac{k_\parallel c}{\omega}\right)^2 \frac{v_A^2}{c^2} = \eta_\parallel^2 \left(\frac{v_A^2}{c^2}\right), \tag{6-12b}$$

$$N_\perp^2 \equiv \frac{k_\perp^2 v_A^2}{\omega^2} = \eta_\perp^2 \left(\frac{v_A^2}{c^2}\right). \tag{6-12c}$$

The quantities $N_\perp$ and $N_\parallel$ are called the Alfvén refractive indices. Note that when $\omega \ll \Omega_i$, $\bar{A} \to 1$, the factor in square brackets in Eq. (6-11) approaches 1 and the fast wave dispersion relation becomes $\omega^2 = k^2 v_A^2 = (k_\perp^2 + k_\parallel^2) v_A^2$. It may be seen from Eqs. (6-11) and (6-12) that

$$N_\perp^2 = 1 \qquad \text{when} \qquad N_\parallel^2 = 0 \tag{6-13a}$$

and that (for the fast-wave branch)

$$N_\parallel^2 = \Omega_i/(\Omega_i + \omega) \qquad \text{when} \qquad N_\perp^2 = 0 . \tag{6-13b}$$

The fast wave branch of Eq. (6-11) is sketched in Fig. 6.4 for rf frequencies below $(\omega < \Omega_i)$ and above $(\omega > \Omega_i)$ the ion cyclotron frequency.

The Alfvén indices of the fast wave, for $\omega > \Omega_i$ and $\omega < \Omega_i$, remain of order unity within the propagating region (Fig. 6.4). This implies that propagation is possible only in sufficiently large and dense plasmas. In a toroidal geometry $k_\perp$ and $k_\parallel$ can be approximated as [86]

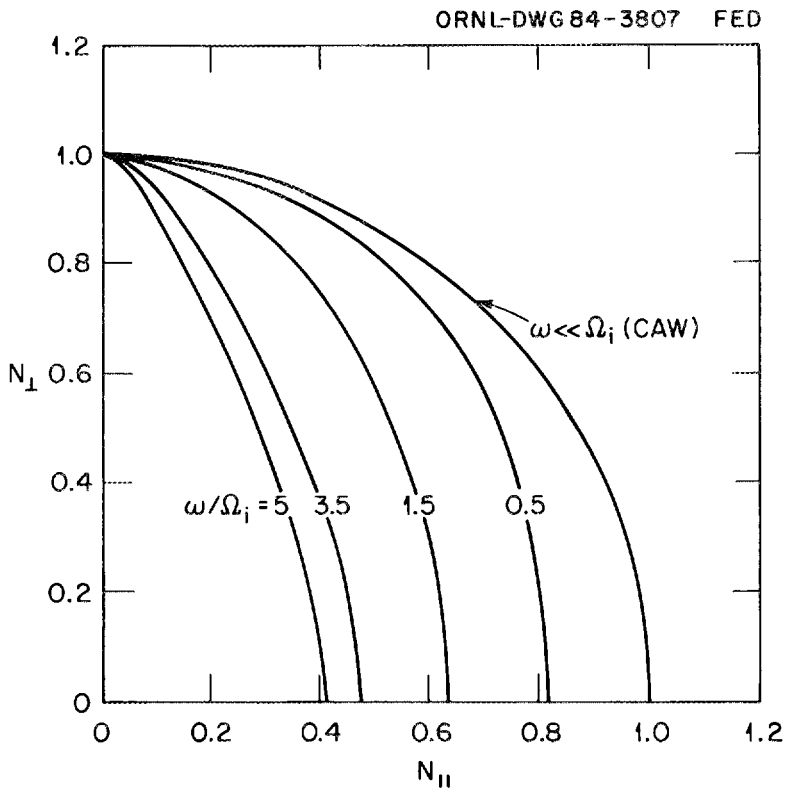

Fig. 6.4. Dispersion curves for fast waves at $\omega/\Omega_i = 0.5$, 1.5, 3.5, and $\omega \ll \Omega_i$. $N_\parallel = \eta_\parallel(v_A c)$ and $N_\perp = \eta_\perp(v_A/c)$ are Alfvén wave refractive indexes. For $\omega \ll \Omega_i$ (CAW) dispersion relation is $N_\perp^2 + N^2{}_\parallel \simeq 1$ [or $\omega^2 = (k_\parallel^2 + k_\perp^2)v_A^2$].

$$k_\perp \sim \pi/a \ ,$$
$$k_\parallel \approx N/R_o \ , \tag{6-14}$$

where N is the toroidal mode number, which is an integer. From Eqs. (6-11) and (6-14), for fast wave propagation we require

$$\left(\frac{\pi}{a}\right)^2 + \left(\frac{\omega + \Omega_i}{\Omega_i}\right)\left(\frac{N}{R_o}\right)^2 \le \left(\frac{\omega}{v_A}\right)^2 \le 1.93 \times 10^{-17} n_e \frac{Z_i^2}{A_i}\left(\frac{\omega}{\Omega_i}\right)^2 \ , \tag{6-15}$$

where Z_i and A_i are the ion charge and relative atomic weight, respectively.

6.4.2 Quasi-Linear Wave Diffusion Coefficient [64]

The acceleration of electrons due to the $E_\parallel$ and $\tilde{B}_\parallel$ field components of traveling waves is given by Eq. (6-2):

$$m_e \frac{dv_\parallel}{dt} = - eE_\parallel - \mu \frac{\partial \tilde{B}_\parallel}{\partial z} \ , \tag{6-16}$$

where $\mu = m_e v_\perp^2/2B_o$. If only $E_\parallel$ is nonzero, the waves are Landau damped by electrons resonant with the wave ($v_\parallel = \omega/k_\parallel$), and the diffusion coefficient is given by Eq. (3-39). If $E_\parallel$ in Eq. (6-16) vanishes, the traveling magnetic field accelerates the electrons. The wave damping is now due to TTMP and the diffusion coefficient is given by Eq. (6-4). In general, however, $E_\parallel$ and $\tilde{B}_\parallel$ are both present and related to each other by Eq. (6-5). Using Eq. (6-5) in Eq. (6-16), the force equation for electrons becomes

$$m_e \frac{dv_\parallel}{dt} = \frac{e}{2\Omega_e}\left(2v_e^2 - v_\perp^2\right)\frac{\partial \tilde{B}_\parallel}{\partial z} \ . \tag{6-17}$$

The Landau damping and TTMP forces are always out of phase for electrons, with TTMP dominating for large $v_\perp$. This is in contrast to

the force equation for the ions (see Sect. 6.2.2). By analogy with the Landau damping and TTMP, the diffusion coefficient can be formed easily with mere substitution. The following expression summarizes the three cases

$$D_{rf}(v_{\parallel}) = \begin{cases} D_L,\ D_{TTMP},\ D_A & v_1 < v_{\parallel} < v_2 \\ 0 & \text{otherwise} \end{cases} , \tag{6-18}$$

where

$$D_L(v_{\parallel}) = \frac{\pi e^2 \langle E_{\parallel}\rangle^2}{m_e^2 v_{\parallel} \Delta k_{\parallel}} \tag{6-19a}$$

is the diffusion coefficient for Landau damping,

$$D_{TTMP}(v_{\parallel}) = \frac{\pi \mu^2 k_{\parallel}^2 \langle \tilde{B}_{\parallel}\rangle^2}{m_e^2 v_{\parallel} \Delta k_{\parallel}} = \frac{\pi k_{\parallel}^2 v_{\perp}^4}{4 v_{\parallel} \Delta k_{\parallel}} \frac{\langle \tilde{B}_{\parallel}\rangle^2}{B_o^2}$$

$$= \frac{1}{4}\left(\frac{v_{\perp}}{v_e}\right)^4 D_L(v_{\parallel}) \tag{6-19b}$$

is the diffusion coefficient for TTMP, and

$$D_A(v_{\parallel}) = \frac{\pi e^2 k_{\parallel}^2 \langle \tilde{B}_{\parallel}\rangle^2}{4\Omega_e^2 m_e^2 v_{\parallel} \Delta k_{\parallel}} (2v_e^2 - v_{\perp}^2)^2$$

$$= \frac{\pi k_{\parallel}^2}{4 v_{\parallel} \Delta k_{\parallel}} (2v_e^2 - v_{\perp}^2)^2 \frac{\langle \tilde{B}_{\parallel}^2\rangle}{B_o^2}$$

$$= \frac{1}{4}\left(2 - \frac{v_{\perp}^2}{v_e^2}\right)^2 D_L(v_{\parallel}) \tag{6-19c}$$

is the diffusion coefficient corresponding to the case when both damping mechanisms (Landau damping and TTMP) are present. (D_A is referred to as the Alfvén wave diffusion coefficient in ref. [64].)

6.4.3 Current Drive Efficiency [64]

The current drive efficiency for low-frequency waves is derived in ref. [64] for various wave types, assuming that D_{rf} is as given by Eq. (6-18). In the limit of small wave amplitudes (low D_{rf} limit) and for a narrow spectrum of wave parallel phase velocities, an approximate expression for $\hat{J}/\hat{P}$ in the low-phase-velocity limit ($\omega/k_{\parallel} \ll v_e$) is given by

$$\frac{\hat{J}}{\hat{P}} = \frac{3}{2} C_W \left(\frac{U_2^2 - U_1^2}{U_2^3 - U_1^3}\right) \equiv \frac{C_W}{\langle U_a \rangle} , \tag{6-20}$$

where U_1 and U_2 are the dimensionless velocities, representing the slowest ($U_1 = v_1/v_e$) and fastest ($U_2 = v_2/v_e$) parallel phase velocities in the spectrum ($v_1 < v_{\parallel} < v_2$); C_W is a constant that depends only on the wave type; and $\langle U_a \rangle$ is an average resonant $U_{\parallel}$ defined as

$$\langle U_a \rangle = \frac{2}{3} \left(\frac{U_2^3 - U_1^3}{U_2^2 - U_1^2}\right) = \frac{2}{3} \left(\frac{v_2}{v_e}\right) \left[\frac{1 - (v_1/v_2)^3}{1 - (v_1/v_2)^2}\right] . \tag{6-21}$$

The constant C_W is determined numerically to fit the results obtained by a numerical solution of the 2-D Fokker-Planck equation. For $Z_{eff} = 1$, they are approximately given by [64]

$$C_A \approx C_{TTMP} \approx 13 , \tag{6-22a}$$

$$C_L \approx 8 , \tag{6-22b}$$

where C_L, C_{TTMP}, and C_A denote the cases of Landau damping, magnetic pumping (TTMP), and Alfvén waves (the combination of the previous two), respectively. The coefficients C_W obtained from more accurate calculations [87] are listed in Table 6.1.

Table 6.1. The coefficients C_W for the three types of current drive by low-frequency wavs [87]

Z_{eff}	C_L	C_{TTMP}	C_A
1	7.52	16.98	16.18
2	3.76	10.34	10.14
5	1.50	5.10	5.20
10	0.75	2.84	2.96

The ratio $\hat{J}/\hat{P}$ has been determined numerically for a wide range of parameters in ref. [64]. Figure 6.5 shows $\hat{J}/\hat{P}$ as a function of the weighted average parallel velocity $\langle U_a \rangle$, defined by Eq. (6-21), for various types of waves in the small D_{rf} limit. Rough semianalytic fits to the data shown in Fig. 6.5 indicate

$$\frac{\hat{J}}{\hat{P}} \simeq \frac{C_W}{\langle U_a \rangle} + 1.4 \langle U_a \rangle^2 + y_W \ , \tag{6-23}$$

where y_W is a constant: $y_A \simeq y_{TTMP} \simeq 5$ and $y_L \simeq 2$.

Once again, two favorable wave phase velocity regimes are apparent from Fig. 6.5 [or Eq. (6-23)]. For high-phase-velocity waves ($\hat{J}/\hat{P} \sim \langle U_a \rangle^2$), a similar behavior is seen, for example, for LH waves [Eq. (3-55)]. For low-phase-velocity waves, $\hat{J}/\hat{P} \sim 1/\langle U_a \rangle$. It would, therefore, be preferable to have either very fast waves (i.e., $\langle U_a \rangle \gg 1$) or very slow waves (i.e., $\langle U_a \rangle \ll 1$). Obviously, there are limits on how fast or how slow the wave phase velocity could be. For example, in hot plasmas (i.e., $T_e \sim 10$–20 keV, a temperature representative of reactor plasmas), the wave accessibility represents a limit on the fastest phase velocity, which at $\langle U_a \rangle \sim 4$–$5$ is nearly the speed of light. For low-phase-velocity waves, $\langle U_a \rangle \sim 0.1$–$0.2$ would probably be the limit to avoid ion Landau damping. The damping of the

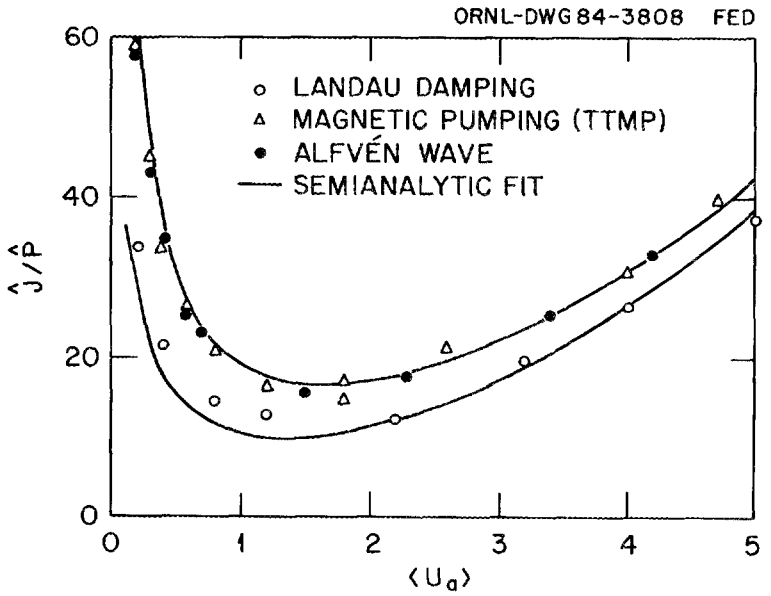

Fig. 6.5. $\hat{J}/\hat{P}$ vs $\langle U_a \rangle$ for three wave types in the low-D_{rf} limit: Landau damping (open circles), magnetic pumping (x's), and Alfvén waves (closed circles). The solid curves ar rough semianalytic fits to the data. The upper curve (TTMP and Alfvén) obeys $\hat{J}/\hat{P} \simeq 13/\langle U_a \rangle + 1.4\langle U_a \rangle^2 + 5$ and the lower curve (Landau damping) obeys $\hat{J}/\hat{P} \simeq 8/\langle U_a \rangle + 1.4\langle U_a \rangle^2 + 2$. In all cases a narrow spectrum is assumed: $\Delta v_{\parallel} = (v_2 - v_1) = 0.2\ v_e(\Delta U_{\parallel} = 0.2)$. (ref. [64]).

wave on the ions will be nearly absent if $v_{\parallel}(=\omega/k_{\parallel})$ is large enough (i.e., several times the ion thermal velocity v_i). We define this ratio as

$$\alpha \equiv \omega/(k_{\parallel} v_i) \gtrsim 6 \ . \tag{6-24}$$

In terms of wave refractive indices $(\eta_{\parallel} = \omega/ck_{\parallel} = v_{\parallel}/c)$, we rewrite current drive efficiency in the low-phase-velocity limit [Eq. (6-20)] as

$$\frac{\hat{J}}{\hat{P}} = \frac{3}{2} C_W \frac{v_e}{c} \left(\frac{\eta_2^{-2} - \eta_1^{-2}}{\eta_2^{-3} - \eta_1^{-3}}\right)$$

$$= \frac{3}{2} C_W \frac{\eta_2 v_e}{c} \left[\frac{1 - (\eta_2/\eta_1)^2}{1 - (\eta_2/\eta_1)^3}\right]$$

$$= C_W \left(\frac{v_e}{c}\right) \langle \eta_a \rangle = C_W \left(\frac{T_e}{511}\right)^{1/2} \langle \eta_a \rangle \ , \tag{6-25}$$

where $\eta_1 = c/v_1$, $\eta_2 = c/v_2$, and

$$\langle \eta_a \rangle \equiv \frac{3}{2} \eta_2 \left[\frac{1 - (\eta_2/\eta_1)^2}{1 - (\eta_2/\eta_1)^3}\right] \equiv \frac{(c/v_e)}{\langle U_a \rangle} \ . \tag{6-26}$$

We discuss some of the low-frequency-wave drivers in the following three subsections.

6.4.4 Compressional Alfvén Wave (CAW) [64,88]

As mentioned previously, the CAW is the fast wave branch of the Alfvén waves and exists as cavity eigenmode at relatively low frequencies $(\omega \ll \Omega_i)$, ranging from several hundreds of kilohertz to a few tens of megahertz. These waves have the dispersion relation [see Eq. (6-11) and the discussions following thereafter]

$$\omega^2 = (k_\parallel^2 + k_\perp^2)v_A^2 \ , \tag{6-27}$$

with the desirable characteristic of low-phase velocity, $\omega/k_\parallel v_e \ll 1$. To avoid ion Landau damping, we require $\alpha \equiv \omega/(k_\parallel v_i) \gtrsim 6$. To avoid ion cyclotron damping at higher harmonics, the frequency should be chosen such that $\omega < \Omega_i/2$. In terms of α, the dispersion relation [Eq. (6-27)] takes the convenient form

$$k_\perp^2 = k_\parallel^2(\alpha^2\beta_t/4 - 1) \tag{6-28}$$

or

$$\alpha \equiv \left(\frac{\omega}{k_\parallel v_i}\right) = \frac{2}{\beta_t^{1/2}}\left(1 + \frac{k_\perp^2}{k_\parallel^2}\right)^{1/2} \geq 6 \ , \tag{6-29}$$

where β_t is the average toroidal beta given by Eq. (1-26) $[\beta_t \equiv 2\mu_o n(T_e + T_i)/B_o^2 \simeq 4\mu_o nT/B_o^2]$.

According to Eqs. (6-20) or Eq. (6-25), current drive efficiency is maximized by exciting the slowest phase velocities (smallest $U_\parallel = v_\parallel/v_e = \omega/k_\parallel v_e$ or largest $\eta_\parallel = c/v_\parallel = ck_\parallel/\omega$), subject to Eq. (6-29). Thus, it is advantageous to have α values not much greater than 6. However, note that even for the lowest order perpendicular mode $k_\perp \approx \pi/a$ and $k_\parallel = N/R_o$

$$\alpha = 2\beta_t^{-1/2}\ \left[1 + (\pi R_o/aN)^2\right]^{1/2} \ , \tag{6-30}$$

which indicates that α (in turn $\omega/k_\parallel$) does not decrease significantly unless N (toroidal mode number) is very large. By decreasing N the phase velocity increases, which yields higher $\hat{J}/\hat{P}$. Because of the necessity of a large number of coils (or a complex antenna design) to excite a high N mode, there is, however, a practical upper limit on N;

$N \sim 10$–20. From Eq. (6–30) we see that the minimum α is $\alpha = 2\beta_t^{-1/2}$, which is optimum (i.e., $\alpha \simeq 6$) for $\beta_t \simeq 10\%$.

As an example, consider a reactor plasma with $T_e \simeq T_i \simeq 15$ keV, $n_e \simeq 10^{20}$ m^{-3}, $a \simeq 1.25$ m, $R_o \simeq 5$ m, $B_o = 4$ T, and an average mass of 2.5 for D–T particles. Taking $N = 20$, we find $\omega/k_{\parallel}v_i \simeq 8.6$, $f = \omega/2\pi = 4.15$ MHz, and $\lambda_{\parallel} = 2\pi/k_{\parallel} = 1.57$ m. For the parameters given, $\beta_t = 7.5\%$ and the ion cyclotron frequency $(\Omega/2\pi)$ is 30 MHz for deuterium (20 MHz for tritium). Because $\omega < \Omega_T/2$, ion cyclotron damping is negligible. Knowing ω and $k_{\parallel}$, $U_{\parallel} = v_{\parallel}/v_e = \omega/k_{\parallel}v_e \simeq 0.13$ and $\eta_{\parallel} \simeq 46$. For a narrow wave spectrum, $\langle U_a \rangle \simeq U_{\parallel} \simeq 0.13$. With these numbers the current drive efficiency $\hat{J}/\hat{P} \simeq 100$. In terms of practical units (i.e., the total wave power required to sustain the total plasma current [see Eq. (1–8)]), we have

$$\frac{I_{tot}}{P_{tot}} \simeq \frac{0.015}{R_o}\left(\frac{20}{\ell n\,\Lambda}\right)\left(\frac{T_e}{10}\right)\left(\frac{10^{20}}{n}\right)\frac{\hat{J}}{\hat{P}}$$

$$\simeq 0.5 \text{ A/W} . \qquad (6\text{–}31)$$

These crude estimates indicate favorable current drive efficiencies. For similar reactor parameters, the optimal current drive efficiency, for example, for LH waves would be around $\hat{J}/\hat{P} \simeq 20$–$30$, requiring a factor of 3 to 4 as much power as the CAW to generate the same current. The attractiveness of CAW (or the low-frequency wave regime, in general) should be viewed very cautiously, however, because the scheme could be susceptible to a large reduction in efficiency due to electron trapping effects, if these exist. As pointed out previously, the expressions given for the efficiency factor do not consider the neoclassical effects of trapped electrons. The neoclassical effects are not too important in the case of LH waves. This is because the current is carried by superthermal resonant tail electrons ($U_{\parallel} \gg 1$), which are nearly all circulating. The current carried by thermal background electrons is negligible, so that trapped electron effects do not matter. In the low-frequency regime, where the wave phase velocity is low, the wave is resonant with trapped

electrons ($U_{\parallel} \ll 1$), which carry no current. It is unclear how large a toroidal current can really be generated. Several arguments are given in ref. [64] to justify the fact that the resonant electrons are trapped presents no problem.

6.4.5 Low-Phase-Velocity Magnetosonic Wave [64,66]

Here, the frequency regime of interest is $\omega > \Omega_i$ with $\omega/k_{\parallel}v_e \ll 1$. To avoid ion Landau damping it is required that $\alpha \equiv \omega/(kv_i) \geq 6$. Ion cyclotron damping is negligible, provided $\omega/\Omega_i \geq 5$. Under these assumptions, magnetosonic wave (fast wave branch of the ICRF waves) damping is mainly due to TTMP, and Eq. (6-20) applies

$$\frac{\hat{J}}{\hat{P}} = 19.5 \left(\frac{v_e}{v_2}\right) \left[\frac{1 - (v_1/v_2)^2}{1 - (v_1/v_2)^3}\right]$$

$$= 19.5 \left(\frac{\eta_2 v_e}{c}\right) \left[\frac{1 - (\eta_2/\eta_1)^2}{1 - (\eta_2/\eta_1)^3}\right] , \qquad (6\text{-}32)$$

where $v_2/v_e \ll 1$ (or $\eta_2 \gg c/v_e$). As an application we consider plasma parameters chosen for the previous example in Sect. 6.4.4. We select $f = \omega/2\pi = 150$ MHz, such that $\omega/\Omega_D = 5$ ($\omega/\Omega_T > 5$). As in the case of CAW, maximization of $\eta_{\parallel}$ maximizes $\hat{J}/\hat{P}$. From the dispersion relation [Eq. (6-11)] and Fig. 6.4, we see that the largest $\eta_{\parallel}$ ($N_{\parallel}$) occurs near the cutoff [Eq. (6-13b)] $N_{\parallel} \equiv \eta_{\parallel}^2 v_A^2/c^2 = \Omega_i/(\Omega_i + \omega) = 1/6$. For an effective ion mass of 2.5, $v_A/c = 1.84 \times 10^{-2}$ and $\eta_{\parallel} \simeq 22$. The corresponding wave number is $k_{\parallel} \simeq 70\ m^{-1}$ (or $\lambda_{\parallel} = 2\pi/k_{\parallel} \simeq 9$ cm), which gives a toroidal mode number $N = k_{\parallel}R_o \simeq 250$. Although at frequencies above 100 MHz the use of ridged or dielectric waveguide antennas may be possible, it will be difficult to design a traveling fast wave antenna with such a short $\lambda_{\parallel}$ (~ 9 cm). The very large mode number makes it almost impossible to excite a single mode with unique characteristics. The problem with multimode excitation is that the modes interfere constructively near the antenna (as they are driven by the same local antenna fields) but destructively elsewhere [86]. The near fields,

thus produced, may cause anomalously large damping at the plasma edge thus creating hollow current density profiles.

Returning to the efficiency factor, assuming a narrow wave spectrum (i.e., narrow range of phase velocities with $\eta_2/\eta_1 \sim 0.8$–0.9), we approximate Eq. (6-32) as

$$\frac{\hat{J}}{\hat{P}} \simeq 14\ \eta_2(v_e/c) \simeq 0.6\ \eta_2 T_e^{1/2}\ .$$

With $\eta_{\parallel} \simeq \eta_2 \simeq 22$ and $T_e = 15$ keV, we find $\hat{J}/\hat{P} \simeq 50$, which is competitive with other drivers (somewhat less attractive than CAW, but better than LH). In practical units it gives $I_{tot}/P_{tot} \simeq 0.25$ A/W. Again, because of the choice of phase velocities $\omega/(k_{\parallel}v_e) \ll 1$, the majority of the resonant electrons are magnetically trapped. The neoclassical effects discussed previously could substantially influence the favorable efficiencies predicted here.

6.4.6 <u>High-Phase-Velocity Magnetosonic Wave</u> [71,88]

It is also possible to broadcast magnetosonic waves ($\omega > \Omega_i$) at high phase velocities $\omega/(k_{\parallel}v_e) > 1$. In this case, the long $\lambda_{\parallel}$ make it appropriate to use waveguide couplers. Because of the high phase velocities ($\omega/k_{\parallel}v_e \sim 3$–$4$), the neoclassical effects should not play a significant role. The advantages and various applications of these waves as a current driver are discussed in refs. [71,88].

The high-phase-velocity magnetosonic waves are also damped with TTMP. Because the electron TTMP absorption process is weak at high phase velocities ($v_{\parallel}/v_e > 1$), the other damping mechanisms (i.e., ion cyclotron harmonic damping) may compete with the weak electron damping, tending to reduce the current drive efficiency. It is, however, possible to avoid cyclotron harmonic damping in a D-T reactor if the frequency is chosen to satisfy $2\Omega_{T,max} < \omega < 2\Omega_{D,min}$. These inequalities can be satisfied if the plasma aspect ratio exceeds $R_o/a \simeq 5$ [71]. Thus, this scheme favors large aspect ratio tokamaks. By direct nature of the damping mechanism (TTMP), this scheme works best in the dense, high-beta, high-T_e plasmas (a regime where LH current drive encounters its greatest difficulties). Current drive

efficiencies achievable with this scheme are somewhat better than those of LH waves (see Fig. 1.2).

REFERENCES

[1] T. Ohkawa, "New Methods of Driving Plasma Current in Fusion Devices," Nucl. Fusion 10, 185 (1970).

[2] N. J. Fisch, "Confining a Tokamak Plasma with RF-Driven Current," Phys. Rev. Lett. 41, 873 (1978); errata Phys. Rev. Lett. 42, 410 (1979).

[3] D. F. H. Start, P. R. Collins, E. M. Jones, A. C. Riviere, and D. R. Sweetman, "Observation of Beam-Induced Currents in Toroidal Plasmas," Phys. Rev. Lett. 40, 1497 (1978).

[4] J. G. Cordey, E. M. Jones, D. F. H. Start, A. R. Curtis, and I. P. Jones, "A Kinetic Theory of Beam Induced Plasma Currents," Nucl. Fusion 29, 249 (1979).

[5] D. F. H. Start and J. G. Cordey, "Beam-Induced Currents in Toroidal Plasmas of Arbitrary Aspect Ratio," Phys. Fluids 23, 1477 (1980).

[6] J. W. Connor and J. G. Cordey, "Effects of Neutral Injection Heating upon Toroidal Equilibria," Nucl. Fusion 14, 185 (1974).

[7] W. H. M. Clark et al., "Measurements of the Beam-Driven Current in the DITE Tokamak," Phys. Rev. Lett 45, 1101 (1980).

[8] J. G. Cordey, "A Review of Non-Inductive Current Drive Theory," Plasma Phys. 25, 361 (1983).

[9] D. F. H. Start, ed., Non-Inductive Current Drive in Tokamaks, Vols. I and II (Proceedings of the IAEA Technical Committee Meeting, Culham Laboratory, April 18-21, 1983), CLM-CD, Culham Laboratory 1983.

[10] J. G. Cordey, "A Review of Current Drive by Fast Ion Injection," in ref [9], pp. 1-10.

[11] D. R. Mikkelsen and C. E. Singer, "Optimization of Tokamak Reactors with Beam-Driven Current," in ref. [9], pp. 11-33.

[12] D. R. Mikkelsen "Neutral Beam Current Drive in TFTR," in ref. [9], pp. 62-70.

[13] D. R. Mikkelsen and C. E. Singer, "Optimization of Steady-State Beam Driven Tokamak Reactors," Nucl. Technol./Fusion 4(2), 237 (1983).

[14] D. A. Ehst, V. Bailey, J. Benford, M. DiCapua, H. Helava, and G. A. Proulx, "Relativistic Electron Beam Current Drive for Tokamak Reactors," Bull. Am. Phys. Soc. 26, 965 (1981).

[15] D. A. Ehst, "Relativistic Electron Beam Current Drive," in FED-A, An Advanced Performance FED Based on Low Safety Factor and Current Drive, ORNL/FEDC-83/1, Oak Ridge Natl. Lab., 1983.

[16] C. F. F. Karney and N. J. Fisch, "Numerical Studies of Current Generation by Radio-Frequency Traveling Waves," Phys. Fluids 22, 1817 (1979).

[17] V. V. Parail and G. V. Preverzev, "Dynamics of Current Driven by Lower Hybrid Waves in a Tokamak," Sov. J. Plasma Phys. 9, 341 (1983).

[18] J. G. Cordey, T. Edlington, and D. F. H. Start, "A Theory of Currents Induced by Radio-Frequency Waves in Toroidal Plasmas," Plasma Phys. 24, 73 (1982).

[19] W. Hooke, "Review of Experiments on Current Drive in Tokamaks by Means of RF Waves," Plasma Phys. 26, 133 (1984).

[20] S. Bernabei et al., "Lower-Hybrid Current Drive in the PLT Tokamak," Phys. Rev. Lett. 49, 1255 (1982).

[21] F. Jobes et al., "Current Drive Experiments on the PLT Tokamak," PPPL-1939, Princeton Plasma Physics Lab., 1983.

[22] M. Porkolab, "Survey of Lower Hybrid Experiments," IEEE Trans. Plasma Sci. 12, 107 (1984).

[23] G. Tonon et al., "Lower Hybrid Current Drive and Heating on Wega Tokamak," in Proceedings of the Ninth International Conference on Plasma Physics and Controlled Nuclear Fusion Research, Baltimore, September 1-8, 1982, Vol. I, IAEA, Vienna, 1983, p. 179.

[24] Yu. N. Dnestrovskij, S. N. Krasheninnikov, V. V. Parail, and G. V. Pereverzev, "Generation of a Steady-State Current in a Tokamak with Lower Hybrid and Cyclotron Waves," in Proceedings of the Ninth International Conference on Plasma Physics and Controlled Nuclear Fusion Research, Baltimore, September 1-8, 1982, Vol. I, IAEA, Vienna, 1983, p. 189.

[25] S. Tanaka et al., "Plasma Current Drive and Sustainment by Lower-Hybrid Wave in the WT-2 Tokamak," in Proceedings of the Ninth International Conference on Plasma Physics and Controlled Nuclear Fusion Research, Baltimore, September 1-8, 1982, Vol. I, IAEA, Vienna, 1983 p. 199.

[26] M. Porkolab et al., "Lower Hybrid Heating and Current Drive Experiments on the Alcator C and Versator II Tokamaks," in Proceedings of the Ninth International Conference on Plasma Physics and Controlled Nuclear Fusion Research, Baltimore, September 1-8, 1982, Vol. I, IAEA, Vienna, 1983, p. 227.

[27] W. Hooke et al., "Lower Hybrid Heating and Current Drive on PLT," in Proceedings of the Ninth International Conference on Plasma Physics and Controlled Nuclear Fusion Research, Baltimore, September 1-8, 1982, Vol. I, IAEA, Vienna, 1983, p. 239.

[28] F. Alladio et al., "Lower Hybrid Heating Experiments in the Frascati Tokamak (FT)," in Proceedings of the Ninth International Conference on Plasma Physics and Controlled Nuclear Fusion Research, Baltimore, September 1-8, 1982, Vol. II, IAEA, Vienna 1983, p. 41.

[29] D. K. Bhadra, C. Chu, R. W. Harvey, and R. Prater, "Studies of Radio Frequency Current Drive in a Plasma," Plasma Phys. 25, 361 (1983).

[30] G. Tonon, "Heating and Current Drive by LH-Waves on Toroidal Plasmas: Problems and Perspectives," Plasma Phys. 26, 145 (1984).

[31] M. Porkolab et al., "Lower Hybrid Experiments at the 1 MW Level on Alcator C: Heating and Current Drive," in Proceedings of the Fourth International Symposium on Heating in Toroidal Plasmas, Rome, Italy, March 21-28, 1984, CONF-840311 (to be published); PFC/CP-84-7, Massachusetts Institute of Technology, 1984.

[32] D. A. Ehst, "Design Constraints for Steady-State Tokamak Reactors Driven by Lower-Hybrid Waves," Nucl. Fusion 19, 1369 (1979).

[33] S. Y. Yuen, D. Kaplan, and D. R. Cohn, "Characteristics of Lower-Hybrid-Wave-Driven Steady-State Tokamak Power Reactor," Nucl. Fusion 20, 159 (1980).

[34] R. Prater et al., "Conceptual Design of RST — An RF-Driven Steady-State Tokamak," EPRI-AP-1351, General Atomic Co., San Diego, March, 1980.

[35] T. Yamamoto, "Study of the Current Drive by the Lower Hybrid Wave in a Tokamak," in ref. [9], pp. 224-249.

[36] B. Lloyd et al., "Lower Hybrid Current Drive Experiments on the Alcator C and the Versator II Tokamaks," in ref. [9], pp. 250-277.

[37] F. Santini, F. DeMarco, E. Barbato, and A. Tuccillo, "Interaction of Lower Hybrid Waves with Fast Electron Tails in FT," in ref. [9], pp. 278-297.

[38] R. W. Motley et al., "Lower Hybrid Current Drive in the PLT Tokamak," in ref. [9], pp. 299-312.

[39] S. Tanaka et al., "Toroidal Plasma Current Start-up and Sustainment by RF in the WT-2 Tokamak," in ref. [9], pp. 327-335.

[40] V. V. Alikaeev et al., "Experiments on Current Drive by Lower Hybrid Waves in the T7 Tokamak," in ref. [9], pp. 313-326.

[41] N. J. Fisch and A. H. Boozer, "Creating an Asymmetric Plasma Resistivity with Waves," Phys. Rev. Lett. 45, 720 (1980).

[42] T. M. Antonsen and K. R. Chu, "Radio Frequency Current Generation by Waves in Toroidal Geometry," Phys. Fluids 25, 1295 (1982).

[43] N. J. Fisch, "Current Generation in a Relativistic Plasma," Phys. Rev. A 24, 3245 (1981).

[44] O. C. Eldridge, "On Currents Induced in Tokamaks by Electron Cyclotron Heating," ORNL/TM-7503, Oak Ridge Natl. Lab., 1980.

[45] C. F. F. Karney and N. J. Fisch, "Currents Driven by Electron Cyclotron Waves," Nucl. Fusion 21, 1549 (1981).

[46] V. S. Chan, S. C. Chiu, J. Y. Hsu, and S. K. Wong, "Kinetic Theory of Electron Cyclotron Current Drive in a Toroidal Device," Nucl. Fusion 22, 787 (1982).

[47] D. F. H. Start et al., "Observation of a Plasma Current Driven by RF Waves at the Electron Cyclotron Resonance in the Culham Levitron," Phys. Rev. Lett. 48, 624 (1982).

[48] M. W. Alcock, B. Lloyd, A. W. Morris, D. C. Robinson, and D. F. H. Start, "High-Beta Poloidal Plasmas and Current Drive by ECRH on Tosca," in Proceedings of the Ninth International Conference on Plasma Physics and Controlled Nuclear Fusion Research, Baltimore, September 1-8, 1982, Vol. II, IAEA, Vienna 1983, p. 51.

[49] D. F. H. Start, M. R. O'Brien, and P. M. V. Grace, "The Effect of a Relativistic Resonance Condition on the Fokker-Planck Theory of ECRH Current Drive," Plasma Phys. 25, 1431 (1983).

[50] C. N. Lashmore-Davies, "A Review of ECRH Current Drive Theory," in ref. [9], pp. 473-495.

[51] R. A. Cairns, J. Owen, and C. N. Lashmore-Davies, "The Effect of Relativistic Correction to the Resonance Condition on Electron Cyclotron Current Drive," in ref.-[9], pp. 496-501.

[52] T. Edlington, "ECRH Current Drive Experiments at Culham," in ref. [9], pp. 514-520.

[53] R. A. Cairns, J. Owen, and C. N. Lashmore-Davies, "Effects of the Relativistic Correction to the Resonance Condition on Electron Cyclotron Current Drive," Phys. Fluids 26, 3475 (1983).

[54] N. J. Fisch, "Current Generation by Minority-Species Heating," Nucl. Fusion 21, 15 (1981).

[55] S. C. Chiu et al., "Current Driven by Asymmetrical Minority Heating in ICRF," Nucl. Fusion 23, 499 (1983).

[56] V. S. Chan and S. C. Chiu, "Minority ICRF Current Drive in Toroidal Geometry," in ref. [9], pp. 71-82.

[57] K. Okano, "Current Drive by ICRF Heating of Alpha-Particles and Beam Ions," in ref. [9], pp. 83-102.

[58] J. M. Dawson, "Current Drive by (1) Injection of Moderately Heavy Ions at MeV/Nucleon; (2) Plasma Synchrotron Radiation," in ref. [9], pp. 366-375.

[59] D. K. Bhadra, C. Chu, and U. A. Peuron, "New Scheme for Current Drive in a Tokamak Reactor," Nucl. Technol./Fusion 3, 335 (1983).

[60] K. Okano, N. Inoue, T. Uchida, R. Sugihara and Y. Ogawa, "Current Generation by Interaction of Alpha Particles with ICRF Waves," in Proceedings of the Ninth International Conference on Plasma Physics and Controlled Nuclear Fusion Research, Baltimore, September 1-8, 1982, Vol. II, IAEA, Vienna, 1983, p. 557.

[61] D. K. Bhadra and C. Chu, "Radio-Frequency Current Drive in a Fusion Producing Plasma," Phys. Rev. Lett. 48, 1824 (1982).

[62] D. F. H. Start, "Non-Inductive Current Drive in Tokamaks," Report on the IAEA Technical Committee Meeting, Culham Laboratory, April 18-21, 1983; Nucl. Fusion 23, 1411 (1983).

[63] A. Hasegawa, "Toroidal Current Production by Kinetic Alfvén Wave," Nucl. Fusion 20, 1158 (1980).

[64] N. J. Fisch and C. F. F. Karney, "Current Generation with Low-Frequency Waves," Phys. Fluids 24, 27 (1981).

[65] N. J. Fisch, "Current Generation in Tokamaks by Phased Injection of Pellets," Nucl. Fusion 24, 378 (1984).

[66] D. A. Ehst, "Wave-Driver Options for Low Aspect Ratio Steady-State Tokamak Reactors," ANL/FPP/TM-141, Argonne Natl. Lab., 1981.

[67] V. B. Krapchev, D. W. Hewett, and A. Bers, "Analytic Solution of the 2-D Fokker-Planck Equation for LH Current Drive," in Proceedings of the Fourth International Symposium on Heating in Toroidal Plasmas, Rome, Italy, March 21-28, 1984, CONF-840311 (to be published); PFC/CP-84-2, Massachusetts Institute of Technology, 1984.

[68] K. Hizanidis, D. W. Hewett, and A. Bers, "Solution of the Relativistic 2-D Fokker-Planck Equation for LH Current Drive," in Proceedings of the Fourth International Symposium on Heating in Toroidal Plasmas, Rome, Italy, March 21-28, 1984, CONF-840311 (to

be published); PFC/CP-84-4, Massachusetts Institute of Technology, 1984.

[69] P. Bonoli, R. Englade, and M. Porkolab, "Realistic Modeling of Lower Hybrid Current Drive with Multiple Codes," in Proceedings of the Fourth International Symposium on Heating in Toroidal Plasmas, Rome, Italy, March 21-28, 1984, CONF-840311 (to be published); PFC/CP-84-6, Massachusetts Institute of Technology, 1984; R. Englade, P. Bonoli, and M. Porkolab, "Numerical Simulation of Current Drive by Lower Hybrid Waves," in ref. [9], pp. 178-189.

[70] M. Cox and D. F. H. Start, "A 2-D Fokker-Planck Treatment of the ICRF Enhancement of Beam-Driven Currents," Nucl. Fusion 24, 399 (1984).

[71] Y-K. M. Peng and P. H. Rutherford, eds., FED-A An Advanced Performance FED Based on Low Safety Factor and Current Drive, ORNL/FEDC-83/1, Oak Ridge Natl. Lab., 1983, Chap. 4.

[72] Starfire Design Team, Plasma Heating and Current Drive in Starfire-A Commerical Tokamak Fusion Power Plant Study, ANL/FPP-80-1, Argonne Natl. Lab., 1980, Vol. 1, Chap. 7.

[73] V. S. Chan, C. S. Liu, P. L. Andrews, and F. W. McClain, "Nonlinear Theory of Lower Hybrid Current Drive II," in Proceedings of the Fourth International Symposium on Heating in Toroidal Plasmas, Rome, Italy, March 21-18, 1984, CONF-840311 (to be published).

[74] V. V. Parail and G. V. Pereverzev, "The Fan Instability and Lower Hybrid Current Drive," (translated from the Russian) ORNL-tr-4995, Oak Ridge Natl. Lab., 1983.

[75] C. F. Kennel and F. Engelmann, "Velocity Space Diffusion from Weak Plasma Turbulence in a Magnetic Field," Phys. Fluids 9, 2377 (1966).

[76] J. G. Cordey and W. G. F. Core, "Energetic Particle Distribution in a Toroidal Plasma with Neutral Injection Heating," Phys. Fluids 17, 1626 (1974).

[77] J. G. Cordey, "Effects of Particle Trapping on the Slowing-Down of Fast Ions in a Toroidal Plasma," Nucl. Fusion 16, 499 (1976).

[78] J. D. Gaffey, "Energetic Ion Distribution Resulting from Neutral Beam Injection in Tokamaks," J. Plasma Phys. 16, 149 (1976).

[79] S. P. Hirshman, "Classical Collisional Theory of Beam-Driven Plasma Currents," Phys. Fluids 23, 1238 (1980).

[80] P. Bonoli, "Linear Theory of Lower Hybrid Heating," IEEE Trans. Plasma Sci. 12, 95 (1984).

[81] E. Canobbio and R. Croci, "On the Interpretation of LH Current Drive Experiments," in ref. [9], pp. 155-160.

[82] V. V. Parail and O. P. Pogutse, "The Kinetic Theory of Runaway Electron Beam Instability in a Tokamak," Nucl. Fusion 18, 303 (1978).

[83] P. B. Parks and F. B. Marcus, "Current Production by Cyclotron Heating of Electrons Passing Through an Axial Magnetic Field Gradient," Nucl. Fusion 21, 1207 (1981).

[84] K. Okano, N. Inoue, and T. Uchida, "Scaling Law of ICRF-Wave-Enhanced Beam-Driven Current," Nucl. Fusion 23, 235 (1983).

[85] J. M. Dawson and P. K. Kaw, "Current Maintenance in Tokamaks by Use of Synchrotron Radiation," Phys. Rev. Lett. 48, 1730 (1982).

[86] T. H. Stix, "Fast-Wave Heating of a Two-Component Plasma," Nucl. Fusion 15, 737 (1975).

[87] C. F. F. Karney and N. J. Fisch, "Efficiency of Current Drive by Fast Waves," PPPL-2128, Princeton Plasma Physics Lab., 1984.

[88] D. A. Ehst, "Driver Options and Burn Cyclo Selections Based on Power Reactor Considerations," in ref. [9], pp. 443-466.

ORNL/TM-9296
Dist. Category UC-20 a,d,f,g

INTERNAL DISTRIBUTION

1. L. A. Berry
2. W. A. Houlberg
3. H. H. Haselton
4. J. Sheffield
5. D. Akers
6. D. B. Batchelor
7. S. K. Borowski
8. J. Dunlap
9. D. Swain
10. T. Uckan
11. J. F. Lyon
12. T. E. Shannon
13. J. H. Harris
14. M. J. Saltmarsh
15. R. A. Dory
16. Y-K. M. Peng
17-21. N. A. Uckan
22. D. R. Baumgardner
23-24. Laboratory Records Department
25. Laboratory Records, ORNL-RC
26. ORNL Patent Office
27. Document Reference Section
28. Central Research Library
29. Fusion Energy Division Library
30. Fusion Energy Division Publications Office

EXTERNAL DISTRIBUTION

31. Office of the Assistant Manager for Energy Research and Development, Department of Energy, Oak Ridge Operations, Box E, Oak Ridge, TN 37830
32. J. D. Callen, Department of Nuclear Engineering, University of Wisconsin, Madison, WI 53706
33. R. W. Conn, Department of Chemical, Nuclear, and Thermal Engineering, University of California, Los Angeles, CA 90024
34. S. O. Dean, Director, Fusion Energy Development, Science Applications, Inc., 2 Professional Drive, Gaithersburg, MD 20760
35. H. K. Forsen, Bechtel Group, Inc., Research Engineering, P.O. Box 3965, San Francisco, CA 94105
36. R. W. Gould, Department of Applied Physics, California Institute of Technology, Pasadena, CA 91125
37. W. M. Stacey, Jr., School of Nuclear Engineering, Georgia Institute of Technology, Atlanta, GA 30332
38. G. A. Eliseev, I. V. Kurchatov Institute of Atomic Energy, P.O. Box 3402, 123182 Moscow, U.S.S.R.
39. V. A. Glukhikh, Scientific-Research Institute of Electro-Physical Apparatus, 188631 Leningrad, U.S.S.R.
40. I. Spighel, Lebedev Physical Institute, Leninsky Prospect 53, 117924 Moscow, U.S.S.R.
41. D. D. Ryutov, Institute of Nuclear Physics, Siberian Branch of the Academy of Sciences of the U.S.S.R., Sovetskaya St. 5, 630090 Novosibirsk, U.S.S.R.
42. J. Schmidt, Princeton Plasma Physics Laboratory, P.O. Box 451, Princeton, NJ 08540
43. D. Cohn, MIT Plasma Fusion Center, NW16-140, Cambridge, MA 02139
44. B. G. Logan, Lawrence Livermore National Laboratory, P.O. Box 5511, Livermore, CA 94550
45. B. Montgomery, MIT Plasma Fusion Center, 167 Albany Street, Cambridge, MA 02139

46. T. K. Fowler, Lawrence Livermore National Laboratory, P.O. Box 5511, Livermore, CA 94550
47. V. T. Tolok, Kharkov Physical-Technical Institute, Academical St. 1, 310108 Kharkov, U.S.S.R.
48. R. Varma, Physical Research Laboratory, Navrangpura, Ahmedabad, India
49. Bibliothek, Max-Planck Institut fur Plasmaphysik, D-8046 Garching bei Munchen, Federal Republic of Germany
50. Bibliothek, Institut fur Plasmaphysik, KFA, Postfach 1913, D-5170 Julich, Federal Republic of Germany
51. Bibliotheque, Centre de Recherches en Physique des Plasmas, 21 Avenue des Bains, 1007 Lausanne, Switzerland
52. Bibliotheque, Service du Confinement des Plasmas, CEA, B.P. 6, 92 Fontenay-aux-Roses (Seine), France
53. Documentation S.I.G.N., Department de la Physique du Plasma et de la Fusion Controlee, Centre d'Etudes Nucleaires, B.P. No. 85, Centre du Tri, 38041 Cedex, Grenoble, France
54. Library, Culham Laboratory, UKAEA, Abingdon, Oxfordshire, OX14 3DB, England
55. Library, FOM Institut voor Plasma-Fysica, Rijnhuizen, Jutphaas, The Netherlands
56. Library, Institute of Physics, Academia Sinica, Beijing, Peoples Republic of China
57. Library, Institute of Plasma Physics, Nagoya University, Nagoya 464, Japan
58. Library, International Centre for Theoretical Physics, Trieste, Italy
59. Library, Laboratorio Gas Ionizzati, Frascati, Italy
60. Library, Plasma Physics Laboratory, Kyoto University, Gokasho Uji, Kyoto, Japan
61. Plasma Research Laboratory, Australian National University, P.O. Box 4, Canberra, A.C.T. 2000, Australia
62. Thermonuclear Library, Japan Atomic Energy Research Institute, Tokai, Naka, Ibaraki, Japan
63. W. B. Ard, McDonnell Douglas Astronautics Company, P.O. Box 516, St. Louis, MO 63166
64. H. L. Berk, Institute for Fusion Studies, University of Texas, Austin, TX 78712
65. R. A. Dandl, Applied Microwave Plasma Concepts, Inc., 2210 Encinitas Boulevard, Encinitas, CA 92024
66. A. J. Favale, Grumman Aerospace Company, P.O. Box 31, Bethpage, NY 11714
67. H. Ikegami, Institute of Plasma Physics, Nagoya University, Nagoya 464, Japan
68. N. A. Krall, JAYCOR, P.O. Box 85154, San Diego, CA 92138
69. J. B. McBride, Science Applications, Inc., P.O. Box 2351, La Jolla, CA 92037
70. F. L. Ribe, University of Washington, College of Engineering, AERL Building FL-10, Seattle, WA 98195
71. A. Opdenaker, Office of Fusion Energy, Office of Energy Research, Mail Station G-256, U.S. Department of Energy, Washington, DC 20545
72. H. Weitzner, Courant Institute of Mathematical Sciences, New York University, 251 Mercer Street, New York, NY 10012

73. N. A. Davies, Office of Fusion Energy, Office of Energy Research, Mail Stop G-256, U.S. Department of Energy, Washington, DC 20545
74. P. M. Stone, Reactor Systems and Applications Branch, Office of Fusion Energy, Office of Energy Research, Mail Stop G-256, U.S. Department of Energy, Washington, DC 20545
75-310. Given distribution as shown in TID-4500 Magnetic Fusion Energy (Category Distribution UC-20 a,d,f,g: Plasma Systems, Fusion Systems, Experimental Plasma Physics, Theoretical Plasma Physics)

☆U.S. GOVERNMENT PRINTING OFFICE: 1984-544-045/4271